

# Microscale Transport Mechanisms: Effect of Electrokinetic and Interfacial Interactions

BY

Glareh Azadi

B.Sc., University of New Hampshire, 2008

A DISSERTATION SUBMITTED IN PARTIAL FULFILLMENT OF THE  
REQUIREMENTS FOR THE DEGREE OF DOCTOR OF PHILOSOPHY  
IN THE Center for Biomedical Engineering, School of Engineering AT BROWN  
UNIVERSITY

PROVIDENCE, RHODE ISLAND

May 2014

© Copyright 2014 by Glareh Azadi

All Rights Reserved

This thesis by Glareh Azadi is accepted in its present form by the  
Center for Biomedical Engineering, School of Engineering as satisfying the  
thesis requirement for the degree of  
DOCTOR OF PHILOSOPHY

Date .....  
Prof. Anubhav Tripathi, Advisor

Recommended to the Graduate Council

Date .....  
Prof. Gary Wessel, Reader

Date .....  
Prof. Robert Hurt, Reader

Date .....  
Prof. Diane Hoffman-Kim, Reader

Date .....  
Prof. Martin Maxey, Reader

Date .....  
Prof. Arijit Bose, Reader

Approved by the Graduate Council

Date .....  
Peter M. Weber, Dean of the Graduate School

## The Vita of Glareh Azadi

Glareh Azadi was born in Kermanshah, Iran on April 12th, 1980. She graduated *Summa Cum Laud* from the University of New Hampshire (UNH) with a B.S. in Chemical Engineering in 2008. At UNH, she first joined the Nanostructured Polymers Research Center, studying polymer synthesis and morphology. Later, she became interested in the field of microfluidics and joined the Fluid Mechanic lab, where she learned the basic concept of microfluidics. She received an undergraduate research fellowship on studying enzymatic reactions in microfluidics and presented her result in the undergraduate research conference at UNH. She also had the opportunity to become a teaching assistant (TA) for Organic Chemistry and supervise the laboratory section of the course during her senior year at UNH. She received multiple scholarships and awards including, AIChE Donald F. Othmer Academic Excellence Award, International Student Award, and Dean's scholarship.

She was admitted to the PhD program at Brown university in 2008 under the guidance of Dr. Anubhav Tripathi. While at Brown, she was a head teaching assistant for Fluid Dynamics for three semesters, teaching assistant for Transport and Biotransport Processes for three semesters, teaching assistant for Engineering Design for one semester, and teaching assistant for Mechanics of Solids and Structures for one semester. She was also given the opportunity to present her research in the American Institute of Chemical Engineers (AIChE) in 2010 and 2012. Her research experience resulted in the following publications:

1. Azadi, G., Chauhan, A., and Tripathi, A. *Dilution of protein-surfactant complexes: A fluorescence study*. Protein Science, 2013(In Press).
2. Azadi, G., Gustafson, E., Wessel. G., and Tripathi, A. *Rapid detection and quantification of specific proteins by immunodepletion and microfluidic separation*. Biotechnol. J. 2012, 7, 10081013.
3. Azadi, G., Seward, M., Larsen, M.U., Shapley, N.C., and Tripathi, A. *Improved Antimicrobial Potency through Synergistic Action of Chitosan Microparticles and Low Electric Field*. Applied Biochemistry and Biotechnology.2012, Volume 168, Issue 3, pp 531-541.
4. Azadi, G., and Tripathi, A. *Surfactant-induced electroosmotic ow in microuidic capillaries*. Electrophoresis 2012, 33, 20942101.

## Acknowledgments

I would like to thank my advisor Dr. Anubhav Tripathi for his guidance and support. I am also thankful to my collaborators Dr. Gary Wessel, Dr. Martin Maxey and Dr. Anuj Chauhan for valuable discussions and insights. I am indebted to Dr. Charles Vaslet who patiently taught me on bacteria culture and protein expression. My friends and lab mates Dr. Stephanie McCalla, Dr. Elejdis Kulla, Dr. Jinkee Lee, Dr. Kenneth Morabito, Yasaman Mani, Stephanie Angione, Jingjing Wang and Michael Godfrin for making my graduate experience full of good memories. My special thank is to Dr. Amir Moradifam for helping me get through the most difficult challenges of my life.

Finally, I am eternally thankful to my mother and role model Nasrin. Although she was not physically with me, her spirit has always given me strength and determination to move ahead. I am forever thankful to my sister Nasim, my brother Saeid and my father Ardeshir for their unconditional love and for standing by me even in distance during the times of frustration and confusion. I could have not finished this work without their endless love and support.

## Dedication

In loving memory of my mother NASRIN

ABSTRACT OF “Microscale Transport Mechanisms: Effect of Electrokinetic and Interfacial Interactions” BY Glareh Azadi, Ph.D., BROWN UNIVERSITY, May 2014.

Electrokinetic transport, as a non-mechanical tool in driving the fluid is widely used in microfluidics. This mode of transport is highly desirable due to simple integration, precise flow control by an external electric field and applicability over a wide range of sample conductivities. Fluid transport by electrokinetic techniques is dominated by surface and interfacial interactions through electrostatic attractions around charged particles (electrophoresis) or adjacent to the channel surface (electroosmosis). Miniaturization at microscale provides a high surface to volume ratio where the surface forces and interfacial effects are significantly enhanced compare to macroscale geometries. For a successful design of an optimum microfluidic device, these interactions need to be precisely quantified and controlled. This thesis focuses on studying the interfacial and electrokinetic interactions in micro-geometries, with the goal of designing an optimal platform for separation and detection of biomolecules. First, the interaction of proteins with surfactant molecules was studied to address some of the fundamental issues in microchip electrophoresis such as simultaneous quantification and detection. This work was followed by developing a rapid method for detection and quantification of proteins by electrophoresis and immunodepletion techniques. In order to quantify the effect of surfactant adsorption on electrokinetic flow, electroosmotic mobility measurements were performed at the solid-liquid interface of plastic microcapillaries (poly methylmethacrylate, PMMA). In addition, the electrokinetic effects with respect to electroporation of the cell wall were applied to develop an

effective technique for inhibition of gram-negative bacteria(*E.Coli*). Finally, the dispersion of a semi-infinite suspension of particles was investigated in a capillary, in order to study the effects of hydrodynamic interactions and capillary confinement on the diffusive behavior of the particles.

# Contents

<b>The Vita of Glareh Azadi</b>	<b>iii</b>
<b>Acknowledgments</b>	<b>v</b>
<b>Dedication</b>	<b>vi</b>
<b>1 Introduction</b>	<b>1</b>
1.1 Microchip protein electrophoresis . . . . .	2
1.2 Application of microchip electrophoresis in detection of a target protein	3
1.3 Application of biopolymers and electric field in bacteria inhibition . .	4
1.4 Electroosmotic flow in plastic microchip devices . . . . .	5
1.5 Dispersion of a semi-infinite suspension plug under oscillatory flow . .	6
1.5.1 Dispersion of a suspension plug formed by magnetic sweeping	7
1.6 Manuscripts . . . . .	7
<b>2 Dilution of Protein-Surfactant complexes: A Fluorescence Study</b>	<b>9</b>
2.1 Abstract . . . . .	9
2.2 Introduction . . . . .	10

2.3	Material and Methods . . . . .	13
2.3.1	Chemicals . . . . .	13
2.3.2	Protein–surfactant preparation . . . . .	13
2.3.3	Fluorescence measurements . . . . .	14
2.4	Optimum SDS and Dye concentration . . . . .	15
2.5	Dilution of SDS-Dye . . . . .	15
2.6	Dilution of Protein-SDS-Dye . . . . .	17
2.7	Effect of Protein Concentration . . . . .	21
2.8	Effect of cationic surfactant CTAB . . . . .	23
2.9	Conclusions . . . . .	25
<b>3</b>	<b>Electrophoretic Detection of a Target Protein on a Microfluidic platform</b>	<b>27</b>
3.1	Abstract . . . . .	27
3.2	Introduction . . . . .	28
3.3	Materials and Methods . . . . .	30
3.3.1	Sample preparation . . . . .	30
3.3.2	Control experiment . . . . .	32
3.4	FLAG protein detection in a bacterial lysate . . . . .	33
3.5	FLAG protein detection in a target-free protein complex . . . . .	39
3.6	Conclusions . . . . .	42
<b>4</b>	<b>Synergistic action of Chitosan and low voltage pulsed electric field in bacterial inhibition</b>	<b>44</b>

4.1	Abstract . . . . .	44
4.2	Introduction . . . . .	45
4.3	Materials and Methods . . . . .	48
4.3.1	Materials . . . . .	48
4.3.2	Preparation of chitosan microparticles(CSMP) . . . . .	49
4.3.3	Characterization of CSMP . . . . .	50
4.3.4	Bacteria culture and inhibition assay . . . . .	50
4.4	E. coli inhibition: Effect of CSMP concentration . . . . .	52
4.5	E. coli inhibition: combination of CSMP and electric field . . . . .	54
4.6	E. coli inhibition: Colony growth results . . . . .	57
4.7	Conclusions . . . . .	59
<b>5</b>	<b>Effect of surfactant adsorption on the electrokinetic properties of poly methylmetcarylate(PMMA)</b>	<b>61</b>
5.1	Abstract . . . . .	61
5.2	Introduction . . . . .	63
5.3	Materials and Methods . . . . .	67
5.3.1	Materials and Reagents . . . . .	67
5.3.2	Instrumentation and Method . . . . .	69
5.4	Surface chemistry of PMMA . . . . .	70
5.5	Effect of ionic and non-ionic surfactants . . . . .	73
5.5.1	Effect of negatively charged ionic surfactant: SDS . . . . .	74
5.5.2	Effect of positively charged ionic surfactant: CTAB . . . . .	77

5.5.3	Effect of non-ionic surfactant: Brij35 . . . . .	79
5.6	Effect of mixed surfactants . . . . .	80
5.7	Effect of neutral polymers . . . . .	83
5.8	Effect of surfactant structure: chain length . . . . .	84
5.9	Estimation of cohesive energy of adsorption . . . . .	89
5.10	Mechanism of surfactant adsorption on PMMA . . . . .	92
5.11	Conclusions . . . . .	95
<b>6</b>	<b>Dispersion of a semi-infinite suspension plug under oscillatory flow</b>	<b>97</b>
6.1	Abstract . . . . .	97
6.2	Introduction . . . . .	98
6.3	Experimental Method . . . . .	100
6.3.1	Image Analysis . . . . .	101
6.4	Theory . . . . .	102
6.5	Results and Discussion . . . . .	103
6.6	Conclusions . . . . .	107
6.7	Acknowledgement . . . . .	108
<b>7</b>	<b>Conclusions</b>	<b>109</b>
<b>A</b>	<b>Dispersion of a suspension plug formed by magnetic sweeping</b>	<b>115</b>
A.1	Experimental Method . . . . .	115
A.1.1	Image analysis . . . . .	116
A.1.2	Formation of force chains by magnetic sweeping . . . . .	117

# List of Tables

2.1	Comparison of the proposed fluorescence model with the experimental values above CMC. Number of micelles is calculated based on the aggregation number and concentration of SDS. . . . .	17
2.2	Comparison of quantum yield of Sypro orange dye with BSA, CA and betagal at 1mg/ml and 15mM SDS. Number of free and bound micelles was calculated using defined ratio of 1.4g SDS/ 1g protein. . . . .	18
2.3	Dilution of free and bound micelles in SDS dominant region. The number of free and bound micelles, $N_{sds}$ and $N_p$ at 15mM as the first point of dilution was determined using the ratio of 1.4g SDS/1g protein. Below 15mM $N_{sds}$ was calculated based on the dilution factor, $N_p$ was estimated using Eq 2.2. . . . .	20
2.4	Comparison of the proposed fluorescence model with the experimental values at various BSA concentrations for the first dilution point(15mM) SDS. Values of $N_{sds}$ and $N_p$ were determined using the ratio of 1.4g SDS/ 1g protein. . . . .	22

3.1 Quantification of the immunodepleted FLAG protein. The listed values are the average of three independent experiments( mean  $\pm$  standard deviation). . . . . 37

# List of Figures

2.1	Schematic of the dilution concept in protein sizing microchip. Protein-surfactant complex at concentration above the surfactant CMC enters the separation channel. Dilution is performed before the detection point in order to reduce the fluorescent of free micelles by reducing the surfactant concentration below CMC. . . . .	11
2.2	Agilent 2100 electropherogram (a) and psuedogel(protein 230) of BSA, CA and betagal at 0.007mg/ml. 4.5kDA and 240kDa as lower and upper markers. . . . .	14
2.3	(a) Uptake of dye molecules by SDS micelles with constant dye concentration (5X). The inset shows the uptake of dye molecules at different concentrations by fixed concentration of SDS at 15mM. (b) Dilution of SDS-Dye with 15mM SDS and 5x sypro orange dye. The signal is normalized with respect to maximum and minimum values. The error bars are obtained from three consecutive measurements. Conditions: 1x Tris-glycine buffer, pH 8.6, room temperature. . . . .	16

2.4	Dilution of SDS-protein complex .The inset shows the fluorescent profile of proteins after subtracting the background SDS fluorescence. The error bars are obtained from three consecutive measurements. Conditions: 15mM SDS, 1mg/ml protein, denatured by heat (5min at 95°C) and beta mercaptoethanol(0.2M), 5x sypro orange dye, 1x Tris-glycine buffer at 8.6 pH, room temperature. . . . .	19
2.5	Effect of protein concentration on the dilution of SDS-BSA complex. The inset shows the fluorescence profile of the protein after subtracting the background SDS fluorescence. Conditions: 15mM SDS, 1x Tris-glycine buffer at 8.6 pH, 5x sypro orange dye, room temperature. Protein was denatured by heat(5min at 95°C) and betamercaptoethanol(0.2M). . . . .	23
2.6	Effect of CTAB concentration on the dilution of SDS-BSA complex. The inset shows the fluorescence profile of the protein after subtracting the background SDS fluorescence. Conditions: 15mM SDS, 1x Tris-glycine buffer at 8.6 pH, 5x sypro orange dye, room temperature. Protein was denatured by heat(5min at 95°C) and betamercaptoethanol(0.2M). . . . .	24
3.1	Schematic of the proposed method. The target is first isolated by immunodepletion with magnetic beads coated against the target. Then after collecting the beads magnetically, the supernatant is analyzed on a microfluidic electrophoresis chip. . . . .	30

3.2	Immunoblot using a conventional Western method. Lanes 1, 2 and 3 correspond to 100, 70 and 35 micrograms of protein loaded per lane that was then stained with Coomassie or labeled by immunoblotting with anti-FLAG antibodies. The asterisk indicates the position of the FLAG-tagged protein species. . . . .	31
3.3	Control experiment. Detection of biotinylated anti-human cTnT antibody( $0.2\mu\text{g}/\mu\text{l}$ ) at three incubation times with streptavidin coated magnetic beads. . . .	34
3.4	Agilent(protein 80) pseudo gel of lysate, elution and incubated samples. All samples, except the elution, are supernatant after incubation with anti-FLAG beads. . . . .	36
3.5	a)Detection of FLAG protein, comparison of two incubation times in depleting the target ( $1.42\mu\text{g}/\mu\text{l}$ ). The adsorption kinetic of FLAG protein is shown in the inset.b)Comparison of eluted and incubated samples after 60 minutes. The elution sample is the eluted FLAG protein from the beads after 60 minutes incubation. The arrow shows the target peak. . . . .	37
3.6	Detection of FLAG protein in a target-free complex sample. The concentration of each non-FLAG protein is constant at $200\text{ng}/\mu\text{l}$ . The inset shows the linear detection range of the target with respect to concentration. . . . .	39
3.7	Detection of depleted target protein in a complex sample. The concentration of FLAG protein ( 50kDa) is varied from $50\text{ng}/\mu\text{l}$ to $200\text{ng}/\mu\text{l}$ , while keeping the non-FLAG protein concentration each at $200\text{ng}/\mu\text{l}$ .	40

3.8	Depletion of FLAG protein in a protein complex at different concentrations. The concentration of each non-FLAG protein was kept constant at 200ng/ $\mu$ l while changing the target concentration. Samples were incubated with anti-FLAG magnetic beads for 10 minutes. Error bars are the standard deviation obtained from three independent studies. .	41
4.1	Colony forming units formed following overnight incubation after subsequent treatment with deionized water or CSMP. The left pane illustrates a representative result obtained after treating cells with deionized water only; the right pane shows cells that grew following introduction of CSMP at a concentration of 1.6 mg/ml suspended in deionized water. Both panes were obtained using dilutions of 1:100,000. . . . .	52
4.2	Growth of cells following treatment with different concentrations of CSMP. DI represents deionized water and values of 0.8 and 3.2 represent the concentration of CSMP in mg/ml prior to serial dilution. . .	53
4.3	Colony forming units formed following overnight incubation after subsequent treatment with deionized water or CSMP at 100V/cm. The left pane illustrates a representative result obtained after treating cells with deionized water only with dilution factor of 1:100,000, the right pane shows survived colonies after chitosan treatment with dilution factor of 1:1000. . . . .	55

4.4	Cell colony counts after electroporation, chitosan introduction, or both. Electrical potentials of 5V and 10V applied across a 1 mm gap correspond to electric field strengths of 50 V/cm and 100 V/cm, respectively. The 0V CSMP data set was performed in triplicate, but the error bar is not visible on the chosen scale. The vertical axis contains a logarithmic scale. . . . .	56
4.5	Comparison of electroporation treatment alone and combined treatment of electroporation and CSMP at high concentration. Final CSMP concentrations of 3.2 mg/ml were able to increase the inhibition effect of electroporation. Electroporation with electric field strengths of 50 V/cm were used. . . . .	57
4.6	Viable colonies following various treatment combinations involving CSMP and 50 V/cm electroporation. Panes (A-C) depict cells that grew following combined treatment with 50 V/cm sustained electric field and 1.6 mg/ml CSMP. The respective dilution factors were: (A) 1:1,000, (B) 1:100,000, and (C) 1:10,000. (D) and (E) experienced electroporation only and had dilution factors of 1:1,000 and 1:100,000 respectively. The control treatment using deionized water and no electroporation appears in frame (F). This control plate was created from bacteria that were diluted by a factor of 1:100,000. . . . .	58
5.1	Chemical structures of surfactants, PMMA, PDMA and polymer used as a coating material. . . . .	68

5.2	Schematic of the EOF detection platform. Microfluidic PMMA capillary (length 12 cm, i.d. $180\mu\text{m}$ ) connected between two reservoirs. Microscope detection system consists of HV power supply (voltage 1500 V), microscope optics, excitation lamp and photodiode. Detection point was located at 6 cm. The migration time of the neutral dye is taken at the point where the photomultiplier (PMT) signal reaches a steady value. . . . .	70
5.3	Critical micelle concentration (CMC) determination of the surfactants. The fluorescence signal is normalized with respect to maximum and minimum values. Sypro orange concentration was constant at 5x. . .	74
5.4	Effect of SDS on EOF in PMMA microcapillaries. The inset shows the plot of theoretical and experimentally measured current values. Error bars are obtained from three independent experiments. . . . .	76
5.5	Effect of CTAB on EOF in PMMA microcapillaries. The inset shows the plot of theoretical and experimentally measured current values. Error bars are obtained from three independent experiments. . . . .	78
5.6	Effect of Brij35 on EOF in PMMA microcapillaries. The inset shows the plot of theoretical and experimentally measured current values. Error bars are obtained from three independent experiments. . . . .	80
5.7	Effect of mixed surfactants on EOF in PMMA microcapillaries. For each data point the concentration of SDS was fixed at 0.5mM. The inset shows the experimental current. . . . .	82

5.8	Effect of HMPC, PDMA and Brij35 mixed with SDS on EOF mobility in a PMMA microcapillary. . . . .	84
5.9	Critical micelle concentration (CMC) determination of the surfactants. The fluorescence signal is normalized with respect to maximum and minimum values. Sypro orange concentration was constant at 5x. . . . .	86
5.10	Experimental currents measurements. The inset shows the counterion association constant with respect to chain length $n_c$ . . . . .	87
5.11	The effect of surfactant concentration on EO mobility in a PMMA microcapillary. Solid lines were added to guide the eye. Conditions: 1mM KCl, pH 8.5 at 25°C. Constant Voltage:1500 V. . . . .	88
5.12	Variation of the slope of the mobility curve as a function of alkyl chain length. The inset shows the linear portion of the mobility curve plotted with logarithmic scale of concentration. Solid lines represent linear fits. . . . .	90
5.13	Variation of the concentration of alkyltrimethyl ammonium bromides at zero-mobility as a function of alkyl chain length. . . . .	91
5.14	(a) Electro-osmotic flow in KCl electrolyte.(b) Monomeric surfactant adsorption through electrostatic and hydrophobic interactions.(c) Transition from dilute to packed surfactant monolayer at higher concentrations.(d) Formation of hemimicelles above critical micelle concentration (CMC). . . . .	94
6.1	A: Paramagnetic spheres(10x Obj). B: Particle position as a function of time. Condition: $Q = 20\mu\text{l}/\text{min}$ , $T=40$ sec. . . . .	100

6.2	The glass capillary is connected to the syringe pump at one end, while the other end is placed vertically in the suspension solution. The semi-infinite plug is subjected to oscillatory flow for the duration of half period( $T/2$ ) in each direction at a set flow rate. Images are taken with a CCD camera at the end of each oscillation cycle. . . . .	101
6.3	Image analysis by measuring the plug extension at the maxima of the parabolic profile. $L_0$ and $L_t$ are plug length at $t = 0$ and $t$ at the end of one cycle. $D$ is the capillary diameter. . . . .	102
6.4	Average position of particles at $\phi = 1\%$ at different strain amplitudes. The average shear rate varies from $0.3s^{-1}$ to $1.1s^{-1}$ , corresponding to $5\mu l/min$ , $T = 10$ sec to $20\mu l/min$ , $T = 20$ sec. $N$ is the number of cycles, $L$ is the plug length and $D$ is the capillary length. Two sets of data for $\gamma = 2.7$ was obtained by varying the flow rate and time period. The astrict shows the resulting strain amplitude at $20\mu l/min$ and $T = 10$ . . . . .	104
6.5	The transient growth of the semi-infinite suspension plug at $24\%$ volume fraction at different strain amplitudes. The average shear rate varies from $0.3s^{-1}$ to $1.1s^{-1}$ , corresponding to $5\mu l/min$ , $T = 10$ sec to $20\mu l/min$ , $T = 20$ sec. $N$ is the number of cycles, $L$ is the plug length and $D$ is the capillary length. . . . .	106

6.6	The transient growth of the semi-infinite suspension plug at 42% volume fraction at different strain amplitudes. The average shear rate varies from $0.3s^{-1}$ to $1.1s^{-1}$ , corresponding to $5\mu\text{l}/\text{min}$ , $T = 10$ sec to $20\mu\text{l}/\text{min}$ , $T = 20$ sec. $N$ is the number of cycles, $L$ is the plug length and $D$ is the capillary length. . . . .	107
6.7	Profile of the suspension plug at cycles 2, 5 and 10. A : $\gamma = 2.7$ , B: $\gamma = 5.6$ and C: $\gamma = 8$ for suspension with $\phi = 42\%$ . . . . .	108
A.1	The apparatus consists of a 3-way valve connected to particle-free syringe pump, suspension syringe pump, and the capillary. . . . .	116
A.2	Determination of the plug width by grayscale in Image J. The grayscale profile corresponds to the line chosen at the middle of the plug. . . . .	117
A.3	Plug extension by time for two volume fractions 33% and 53% at various strain amplitudes. . . . .	118

# Chapter 1

## Introduction

The advent of microfluidics has revolutionized the field of life sciences and biomedicine over the past two decades. Miniaturization from macro to micro scale provides a number of advantages, mainly small sample volume, fast analysis time and automation. Despite rapid development of new devices, a better understanding of diffusive and convective transport processes in micro scale is necessary for the optimization and commercialization of the current designs. Due to a large surface to volume ratio, transport processes in these devices are influenced by interfacial effects. The convective transport relies on pressure or electric field driven (electrokinetic) flows. The electrokinetic flows arise from two mechanisms: 1) electrophoretic and 2) electroosmotic. In electrophoretic flow, a charged particle moves under the action of electric field, whereas electroosmotic flow (EOF) is the fluid motion driven by the charged ion cloud adjacent to the solid wall. This thesis explores the influence of interfacial interactions on the diffusion and electrokinetic transport in microscale geometries.

## 1.1 Microchip protein electrophoresis

Microfluidic electrophoresis is a strong analytical tool in protein separation offering high sensitivity, versatility and speed. The mechanism is based on the diffusive and electrokinetic interactions of proteins with surfactant micelles. Prior to analysis, the protein sample is mixed with a buffer containing a surfactant, mainly sodium dodecyl sulfate (SDS) at a concentration above critical micelle concentration (CMC) and beta mercaptoethanol as denaturants. In the next step, the protein sample is heated at 95°C to ensure an irreversible unfolding of protein. Finally, the sample is injected by electrokinetic mode on the chip. The channels are filled with poly dimethylacrylamide (PDMA) as the gel matrix and a hydrophobic fluorescent dye. The protein-surfactant complex is mixed with the dye as it passes through the channels. Due to the hydrophobic nature, the dye also binds to the free surfactant micelles. In order to minimize the fluorescence contribution of free surfactant micelles, the protein-surfactant complex is diluted by addition of buffer before arriving at the detection window. During this step, the surfactant concentration is reduced below CMC, where surfactant molecules are present as monomers. Although separation of proteins is achieved, the quantification of protein based on the intensity of fluorescent signal has not been reported. In the first chapter of this thesis, we study the dilution of protein-surfactant complex as an integrated step in microchip electrophoresis. We analyze the contribution of free and protein bound surfactant micelles on the overall fluorescence by proposing a possible fluorescent model. The quantification of protein sample based on the fluorescence intensity and the effect of a cationic surfactant additive are

investigated.

## **1.2 Application of microchip electrophoresis in detection of a target protein**

With the advent of proteomics, the detection of protein biomarkers has gained increasing attention over the past decade. Conventional techniques in detection of a target protein include gel electrophoresis, Western blot, Nuclear magnetic resonance(NMR) and enzyme linked immunosorbant assay(ELISA). Even though these techniques provide a robust and sensitive detection, they suffer from large sample volume and lengthy analysis time. To this end, a rapid and simple detection technique can be highly beneficial as a quick evaluation for the existence of a target protein in a specific medium. In the second chapter, we propose a method for a parallel detection and quantification of a target protein by a combination of microchip electrophoresis and immunodepletion. The sensitivity of this method is analyzed with respect to the target concentration and non-specific adsorption of other proteins in immunodepletion step. The results are compared to conventional Western blot and elution of target for quantification in immunodepletion.

### 1.3 Application of biopolymers and electric field in bacteria inhibition

Outbreaks of pathogenic bacteria contaminating consumed produce are continuously being reported with *Escherichia coli* O157:H7 and *Salmonella* among the leading pathogenic threats to food safety. Common treatments such as thermal and large scale irradiation are either costly or can not be applied to fresh produce. In response, a mild, incompatible and energy efficient method is needed for fresh and fresh-cut fruits and vegetables. Polymeric nanoparticles with positive surface charge and antibacterial properties are among suitable treatments that can be applied synergistically with a chlorine wash. Furthermore, these particles can be surface modified or encapsulated with antibacterial peptide molecules for enhanced treatment. The antibacterial effect of chitosan as a non-toxic biopolymer is widely recognized in acidic conditions, pH ranges of 5.5-7.0[78, 25, 76]. The antibacterial effects are minimized in neutral and alkaline pH. In order to overcome this problem an electric field can be synergistically applied with particulate chitosan. Irreversible electric field action is an effective inhibition method that is limited in application. The limiting factor in electro-lysis of bacteria is the very high electric field required(16 kV/cm [109]),which is difficult to generate and apply to sufficiently large geometries. It is therefore of interest to incorporate sub-lethal electric field with a natural treatment for an effective inhibition of bacteria. In chapter three, we investigate the combination effect of particulate chitosan and low voltage pulsed electric field in inhibiting *E.coli*.

## 1.4 Electroosmotic flow in plastic microchip devices

In recent years, researchers have focused on plastic substrates (polymers) as a substitute for glass based microfluidics due to the ease of manufacturing [150], relative low cost [35] and flexibility in design and fabrication [65]. However, compared to glass with a known surface chemistry (negative charge of siloxy groups), the surface charge and zeta potential of the plastic substrates varies [71]. This variation arises from a number of additives used during the manufacturing process for the enhancement of physical and chemical properties. For this reason the control of electroosmotic flow (EOF) has been proven challenging in plastic microchips [94]. Depending on surface charge, EOF can exist in opposite direction of electrophoretic flow, minimizing the sensitivity of electrophoretic separation. For this reason a precise control of EOF in plastic devices is necessary. Surface modification through dynamic coating with surfactant is among the simple and low cost method for controlling EOF [60, 55, 120]. In chapter four, we study the effect of surfactant additives on EOF in poly methylmetacrylate (PMMA) microcapillaries. Factors considered are surfactant charge, concentration and chain length.

## 1.5 Dispersion of a semi-infinite suspension plug under oscillatory flow

Dispersion of microspheres and cells has become a critical issue in a number of biological and microfluidic applications. While it is well known that pressure driven flows through a microchannel leads to Taylor dispersion of solute plugs, the dispersion characteristics of particles or cell suspension plugs have not been explored in detail. The dispersion is important at time scales such that the particles sample many streamlines due to interfacial effects at the channel wall and multiparticle hydrodynamic interactions. In most of the microfluidic applications, single or multiple dilutions of reagents are required in order to perform reactions or measurements over a range of concentrations using only one set of sample solutions to fill the inlets. It is often unclear how to design the dilution channel or channels for achieving minimum dispersion of plugs. New insights on particle fluxes and mixing in microchannel flows are needed to develop models for concentration fronts or strongly inhomogeneous flows as opposed to fully populated flows. Even though numerous studies have investigated the dispersion behaviour of fully populated suspensions, no study has been reported on evaluating the dispersion of a plug or semi-infinite plug of particles. In chapter five, we study the transient dispersion of a semi-infinite suspension plug inside a capillary under continuous oscillatory flow.

### 1.5.1 Dispersion of a suspension plug formed by magnetic sweeping

Appendix A discusses the results of a magnetic set up for formation of a plug of particles inside a capillary.

## 1.6 Manuscripts

This thesis is based on and contains the following manuscripts that are published or in preparation for submission in peer-reviewed academic journals.

- Chapter 2: Azadi, G., Chauhan, A., and Tripathi, A. *Dilution of protein-surfactant complexes: A fluorescence study*. Protein Science, 2013(In Press).
- Chapter 3: Azadi, G., Gustafson, E., Wessel. G., and Tripathi, A. *Rapid detection and quantification of specific proteins by immunodepletion and microfluidic separation*. Biotechnol. J. 2012, 7, 10081013.
- Chapter 4: Azadi, G., Seward, M., Larsen, M.U., Shapley, N.C., and Tripathi, A. *Improved Antimicrobial Potency through Synergistic Action of Chitosan Microparticles and Low Electric Field*. Applied Biochemistry and Biotechnology.2012, Volume 168, Issue 3, pp 531-541.
- Chapter 5: Azadi, G., and Tripathi, A. *Surfactant-induced electroosmotic ow in microwidic capillaries*. Electrophoresis 2012, 33, 20942101.
- Chapter 5: Azadi, G., Vlahovska, P.M., and Tripathi, A. *Influence of adsorbed*

*cationic surfactants on electrokinetic properties of a hydrophobic substrate: effect of concentration and chain length.* To be submitted to the Journal of Colloid and Interface Science.

- Chapter 6: Azadi, G, Maxey, M, and Tripathi, A. *Dispersion of a semi-infinite suspension plug under oscillatory flow.* To be submitted to the Journal of Fluid Mechanics.

# Chapter 2

## Dilution of Protein-Surfactant complexes: A Fluorescence Study

### 2.1 Abstract

Dilution of protein-surfactant complexes is an integrated step in microfluidic protein sizing, where the contribution of free micelles to the overall fluorescence is reduced by dilution. This process can be further improved by establishing an optimum surfactant concentration and quantifying the amount of protein based on the fluorescence intensity. To this end, we study the interaction of proteins with anionic sodium dodecyl sulfate (SDS) and cationic hexadecyl trimethyl ammonium bromide (CTAB) using a hydrophobic fluorescent dye (sypro orange). We analyze these interactions fluorometrically with bovine serum albumin, carbonic anhydrase, and beta-galactosidase as model proteins. The fluorescent signature of proteinsurfactant complexes at various dilution points shows three distinct regions, surfactant dominant, breakdown, and

protein dominant region. Based on the dilution behavior of protein-surfactant complexes, we propose a fluorescence model to explain the contribution of free and bound micelles to the overall fluorescence. Our results show that protein peak is observed at 3 mM SDS as the optimum dilution concentration. Furthermore, we study the effect of protein concentration on fluorescence intensity. In a single protein model with a constant dye quantum yield, the peak height increases with protein concentration. Finally, addition of CTAB to the protein-SDS complex at mole fractions above 0.1 shifts the protein peak from 3 mM to 4 mM SDS. The knowledge of proteinsurfactant interactions obtained from these studies provides significant insights for novel detection and quantification techniques in microfluidics.

## 2.2 Introduction

The interactions of proteins with surfactants have been studied extensively due to a wide range of applications in the field of separation, drug delivery, cosmetics and detergency[33, 130], or as a model in mimicking the behavior of cell membrane proteins[146, 157, 121]. Microfluidic electrophoresis is a strong tool in separation and detection of proteins[148, 94]. Even though miniaturization has many advantages, detection of low concentrated proteins in a small sample volume is still challenging. Hydrophobic fluorescent probes are among the methods used to enhance the detection sensitivity in low concentrations[126]. However due to the hydrophobic nature these probes also bind to the free surfactants micelles, creating a high background signal[54]. To overcome this problem, a dilution step has been integrated on the electrophoresis

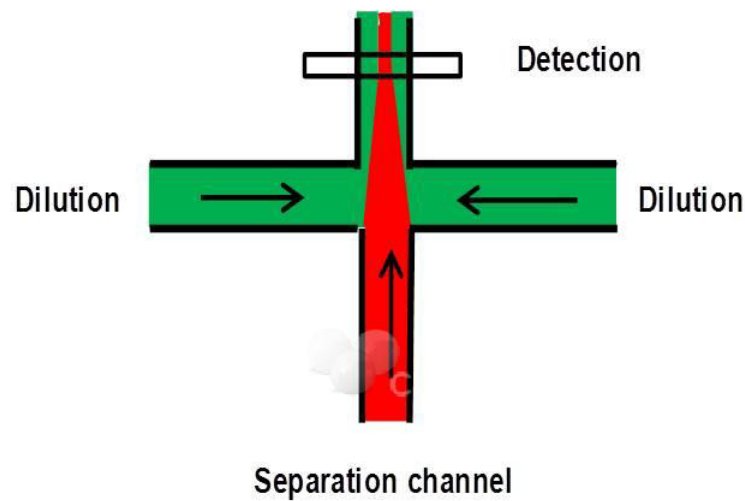


Figure 2.1: Schematic of the dilution concept in protein sizing microchip. Protein-surfactant complex at concentration above the surfactant CMC enters the separation channel. Dilution is performed before the detection point in order to reduce the fluorescent of free micelles by reducing the surfactant concentration below CMC.

microchip to reduce the fluorescent contribution from free surfactant micelles (Figure 2.1 ). Even though detection analysis has been improved to a great extent, no investigation has been performed on establishing an optimum dilution concentration or a correlation between fluorescent peaks (electropherograms) and protein concentration. In addition, current designs require a specific concentration range, limiting the analysis outside this range. To this end, more insights are needed in understanding protein-surfactant-dye interactions at various dilution points, in order to improve the detection and quantification of proteins on microfluidic platforms.

Binding of ionic surfactants to proteins at a certain concentration alters the native structure by initiating the unfolding or denaturing process. It is believed that at low concentrations, the binding of surfactant molecules are governed by electrostatic forces, however at concentrations above critical micelle concentration (CMC)

hydrophobic interactions are dominant[66, 88, 127]. At these high concentrations, the surfactant molecules dynamically bind to protein to induce denaturation, impart additional charges and make proteins structurally similar [138, 99, 81, 119]. By providing a constant charge/mass, separation of proteins is achieved based on the difference in molecular weight. Although the dynamic and kinetics of surfactant-protein interactions has been studied extensively[21, 151, 152, 100, 154], the effect of dilution on the fluorescent intensity of protein-surfactant complexes has not been studied in detail. Moreover, a great volume of literature on interaction of protein and surfactant is focused on single protein Bovine Serum Albumin (BSA)[32, 15, 33, 23, 149, 155]. Due to the wide range of differences in protein structure, it is important to investigate these interactions in a system of multiple proteins with different molecular weights. Understanding the nature of protein-surfactant interactions has been assisted in large by numerous structural analytical techniques such as circular dichroism(CD), nuclear magnetic resonance(NMR), mass spectroscopy(MS) and capillary electrophoresis(CE). Although these complex techniques have greatly advanced the field of protein analysis, their application is limited due to differences in protein structures and properties. Moreover, the procedure is lengthy and requires many hands-on steps. We address some of the key points in dilution of protein-surfactant-dye complex through a rapid and low-tech fluorometric technique. We analyze interactions of three proteins bovine serum albumin(BSA), carbonic anhydrase(CA) and beta-galactosidase(beta-gal) with sodium dodecyl sulfate(SDS), using a hydrophobic dye at different dilution points. In addition, we investigate the effect of cationic surfactant additives such as hexadecyltrimethylammonium bromide(CTAB) added for the pur-

pose of controlling the electro-osmotic flow in capillary electrophoresis[137, 79]. Based on our experimental results a fluorescent model is proposed to explain the interactions of the dye with free and bound surfactant micelles. The presented results on the dilution of protein-surfactant complexes significantly contribute to the development of novel detection and separation techniques in microfluidics platforms.

## **2.3 Material and Methods**

### **2.3.1 Chemicals**

Bovine serum albumin (BSA, 66 kDa), betagalactosidase from *E. coli* (betagal, 465 kDa), carbonic anhydrase from bovine erythrocytes (CA, 28 kDa), sodium dodecyl sulfate (SDS), hexadecyl trimethyl ammonium bromide (CTAB), betamercaptoethanol(DTT), and Tris-Glycine buffer were obtained from Sigma (St. Louis, MO). Sypro Orange protein staining dye (5000X) was purchased from Invitrogen (Carlsbad,CA). Aqueous solutions were prepared using ultra pure DI water (Elga Lab Water, Marlow, UK). All chemicals were used as received. The molecular weight of each protein was determined by gel electrophoresis on Agilent 2100 bioanalyzer (Figure(2.2)), following the manufacture protocol (Protein 230 kit).

### **2.3.2 Protein–surfactant preparation**

Solutions of SDS, CTAB, and protein were prepared in Tris-Glycine buffer (25 mM Tris/192 mM glycine, pH 8.6) and incubated at room temperature on a shaker (Innova 4080 incubator shaker, New Brunswick Scientific) for 1 h. At pH 8.6, all the proteins

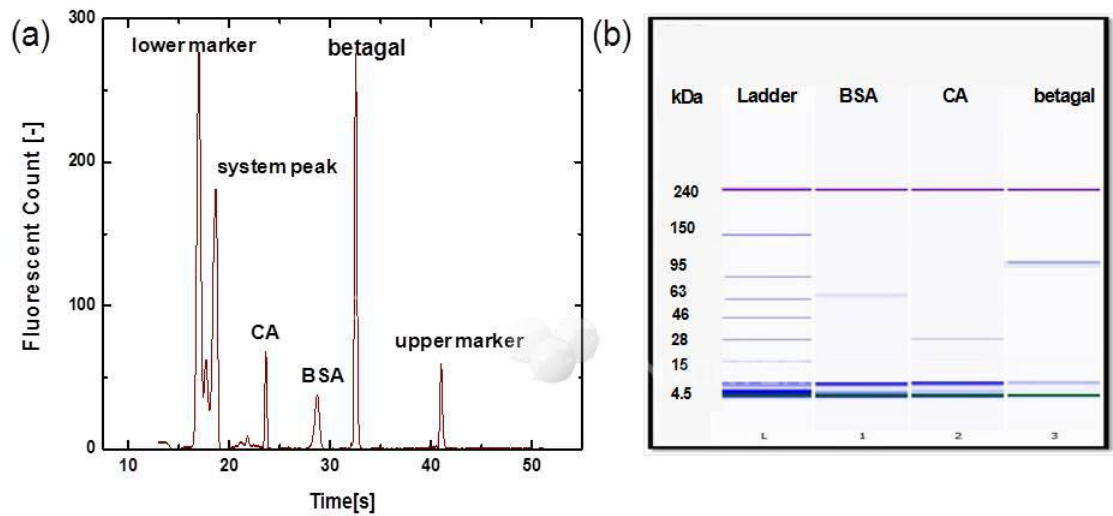


Figure 2.2: Agilent 2100 electropherogram (a) and pseudogel (protein 230) of BSA, CA and betagal at 0.007mg/ml. 4.5kDa and 240kDa as lower and upper markers.

carry a net negative charge as required in electrophoresis separation (isoelectric point of BSA, CA, and betagal are 4.7 [24], 5.9 [7] and 4.6 [141] respectively.) The protein-surfactant complexes were irreversibly denatured by beta-mercaptoethanol (0.2M) and heated (95°C for 5 min). After denaturing, sypro orange dye (5X) was added and the mixture of protein-surfactant-dye was serially diluted. All the experiments were carried out in triplicate at room temperature.

### 2.3.3 Fluorescence measurements

The fluorescence (Ex/Em: 470/570) of stained protein-surfactant solutions was measured at room temperature using a QM-4/2005SE spectrophotometer (Photon Technologies International, Birmingham, NJ). Sample was placed in a 10-mm length, 50 $\mu$ L quartz cuvette (Starna Cells, Atascadero, CA) and data was collected over time at 0.1 Hz. The cuvette was blanked with buffer prior to each measurement.

## 2.4 Optimum SDS and Dye concentration

The concentration of SDS was chosen at 15mM (4.3 mg/ml) three times more than the defined stoichiometry(1.4g SDS/1g protein at  $[sds] > CMC$ )[47, 12], allowing for a complete binding and a full range of study with free and protein bound micelles (protein micelles). The optimum dye concentration was determined by varying the dye concentration with fixed SDS concentration at 15mM(Figure 2.3a.inset). A plateau at 5x dye concentration shows a complete uptake of the dye by micelles. Note that the actual concentration of the dye cannot be determined. Furthermore, the fluorescence intensity of various concentrations of SDS with constant dye at 5x was measured (Figure 2.3a). Two observations can be made from Figure 2.3a, first the sudden increase in fluorescence signal at 4mM marks this concentration as the critical micelle concentration(CMC) of SDS in Tris-Glycine buffer where the hydrophobic dye resides within the micelles and fluoresces more. Second, the fluorescence signal reaches a constant value at 15mM SDS, due to a complete micellar uptake of dye molecules. At this concentration, considering the aggregation number of SDS as 80(74 in water[18]), the number of SDS micelles present is  $1.13 \times 10^{20}$ .

## 2.5 Dilution of SDS-Dye

After establishing the optimum SDS and dye concentration, the effect of dilution on the fluoresce intensity of SDS-Dye complex was investigated with 15mM SDS and 5x dye, and no free dye molecules in the solution. Figure 2.3b shows the normalized plot of fluorescence count versus SDS concentration. Given that the emission of the

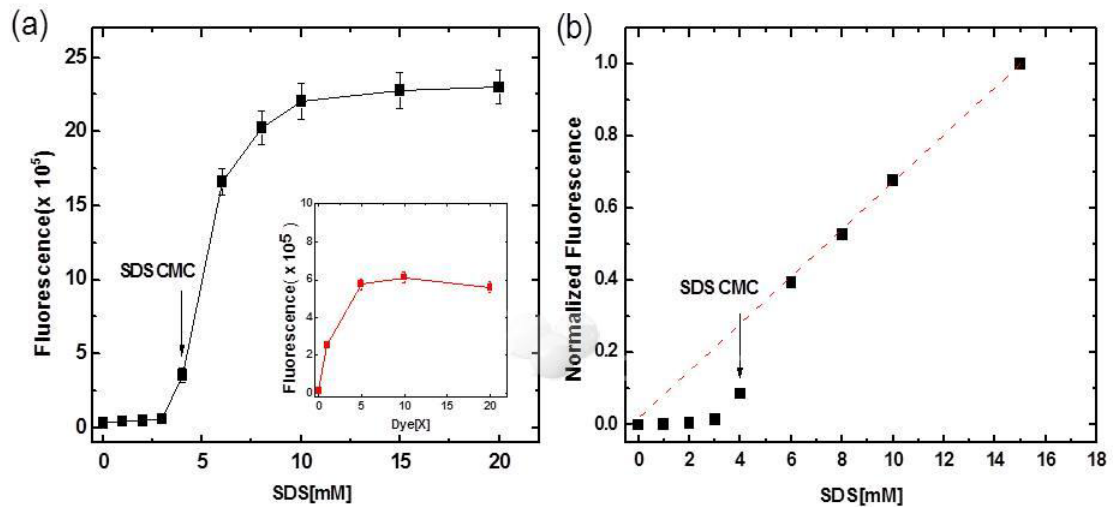


Figure 2.3: (a) Uptake of dye molecules by SDS micelles with constant dye concentration (5X). The inset shows the uptake of dye molecules at different concentrations by fixed concentration of SDS at 15mM. (b) Dilution of SDS-Dye with 15mM SDS and 5x sypro orange dye. The signal is normalized with respect to maximum and minimum values. The error bars are obtained from three consecutive measurements. Conditions: 1x Tris-glycine buffer, pH 8.6, room temperature.

dye is proportional to the number of micelles, the linear decrease in fluorescence intensity suggests a reduction in micellar number density by dilution from 15mM to 6mM SDS. Once the surfactant concentration reaches a critical value, the observed intensity undergoes a sudden decline, and finally vanishes below 4mM(CMC)[92], where SDS molecules are present as monomers. A possible fluorescent model can be proposed as:

$$Fl = \sum_{i=1}^{N_{sds}} (A \times n_{dye} \times \varphi_{sds})_i \quad (2.1)$$

where  $Fl$  is the fluorescence count,  $A$  is the adsorption intensity,  $n_{dye}$  is the number of dye molecules in each micelle,  $\varphi_{sds}$  is the quantum yield of one dye molecule with one SDS micelle, and  $N_{sds}$  is the total number of SDS micelles in the solution. Since

the concentration of the dye is unknown (5x), the exact number of dye molecules in the solution cannot be determined. We can estimate  $\beta = A \times n_{dye} \times \varphi_{sds}$ , assuming equal number of dye molecules per micelle, using the fluorescence count and the number of micelles in the solution. With 15mM SDS and 5x dye as the first dilution point (  $15mMSDS = 1.13 \times 10^{20}$  micelles)  $\beta = 1.48 \times 10^{-14}$  count/micelle.

The fluorescence count of other dilution points up to CMC can be determined using Eq 2.1. The calculated values confirm the linear decrease in number of micelles and are in a good agreement with the experimental values as tabulated in Table 2.1.

Table 2.1: Comparison of the proposed fluorescence model with the experimental values above CMC. Number of micelles is calculated based on the aggregation number and concentration of SDS.

SDS[mM]	#micelles	F1(calculated)	F1(experimental)	error
15mM	$1.13 \times 10^{20}$	$1.67 \times 10^6$	$1.67 \times 10^6$	-
10	$7.53 \times 10^{19}$	$1.11 \times 10^6$	$1.13 \times 10^6$	1.8
8	$6.02 \times 10^{19}$	$8.92 \times 10^5$	$8.82 \times 10^5$	1.1
6	$4.52 \times 10^{19}$	$6.69 \times 10^5$	$6.60 \times 10^5$	1.4

## 2.6 Dilution of Protein-SDS-Dye

After studying the interaction of dye with SDS micelles, the dilution of protein-SDS-dye complex was examined using three model proteins: BSA( 583 amino acids), CA(259 amino acids) and betagal( 1052 amino acids). The starting concentration of SDS, proteins and dye was 15mM, 1mg/ml, and 5x respectively. Proteins were denatured prior to dilution by 0.2M betamercaptoethanol and heat at 95°C for 5 min. Betagalactosidase denatures into four equal subunits each at  $\sim 112$ kDa.

Figure 2.4 shows the fluorescence intensity of protein and protein-free complexes at

various dilutions. Considering the contribution of bound micelles, Eq 2.1 is modified as:

$$Fl = \sum_{i=1}^{N_{sds}} (A \times n_{dye} \times \varphi_{sds})_i + \sum_{j=1}^{N_p} (A \times n_{dye} \times \varphi_p)_j \quad (2.2)$$

where  $N_p$  is the number of bound micelles, and  $\varphi_p$  is the quantum yield of one dye molecule with one bound micelle. Here, we have neglected the contribution of protein alone, assuming a complete binding of SDS molecules to the protein chain at saturated SDS concentration. Note that the individual values of  $A$ ,  $n_{dye}$ , and  $\varphi$  can not be determined, therefore we can only estimate the product of these factors. We have assumed equal number of dye molecules per free and bound micelle, neglecting the possible differences in micellar hydrophobicity and size. Considering constant  $\beta = 1.48 \times 10^{-14}$  count/micelle, calculated in the previous section, we define  $\alpha = A \times n_{dye} \times \varphi_p$ , therefore the difference in fluorescence of proteins at 15mM SDS in Figure 2.4 is attributed to variation in quantum yield of the dye with bound micelles as calculated in Table 2.2. Number of free micelles  $N_{sds}$  and bound micelles  $N_p$  at 15mM SDS was determined using the ratio of 1.4g SDS/g protein.

Table 2.2: Comparison of quantum yield of Sypro orange dye with BSA, CA and betagal at 1mg/ml and 15mM SDS. Number of free and bound micelles was calculated using defined ratio of 1.4g SDS/ 1g protein.

SDS[mM]	$Fl \times 10^6$	$N_{sds} \times 10^{19}$	$N_p \times 10^{19}$	$\beta \times 10^{-14}$	$\alpha \times 10^{-14}$
BSA	2.11	7.63	3.65	1.48	2.68
CA	2.30	7.63	3.65	1.48	3.20
Betagal	1.80	7.63	3.65	1.48	1.84

Our results show that proteins with equal concentration yield different fluorescence

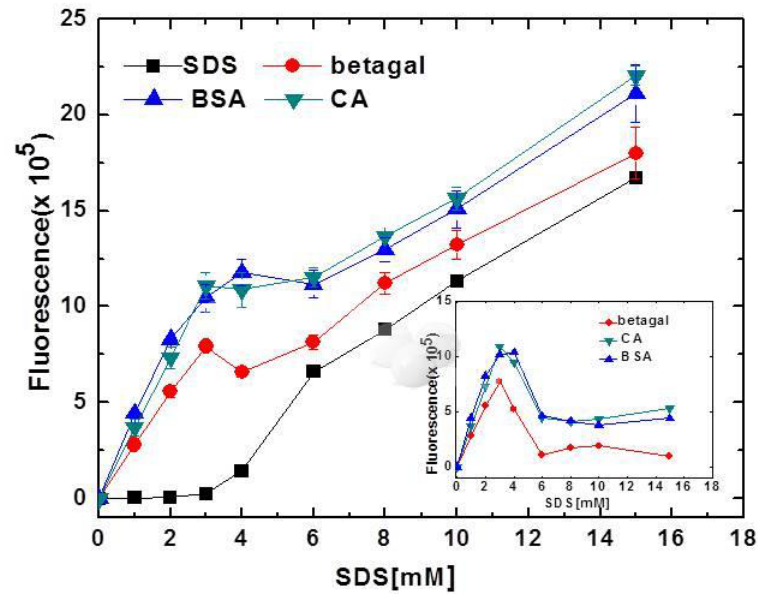


Figure 2.4: Dilution of SDS-protein complex. The inset shows the fluorescent profile of proteins after subtracting the background SDS fluorescence. The error bars are obtained from three consecutive measurements. Conditions: 15mM SDS, 1mg/ml protein, denatured by heat (5min at 95°C) and beta mercaptoethanol(0.2M), 5x sypro orange dye, 1x Tris-glycine buffer at 8.6 pH, room temperature.

intensities. Even though the concept of gel electrophoresis is based on the differences in size only, and dye is used as a marker of migration time, we speculate that for analysis based on fluorescence yield only in a gel-free solution, physical and chemical properties of the dye are key factors to be considered. As shown in Table 2.2, the dye quantum yield with bound micelles is higher than free micelles and varies for each protein. Figure 2.4 shows three distinct regions in the dilution profile of protein-SDS-dye: SDS dominant region: 15mM to 6mM SDS, breakdown region: 6mM to 3mM SDS and protein dominant region: below 3mM SDS. In the SDS dominant region, the dilution curve of protein complex shows a similar slope as protein-free complex, suggesting a linear reduction in the number of free micelles. To evaluate

this argument, the dilution of free and bound micelles is compared in Table 2.3. The number of free micelles at each point was determined based on the dilution factor, whereas the number of bound micelles was calculated based using Eq 2.2. As shown in Table 2.3. free micelles are diluted more significantly compare to bound micelles, resulting in a linear decrease in fluorescence. In the breakdown region, breaking of free SDS micelles results in the release of the dye from these micelles and its uptake by the bound micelles with higher quantum yield. This is evident by a slight increase in fluorescence count within this region as shown in Figure 2.4.

Table 2.3: Dilution of free and bound micelles in SDS dominant region. The number of free and bound micelles,  $N_{sds}$  and  $N_p$  at 15mM as the first point of dilution was determined using the ratio of 1.4g SDS/1g protein. Below 15mM  $N_{sds}$  was calculated based on the dilution factor,  $N_p$  was estimated using Eq 2.2.

SDS[mM]	$N_{sds} \times 10^{19}$	dilution	$N_{BSA} \times 10^{19}$	dilution	$N_{CA} \times 10^{19}$	dilution	$N_{Betagal} \times 10^{19}$	dilution
15	7.63	0	3.65	0	3.65	0	3.65	0
10	5.09	33	2.82	23	2.53	30	3.10	15
8	4.07	20	2.59	8	2.36	7	2.83	9
6	3.05	25	2.49	4	2.19	7	1.98	3

Finally, in the protein dominant region, with no free SDS micelles in the solution, the only fluorescence contribution is from bound micelles. Further dilution in this region results in a rapid reduction in fluorescence (increased slope) due to a decrease in number of protein molecules and consequently the number of bound micelles. In protein electrophoresis, the concentration of SDS is above CMC to ensure a complete binding and unfolding of protein. However, a dilution step is necessary to minimize the contribution of free micelles by reducing the SDS concentration to monomers (below CMC). The electropherograms or the protein peaks are generated by subtracting the

background fluorescence (SDS fluorescence). These peaks are shown as the inset in Figure 2.4 The maximum peak height was obtained at  $\sim 3\text{mM}$  SDS with no free SDS micelles in the solution. By eliminating the contribution of free micelles, this dilution point is considered as the optimum SDS concentration for protein electrophoresis. It is important to note that even though the concentration of proteins is equal, the peak intensities are not identical due to a difference in the dye quantum yield with each protein (Table 2.2).

## 2.7 Effect of Protein Concentration

Effect of protein concentration on dilution of SDS-protein was studied with five concentrations of BSA ranging from  $0.005\text{mg/ml}$  to  $1\text{mg/ml}$  while keeping the SDS concentration constant at  $15\text{mM}$ . The quantum yield of the dye with free and bound micelles was calculated based on the fluorescence counts of protein and SDS at the first point of dilution following the same procedure (Eq 2.2). The variation in fluorescence profiles with respect to protein concentration is shown in Figure 2.5. As the protein concentration increases more binding sites are available for SDS micelles. With constant number of total SDS micelles ( $15\text{mM}$ ), the number of free micelles in the solution is reduced as the number of bound micelles increases (Table 2.4). Higher quantum yield of the dye with bound micelles compare to free micelles results in an increase in fluorescence at higher protein concentration. To evaluate the proposed fluorescence model (Eq 2.1) with different protein concentration, the fluorescence intensity at each protein concentration was calculated at  $15\text{mM}$  SDS(start point of

dilution). The results are in a good agreement with the experimental values as shown in Table 2.4.

Table 2.4: Comparison of the proposed fluorescence model with the experimental values at various BSA concentrations for the first dilution point(15mM) SDS. Values of  $N_{sds}$  and  $N_p$  were determined using the ratio of 1.4g SDS/ 1g protein.

BSA[mg/ml]	$N_{sds}$	$N_p$	Fl(calculated)	Fl(measured)	%error
0	$1.129 \times 10^{20}$	0	-	$1.10 \times 10^6$	-
0.005	$1.127 \times 10^{20}$	$1.827 \times 10^{17}$	$1.102 \times 10^6$	$1.12 \times 10^6$	1.6
0.01	$1.125 \times 10^{20}$	$3.653 \times 10^{17}$	$1.104 \times 10^6$	$1.15 \times 10^6$	4
0.05	$1.110 \times 10^{20}$	$1.827 \times 10^{18}$	$1.12 \times 10^6$	$1.16 \times 10^6$	3
0.5	$9.461 \times 10^{19}$	$1.827 \times 10^{19}$	$1.25 \times 10^6$	$1.33 \times 10^6$	6
1	$7.634 \times 10^{19}$	$3.653 \times 10^{19}$	-	$1.5 \times 10^6$	-

Figure 2.5 shows identical fluorescence profiles with 0.005mg/ml and 0.01mg/ml protein as protein free complex (SDS-dye). At these concentrations, the number of free micelles is three orders of magnitude higher than bound micelles as given in Table 2.4. Hence, the contribution of bound micelles to the overall fluorescence is negligible due to the low concentration of protein. This is evident by an almost invisible protein peak after eliminating the SDS contribution (Figure 2.5 inset).

It is important to note that with low protein concentration the protein peaks are shifted from 3mM to 4mM SDS as the point of micellar breakdown. This observation further emphasizes the significant contribution of free micelles at low protein concentrations. At higher concentration, a distinct protein peak is observed at 3mM SDS. Figure 2.5(inset) shows that the peak height is proportional to the protein concentration. Therefore, it can be concluded that with a single protein model with no variation in the dye quantum yield, the electropherograms can be used in quantification of sample protein. We assume that the overlapping curve of 0.5mg/ml and 1mg/ml samples at concentrations below 3mM SDS is due to the insufficient number

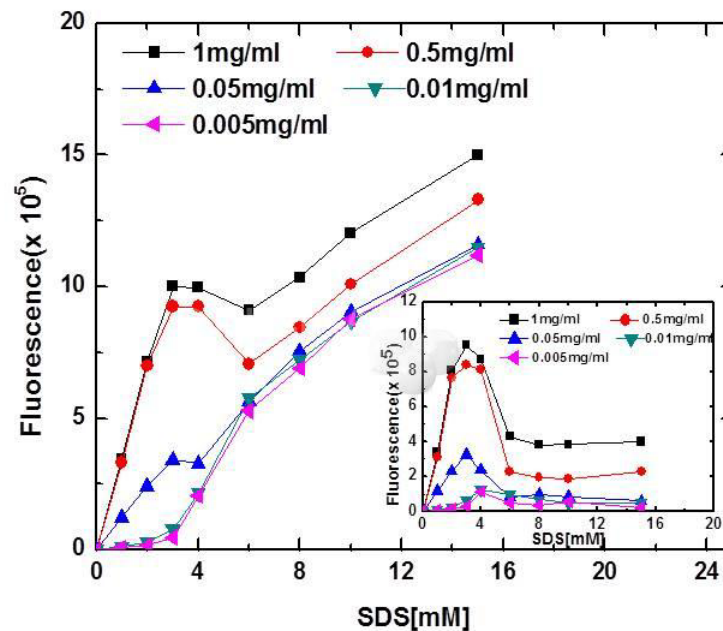


Figure 2.5: Effect of protein concentration on the dilution of SDS-BSA complex. The inset shows the fluorescence profile of the protein after subtracting the background SDS fluorescence. Conditions: 15mM SDS, 1x Tris-glycine buffer at 8.6 pH, 5x sypro orange dye, room temperature. Protein was denatured by heat(5min at 95°C) and betamercaptoethanol(0.2M).

of dye molecules.

## 2.8 Effect of cationic surfactant CTAB

The CMC of CTAB in Tris-Glycine buffer was estimated to be  $\sim 0.4$  mM following the same procedure for determination of CMC for SDS. CTAB concentrations above CMC were added to BSA-SDS complex, providing molar ratios (SDS/CTAB) from 7 to 30. Figure 2.6 shows the effect of CTAB addition on dilution of protein-SDS complex. The increase in fluorescence upon addition of CTAB can be explained by comparing the hydrophobicity of CTAB and SDS micelles. CTAB molecules with 16 carbons in the alkyl chain are more hydrophobic than SDS molecules with 12 carbons.

It is possible that the quantum yield of the dye is higher with more hydrophobic CTAB micelles, or with mixed SDS-CTAB micelles. As shown in Figure 2.6, the fluorescence increases with higher CTAB concentration, due to a larger number of micelles present. Protein peak heights remain approximately constant at 3mM SDS with 0.5 and 0.9mM CTAB, however the intensity is reduced by 27% and 54% with 2mM and 2.5mM CTAB respectively(Figure 2.6 inset). Moreover, the peak is shifted to 4mM SDS at these concentrations. Therefore, addition of CTAB with the purpose of surface modification in presence of SDS at mole fractions above 0.1 significantly affects the dynamic of protein-SDS complex in protein electrophoresis.

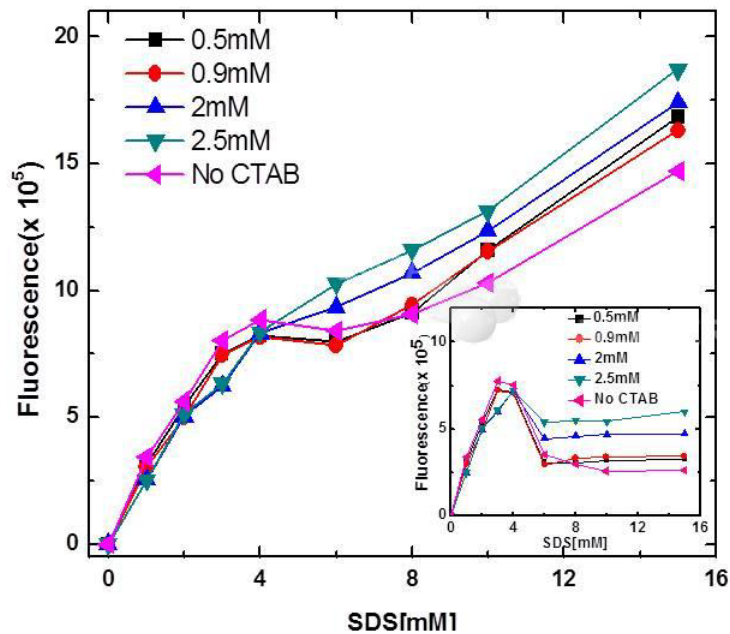


Figure 2.6: Effect of CTAB concentration on the dilution of SDS-BSA complex. The inset shows the fluorescence profile of the protein after subtracting the background SDS fluorescence. Conditions: 15mM SDS, 1x Tris-glycine buffer at 8.6 pH, 5x sypro orange dye, room temperature. Protein was denatured by heat(5min at 95°C) and betamercaptoethanol(0.2M).

## 2.9 Conclusions

We have investigated the effect of dilution of protein-SDS complexes as an essential step for on chip protein electrophoresis by utilizing Sypro orange dye as a fluorescent hydrophobic probe. The most important conclusion is that for protein analysis in a solution (gel-free), even though the binding stoichiometry of SDS to proteins is constant, and that the surfactant at concentrations above CMC makes proteins structurally similar, the overall fluorescence varies with different proteins. As a consequence, the fluorescence intensity of proteins with the same concentration is not equal. However, the quantification of protein based on the peak height can be achieved for a single protein where the quantum yield of the dye is constant. Moreover, the maximum peak height in electropherograms was observed at 3mM SDS, below the SDS CMC value. At this concentration only the SDS micelles bound to protein contribute to the overall fluorescence intensity. Therefore, this concentration can be considered as the optimum SDS concentration in protein electrophoresis. The dilution profile of protein-SDS complexes shows three distinct regions: SDS dominant region above 6mM SDS, breakdown region between 3mM-6mM SDS and the protein dominant region below 3mM SDS. In the SDS dominant region the contribution of SDS micelles to the overall fluorescence signature is more pronounced than bound micelles. The fluorescence in this region is a linear function of free micelles number density. In the breakdown region, micelles start to break to monomers. The released dye is taken by bound micelles with higher quantum yield compare to free micelles, resulting in a slight increase in the fluorescence intensity. Finally in the protein dominant region, with no free SDS

micelles, the contribution of bound micelles becomes significant. Based on the experimental results, we propose a fluorescence model for the interaction of dye with SDS and protein. In this model, the variation in fluorescence arises from the difference in the dye quantum yield with the micelles, assuming equal uptake of dye molecules with free and bound micelles. In a single protein model, quantification of protein concentration based on fluorescence intensities can be achieved with a constant dye quantum yield. This is evident by an increased in protein peak height with increasing concentration. Finally, addition of CTAB as a more hydrophobic surfactant compare to SDS at concentrations above CMC results in a shift in protein peak, where the mole fraction of CTAB was above 0.1. Lower concentrations of CTAB(0.5mM and 0.9mM) did not alter the dynamics of protein-SDS interactions. The presented results on the dilution of protein-surfactant complexes significantly contribute to the development of novel detection and separation techniques in microfluidics platforms, where quantification of protein can be achieved parallel to detection.

## Chapter 3

# Electrophoretic Detection of a Target Protein on a Microfluidic platform

### 3.1 Abstract

Conventional immunoblotting techniques are labor intensive, time consuming and rely on the elution of target protein after depletion. Here we describe a new method for detection and quantification of proteins, independent of washing and elution. In this method, the target protein is first captured by immunodepletion with antibody-coated microbeads. In the second step, both the supernatant after immunodepletion and the untreated protein sample are directly analyzed by microfluidic electrophoresis without further processing. Subsequently, the detection and quantification are performed by comparing the electropherograms of these two samples. This method was tested

using an *Escherichia coli* lysate with a FLAG-tagged protein and anti-FLAG magnetic beads. An incubation of as short as one min was sufficient for detectable depletion (66%) by microchip electrophoresis. Longer incubation (up to 60 min) resulted in more depletion of the target band (82%). Our results show that only 19% of the target is recovered after elution from the beads. By eliminating multiple wash and elution steps, our method is faster, less labor intensive, and highly reproducible. The target protein can still be easily identified even in the case of nonspecific binding at low concentrations. This work highlights the advantages of integrating immunodepletion techniques on a microfluidic platform.

## 3.2 Introduction

Separation and quantification of biomarkers are strong tools in biomedical research for a wide range of applications such as disease detection, toxicology assessment, and research diagnostics. Despite significant improvements in the field of separation and instrumentation, there is still an urgent need for fast and sensitive detection of low concentration biomarkers in complex biological fluids. Characterization of these analytes with a high level of sensitivity is challenging and requires new separation techniques. To this end, microfluidic devices have revolutionized the field of separation by providing, high throughput, rapid analysis, and small sample volume. However, the main challenge remains in detection of the analyte due to significant reduction in the volume (less number of target molecules). Among all the methods developed to improve detection sensitivity, the combination of microfluidics and immuno-affinity

techniques is the most promising. The use of antibodies against the target analyte (antigen) provides robust and highly specific isolation of the analyte, depending on the antibody quality. Combination of this technique with a microfluidic platform ensures sensitive detection of the analyte in miniaturized sample volume. Furthermore, an automated microfluidic platform with minimum preparation steps and the ability of analyzing various analytes simultaneously on a single compact microchip is highly advantageous in rapid point-of-care diagnostics. Among immuno-affinity methods, immunoprecipitation of proteins from the cell lysate is commonly used for the detection and analysis of target proteins. Surface modified microbeads, against the protein of interest, isolate the target from the lysate under native conditions. The protein is then eluted from the beads, separated by gel electrophoresis and analyzed by immunoblotting[36, 118]. Despite its high sensitivity (sub-nanogram range depending on the antibody used[51], immunoblotting is labor intensive and time consuming due to multiple manual steps. Moreover, the precise quantification of proteins is challenged by film or chromogenic detection[73]. Even though protein separation and immunoassays have been performed on a microchip[15, 58, 156, 56, 159] a simpler design with minimum manipulations is highly in demand. All immunoprecipitation techniques using microbeads involve washing and elution steps, which significantly add to analysis time[36, 118, 108, 147, 3]. We propose a new protein detection and quantification method independent of washing or elution as shown in Figure 3.1. Our method utilizes an immunodepletion step followed by microfluidic electrophoretic separation. First, immunodepletion is performed to capture the target protein using antibody coated microbeads. Following this step, the supernatant is loaded on a mi-

crochip for electrophoretic separation. Simultaneously, the untreated protein sample is loaded on the same microfluidic chip. The two electropherograms are then compared for quantification and detection of the target protein. Microfluidic separation allows for fast quantification of the results (less than an hour) which is performed parallel to detection. The result of this technique is compared with traditional (Western) blotting as well as elution of the target from the beads.

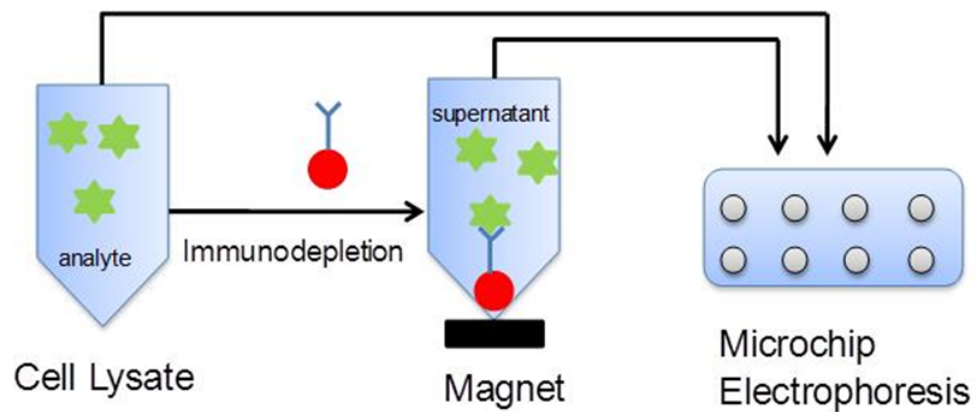


Figure 3.1: Schematic of the proposed method. The target is first isolated by immunodepletion with magnetic beads coated against the target. Then after collecting the beads magnetically, the supernatant is analyzed on a microfluidic electrophoresis chip.

### 3.3 Materials and Methods

#### 3.3.1 Sample preparation

*E. coli* bacteria (BL21DE2) were transfected with the pNO-TAT vector harboring the C-terminal 236 amino acids of the DEAD-box helicase Vasa[48]. Linked in-frame

at the C-terminal most amino acid was a FLAG-tag, an octapeptide sequence (N-Asp-Tyr-Lys-Asp-Asp-Asp-Asp-Lys-C) for which a monoclonal antibody is available either freely soluble, or linked to magnetic beads(M8823; Sigma-Aldrich). Cells were cultured at 37°C for 8-10 hours and induced with 10mM IPTG for 2 hours. After incubation, cells were lysed by addition of lysozyme (10ug/ml; 10 minutes at room temperature) and repeatedly freeze-thawed between -80°C and 37°C. The cellular lysate was centrifuged at 10,000g for 20minutes and the supernatant was collected and stored at -20°C.

For immunoblotting, 100µg, 70µg, and 35µg in lanes 1, 2, and 3 respectively (Figure 3.2) of the cellular lysate was first resolved by 4-10% polyacrylamide gel electrophoresis (PAGE).

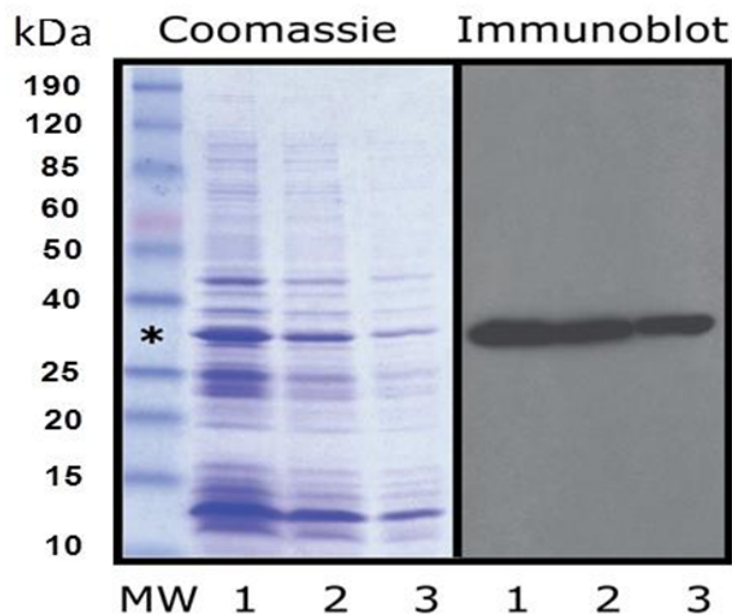


Figure 3.2: Immunoblot using a conventional Western method. Lanes 1, 2 and 3 correspond to 100, 70 and 35 micrograms of protein loaded per lane that was then stained with Coomassie or labeled by immunoblotting with anti-FLAG antibodies. The asterisk indicates the position of the FLAG-tagged protein species.

The amounts of protein used, allows for a broad range of mass ( $\sim 3$ -fold), with reproducibility within dilution. Once resolved, proteins were transferred to nitrocellulose and processed for immuno-labeling as described in [48, 51, 133]. Anti-FLAG antibody M2 (Sigma-Aldrich) was used at 1/5000 dilution in blot for 4 hrs at room temperature, and the blot was then washed several times for 5 minutes each with excess blot. A rabbit anti-mouse secondary antibody conjugated to horseradish peroxidase (Sigma-Aldrich) was diluted 1/5000 and added to the washed blot. After 4 hours incubation at room temperature, the blot was washed as described for the primary antibody and the secondary antibody was detected with an ECL kit (Pierce, Thermo Fisher Scientific) on film following the protocol.

### 3.3.2 Control experiment

Our method was first tested using a single analyte system containing a biotinylated antibody (mouse anti-human troponin T, cTnT; US Biological) and streptavidin magnetic beads (Dynabeads M-270; Invitrogen). The antibody was diluted to  $0.2 \mu\text{g}/\mu\text{l}$  with phosphate buffered saline (PBS).  $10 \mu\text{l}$  of the magnetic beads was washed with PBS buffer twice and incubated with  $5 \mu\text{l}$  of the diluted antibody at room temperature. The required bead volume was calculated based on the binding capacity of the beads ( $10 \mu\text{g}$  antibody per mg of beads). Samples at 1, 5, and 10 minutes incubation time were prepared by mixing on a revolver (Labnet International) except for one minute incubation sample which was manually mixed by pipetting. After each incubation time, the beads were collected by magnetic adsorption and the supernatant

was taken for microchip electrophoresis.

### 3.4 FLAG protein detection in a bacterial lysate

A cellular lysate concentration of  $7.1\mu\text{g}/\mu\text{l}$  was diluted with PBS buffer (0.02M phosphate, 0.15M NaCl) to  $1.42\mu\text{g}/\mu\text{l}$ . The dilution was chosen to accommodate the signal level below the saturation limits of the detector.  $20\mu\text{l}$  (5 times more than the bead capacity, to ensure complete binding) of the diluted lysate was incubated with  $10\mu\text{l}$  of anti-FLAG M2 magnetic beads with binding capacity of 0.6 mg of FLAG protein per 1 ml of packed beads. In order to determine minimum incubation time required for depletion, the beads were incubated at 1, 5, 10 and 60 minutes with the lysate at room temperature. The diffusion time for FLAG proteins was approximately estimated to be  $t = l^2/2D$ . where  $l$  is the average distance between beads, and  $D$  is the diffusivity of FLAG protein. Assuming that  $l$  is  $600\mu\text{m}$ , and  $D$  is  $300\mu\text{m}^2/\text{s}$ ,  $t$  was estimated to be  $\sim 600$  s. Here, we assumed that the capture of the target molecules by the surface is faster than the diffusion time[107]. This reference also reported detection of Flag system in microfluidic affinity columns. The experimental data showed high binding rate. Their analysis showed the mass transport limited regime for almost all the experiments. Hence, the incubation times were varied from low (1 minute) to high diffusion times (60 minutes). Additionally, the selected time interval allows for comparing a broad range of conditions (60-fold) at room temperature for immunoreactivity. The beads were kept in suspension by placing the samples on a revolver. The supernatant was collected following the same procedure as stated above. Elu-

tion carried out on the 60 minutes incubated beads with the lysate. For eluting the target, beads were suspended in  $20\mu\text{l}$  sample buffer plus  $1\mu\text{l}$  of 2-mercaptoethanol after washing with PBS buffer. Following this step, the beads were heated at  $95^\circ\text{C}$  for 5 minutes, and the supernatant was taken for analysis. All samples tested here, with the exception of the elution sample, are supernatants following bead incubation. For microchip electrophoresis, samples were prepared according to Agilent kit and analyzed three times by 2100 Bioanalyzer. The control experiment performed on a biotinylated antibody, as a proof of concept, demonstrates the high efficiency of this method for depleting the target analyte. The amount of adsorption is calculated by comparing the target peak area of each sample with the untreated antibody (Figure 3.3).

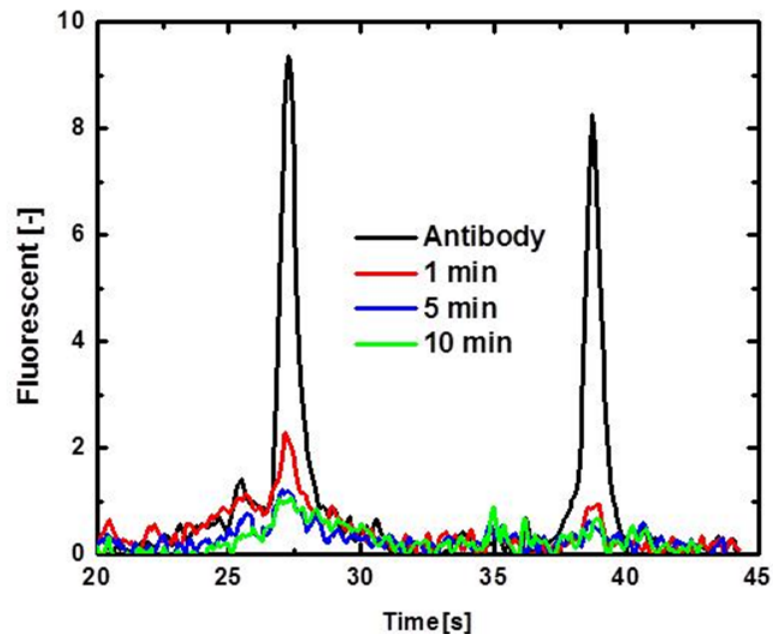


Figure 3.3: Control experiment. Detection of biotinylated anti-human cTnT antibody ( $0.2\mu\text{g}/\mu\text{l}$ ) at three incubation times with streptavidin coated magnetic beads.

One minute incubation results in 95% reduction of the target band. At 5 minutes

and above, 99% depletion was observed. After establishing the high efficiency of our method, the performance of this technique was tested in a more complex system of bacteria lysate (as used in blotting experiment). Cells expressing Vasa-FLAG protein have several major protein bands, including one at approximately 36 kDa, which is the predicted mobility of the DNA-encoded construct. By performing the traditional (Western) immunoblotting, it was verified that the 36kDa band is the FLAG-tag protein (Figure 3.2: lane 1-3 under immune-blot). An alternative approach for this assay is to use a protein chip following elution of proteins from beads that had been pre-incubated with the lysate. This approach was recently demonstrated[147] but still required several hours to be accomplished with multiple manual steps. In the case of the queried bacterial bands here within whole cell lysate, a pre-absorption approach might be sufficient to rapidly detect the band of interest using minimum reagents as demonstrated in our method. Samples were analyzed on an electrophoresis gel. Figure 3.4 (lanes 2-5) clearly shows the depletion of two bands at 12.4 kDa and 36.3 kDa for four incubation times. In comparing the intensities of the two bands in lanes 2-5 with the lysate, the target band is detected by the significant depletion of the 36.3 kDa band. The presence of the 36.3 kDa band in the elution sample (lane 6) not only confirms the presence of the target, but also the effective adsorption of the FLAG proteins on the beads. Even at one minute incubation, a significant depletion of the target protein is clearly observed. This suggests that the time scales for diffusion and reaction for transport and adsorption of FLAG protein were in the range of minutes.

For detection and quantification of the depleted FLAG protein the electropherograms of lysate, 1 and 60 minutes samples are compared in Figure 3.5a. Even though

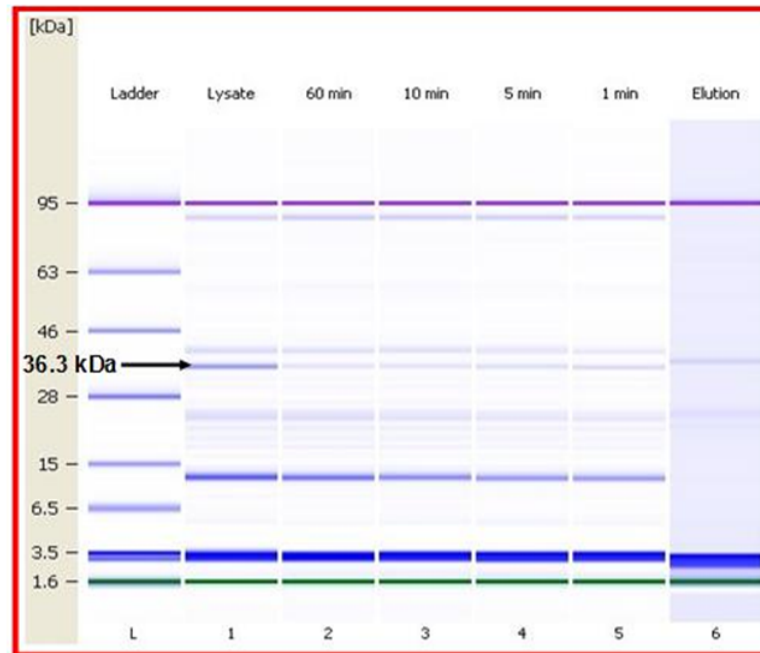


Figure 3.4: Agilent (protein 80) pseudo gel of lysate, elution and incubated samples. All samples, except the elution, are supernatant after incubation with anti-FLAG beads.

one minute incubation is sufficient for the detection of target band on the gel (Figure 3.4) depletion continues at longer incubation times. However, the rate of depletion decreases after 10 minutes of incubation time (embedded graph in Figure 3.5a). This is evident as rate of diffusion transport decreases with decrease in concentration gradient between the bulk and the surface. In order to compare our method with the elution technique, the electropherograms of supernatant and eluted protein after 60 minutes incubation are compared in Figure 3.5b. The presence of a distinct peak at 36.3 kDa, overlaying the 60 minutes target peak, confirms the eluted protein as the FLAG protein.

Quantification of depleted and eluted FLAG protein was performed using the peak

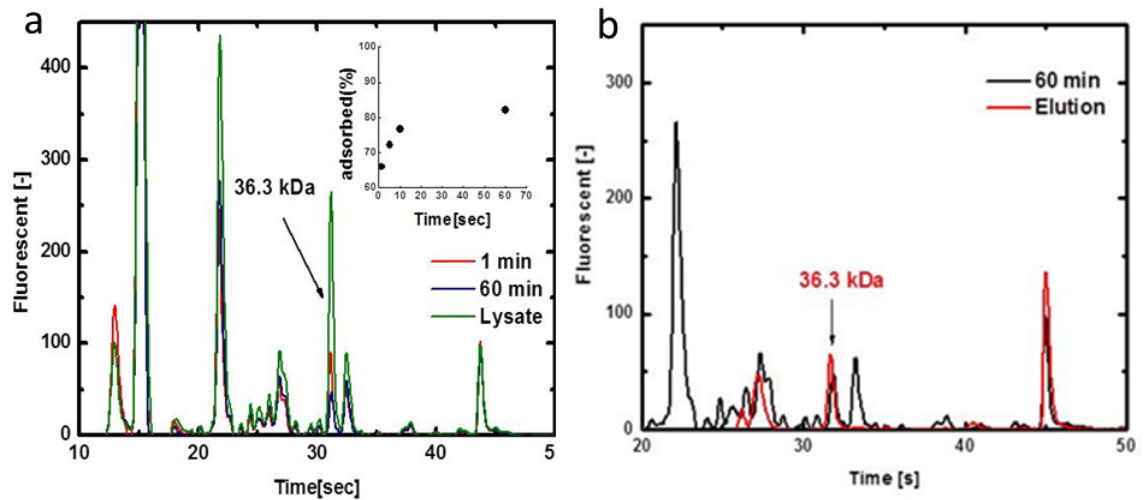


Figure 3.5: a) Detection of FLAG protein, comparison of two incubation times in depleting the target ( $1.42\mu\text{g}/\mu\text{l}$ ). The adsorption kinetic of FLAG protein is shown in the inset. b) Comparison of eluted and incubated samples after 60 minutes. The elution sample is the eluted FLAG protein from the beads after 60 minutes incubation. The arrow shows the target peak.

area (including the non-specific adsorption) and is listed in Table 3.1.

$$\%adsorption = \frac{A_l - A_s}{A_l} \times 100 \quad (3.1)$$

where  $A_l$  and  $A_s$  are the target peak area of lysate and sample respectively.

Table 3.1: Quantification of the immunodepleted FLAG protein. The listed values are the average of three independent experiments( mean  $\pm$  standard deviation).

Sample	12.4kDa peak area	%adsorbed	36.3kDa peak area	%adsorbed	%released
lysate	$244.1 \pm 4.8$	-	$36.5 \pm 1.2$	-	-
1min	$133 \pm 6.8$	45.6	$29.8 \pm 2.1$	66.1	-
5min	$128.3 \pm 4.2$	47.5	$25 \pm 1.3$	72.3	-
10min	$146 \pm 0.6$	40.3	$19.2 \pm 1.5$	76.8	-
60min	$147.6 \pm 3.4$	39.6	$20.7 \pm 5.1$	82.2	-
elution	-	-	-	80.8	19.2

Table 3.1 (column 5) shows more than 66% adsorption of FLAG protein in the first

minute of incubation and that the adsorption of FLAG protein gradually increases, from 66% to 82% after 59 minutes of incubation. The non-specific adsorption of 12.4 kDa band is also shown (column 3) with approximately constant adsorption (43%) in all of the samples. Since the 12.4 kDa peak appears far away from the 36.3 kDa FLAG protein peak, the non-specific binding does not affect the quantification of the target protein. However, the sensitivity of the assay would be limited in cases of interference of the target peak with other protein peaks in the sample. It is important to note that peak interference is a challenge in all the current methods available. More investigations are needed to improve resolution of the peaks by choosing different gel properties[98], or changing the script of the system. Release of only 19% of the FLAG protein from the beads shows that even though the target can be detected after elution, and further improvements are possible by optimizing the elution process, an accurate quantification is not possible by this method. Finally, the dynamic detection range of the target ( $\sim 50$  kDa FLAG) was determined in a protein complex at different concentrations. The complex sample consists of four other proteins, each at  $200 \text{ ng}/\mu\text{l}$ . The target electropherogram peak is shown in Figure 3.6 for one of the sample runs. All the peaks can be easily identified arriving at 35.5 seconds. As shown in Figure 3.6(inset), the fluorescent intensity is linearly proportional to the target concentration.

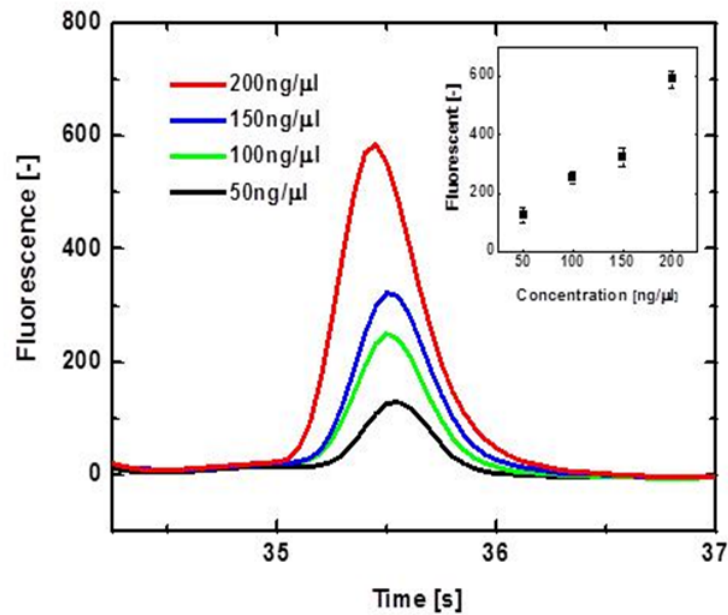


Figure 3.6: Detection of FLAG protein in a target-free complex sample. The concentration of each non-FLAG protein is constant at  $200\text{ng}/\mu\text{l}$ . The inset shows the linear detection range of the target with respect to concentration.

### 3.5 FLAG protein detection in a target-free protein complex

To further evaluate the dynamic detection range of the target, various concentrations of a FLAG protein (50kDa) was mixed with four other proteins: lysozyme, soybean trypsin inhibitor, bovine serum albumin (BSA) and ovalbumin, each at  $200\mu\text{g}/\mu\text{l}$  concentration in PBS buffer. The target concentration was varied from  $50\text{ng}/\mu\text{l}$  to  $200\text{ng}/\mu\text{l}$ , providing a target/complex ratio of 0.06 to 0.25. The complex sample was incubated with anti-FLAG magnetic beads for 10 minutes at room temperature and the supernatant was analyzed by microchip electrophoresis. The effect of non-

specific binding of other proteins on the detection of the target was also investigated by electropherogram peak analysis. These electropherograms are shown in Figure 3.7.

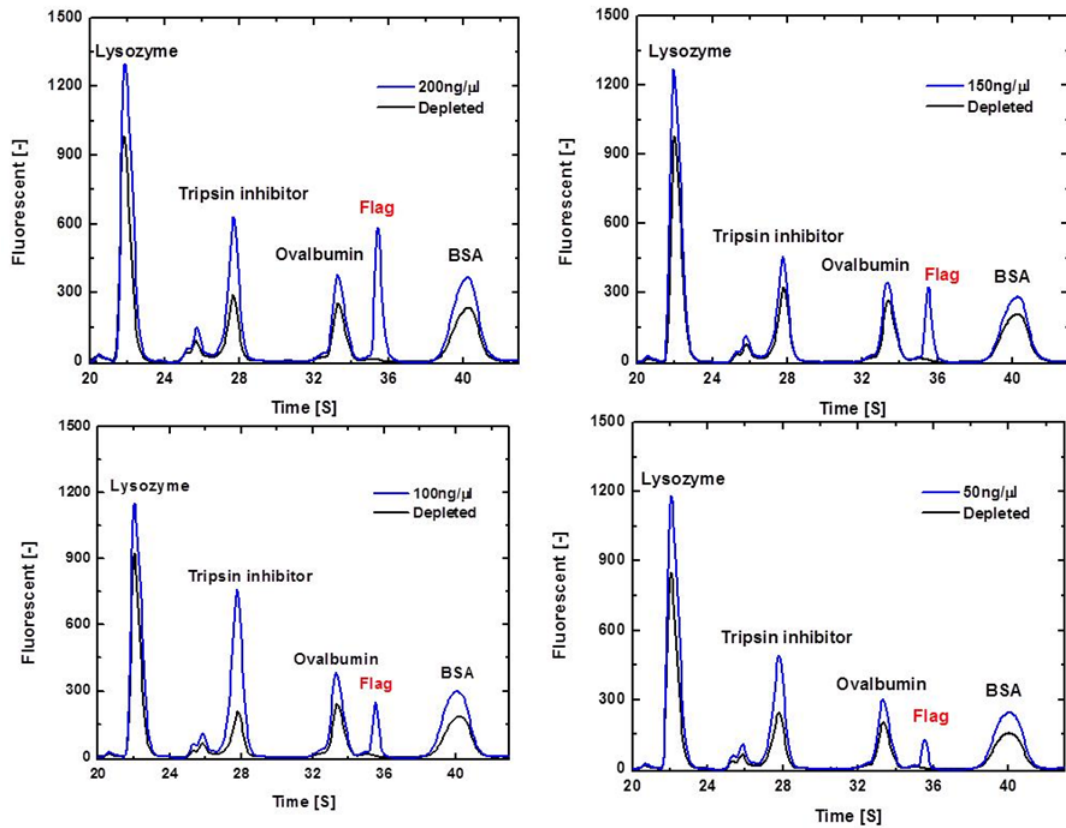


Figure 3.7: Detection of depleted target protein in a complex sample. The concentration of FLAG protein ( 50kDa) is varied from 50ng/ $\mu$ l to 200ng/ $\mu$ l, while keeping the non-FLAG protein concentration each at 200ng/ $\mu$ l.

Figure 3.8 shows the percentage adsorption of each protein in the complex sample. It is important to note that, even though the most significant depletion (95%-100%) was observed in the target band, other proteins in the complex were also depleted (less than 40%) through non-specific adsorption. Our results suggest that even at very low concentration of target (50ng/ $\mu$ l) and in case of non-specific binding of other sample components, the rapid and high specific detection of the target can be achieved.

Speed, simplicity and sensitivity are key factors in designing a diagnostic device.

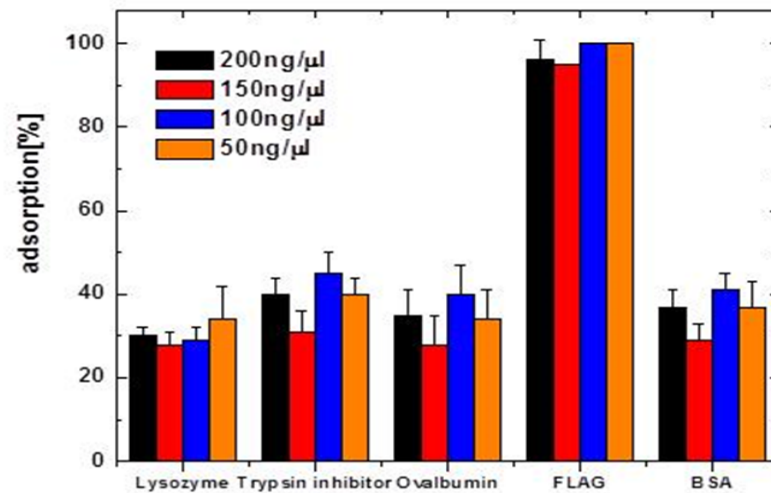


Figure 3.8: Depletion of FLAG protein in a protein complex at different concentrations. The concentration of each non-FLAG protein was kept constant at  $200\text{ng}/\mu\text{l}$  while changing the target concentration. Samples were incubated with anti-FLAG magnetic beads for 10 minutes. Error bars are the standard deviation obtained from three independent studies.

Whether this device is used in the research laboratory or the clinical diagnostic lab, the combination of these criteria ultimately determines its application. Our proposed method is optimally suited in low complexity protein mixtures where each of the bands may be seen individually, or in a whole cell lysate in which some of the bands of interest are in significant relative abundance. Under these conditions, our detection technique is ideal for rapid verification of a target protein (minutes). The efficiency of this method is minimized where the concentration of the target protein is significantly less than other proteins in the mixture, such as HSA (Human serum albumin) in the serum. Here the depleted band would not be amply detected; although a decrease in multiplex heights are suggestive of target protein presence. In more complex systems with multiple peaks, the detection performance can be optimized using different gel

matrices, antibodies, sample buffers and bead properties. In addition, the incubation time and temperature can also be optimized for maximum efficiency. Considering the binding capacity of the beads (0.6mg FLAG protein per 1 ml of beads),  $10\mu\text{l}$  of beads used in the experiments results in binding of  $6\mu\text{g}$  protein to the beads. For the above experiments, the beads were incubated with lysate at almost 5 times the binding capacity ( $20\mu\text{l}$  lysate= $28.4\mu\text{g}$  protein), to ensure maximum adsorption. However, even with the excess amount of protein (more than bead capacity), the specific binding affinity of the beads provides sufficient depletion of the target for quantification purposes. The sensitivity of this method depends on the detection limit of the microchip sizing assay which is  $\sim 50\text{ng}/\mu\text{l}$  before loading on the gel.

### 3.6 Conclusions

By eliminating multiple wash and elution steps, our modified immunodepletion method not only minimizes the analysis time, but also provides a robust and more reliable quantification platform. Even in cases of non-specific binding and at low concentrations, the target protein is significantly depleted and can be identified. Although, the target can be detected by the current bead based immunodepletion techniques, the quantification is limited due to the low recovery of the target after elution from the beads. We emphasize that this new technology is not dependent on an antibody. Lectin, or other specific affinity methods are equally valid. The binding matrix could be a lectin used to study various glycosylated proteins, interacting proteins for which they are already available and thereby selectively adsorb even isoforms of protein

family members, small molecules attached to the beads to interrogate the starting protein mixture, and even cis-elements of a DNA promoter region. Further, the target can be detected in any population of protein mixture, including cellular lysate, serum, or body fluids. The only requirement of this system is that they be soluble during the depletion procedure.

## Chapter 4

# Synergistic action of Chitosan and low voltage pulsed electric field in bacterial inhibition

### 4.1 Abstract

Techniques to inhibit gram-negative bacteria such as Shiga toxin-producing *Escherichia coli* are valuable as the prevalence of large-scale industrial food preparation increases the likelihood of contamination. Chitosan, the deacetylated derivative of chitin, has been demonstrated to inhibit bacteria growth in acidic environments, but is significantly less effective in preventing bacteria grown at  $\text{pH} > 7.0$ . Pulsed electric fields, constituting another method of bacteria inhibition, are difficult to generate at sufficient strength due to the high electric potentials required. This study utilizes adsorption of particulate chitosan in a very low electric field for an increased inhibition of

gram-negative bacteria in neutral or alkaline pH conditions. Chitosan microparticles are demonstrated to flocculate *E. coli*, inhibit growth, and exhibit increased efficacy when combined with a low voltage electric field applied over 2-min intervals. Using sustained pulses of approximately 100 V/cm, it is demonstrated that bacteria viability is reduced by several orders of magnitude. The degree of bacterial inhibition is increased when chitosan microparticles are introduced to the system prior to imposing a small electric field.

## 4.2 Introduction

Since identification as a pathogen in 1982, numerous outbreaks of Shiga toxin-producing *Escherichia coli* (STEC), including the enterohemorrhagic strain *E. coli* 0157:H7, have involved conditions including diarrhea and hemolytic uremic syndrome. Undercooked beef is a common source of STEC infections, but produce and water have also been contaminated[101]. Techniques to inhibit gram-negative bacteria such as pathogenic *Escherichia coli* are valuable as the prevalence of large-scale industrial food preparation increases the likelihood of contamination. Chitosan (CS), an abundant naturally occurring biopolymer, is widely recognized as exhibiting antimicrobial properties in acidic conditions[78, 25, 76]. Among other antibacterial agents, chitosan is biocompatible (non-toxic) and exhibits a higher antibacterial activity[78]. Two mechanisms for inhibition activity of chitosan have been proposed. In the first mechanism, membrane permeability is affected by the interaction between the positively charged chitosan molecules and anions on the cell membrane[135, 57, 77, 110]. The second mechanism

involves RNA inhibition by binding of chitosan to DNA[57, 77, 110, 25]. In addition to adsorption to the cell membrane, it is believed that chitosan affects the hydrophilicity and charge density of the outer membrane[26]. Chitosan has also been investigated as an antimicrobial agent for a number of different applications, including wound dressings and preservatives[111, 14, 68]. Studies have also probed the efficiency of chitosan in drug delivery and as a flocculant[158, 50]. Although the antimicrobial benefits of chitosan have been employed in multiple applications, widespread adoption of chitosan and its derivatives depends on overcoming difficulties associated with its use. Studies that investigate the antibacterial effect of chitosan on various bacteria species utilize acidic test environments, with pH ranges of 5.5-7.0[78, 25, 76]. It is commonly accepted that chitosan is not effective as an antimicrobial additive at neutral and alkaline pH, due to its loss of positive charge and aqueous solubility in such environments. CS microparticles(CSMP) are investigated as a potential method to bypass the low pH required to use conventional molecular chitosan in solution as a microbial inhibitor. The lipid bilayer membrane of the cell has a unique conductance which facilitates the ion exchange. External stimulants, such as organic compounds and detergent as well as transmembrane electric field can modify the membrane ion composition and disturb the permeability of the membrane[27, 132]. Depending on the intensity of the electric field, electroporation occurs either in the bilayer or in the protein channels inside the membrane. Electric fields of 1000 V/cm and higher changes the orientation of lipids and creates hydrophilic pores in the membrane, while lower electric potential targets the protein channels[136]. The use of high intensity localized electric fields to open membrane pores in bacteria is commonly used to

transform bacteria[1] and to open voltage-gated protein channels and create pores in eukaryotic cells. Short, high-voltage pulses on the nanosecond time scale create electric fields that effectively inactivate large bacteria populations when fields greater than approximately 16 kV/cm are employed[109], although much smaller fields on the order of 1 kV/cm were reported in microfluidic environments[142]. Similar to the use of chitosan, irreversible electric field action is an effective bacteria inhibition method that is limited in application. The limiting factor in electro-lysis adoption is the very high electric field required, which are difficult to generate and apply to sufficiently large geometries. Electric field actions and chitosan treatments both utilize membrane permeation to prevent microbial reproduction[57, 77, 142]. Synergistic use of natural antimicrobials and pulsed electric fields has been attempted to inhibit pathogenic bacteria[89]. These treatments utilize a relatively short treatment time in which the sample was exposed to a number of pulses on the micro to nanosecond scale. The effect of incorporating sub-lethal electric voltage as opposed to high intensity pulsed electric field is currently unknown. It is therefore of interest to incorporate sub-lethal electric field with a natural treatment to increase the porosity and inhibit bacteria by altering pores in both the outer and inner membranes. Non-thermal methods of bacteria inhibition such as pulsed electric fields, ultrasonication, high hydrostatic pressure, ionizing radiation and chemical preservatives have been studied and the current understanding is that the methods can be used most effectively in combination, according to the concept of hurdle technologies[116, 89, 82]. A synergistic combination of chitosan microspheres and pulsed electric fields (PEF) is expected to produce effective antimicrobial action at gentle processing conditions.

By introducing CSMP, an immediate flocculation event will occur, creating numerous large microparticle-bacteria aggregates where the bacteria are in direct contact with chitosan[61, 128, 74, 112]. Bacteria locked in the aggregate are affected by the chitosan and are hypothesized to be more susceptible to subsequent pulsed electric field treatments. Potential mechanisms of enhanced susceptibility include destabilization of the outer membrane due to disruption of counterions by chitosan[57] or enhancement of local electric field gradients adjacent to the cell membrane[114]. Due to the difficulties in applying existing technologies in isolation or delivering alternative simple and effective microbial inhibition methods, it is necessary to develop superior, synergistic techniques for inactivating bacteria. An effective, simple combination technology for bacteria inhibition allows for control of pathogenic bacteria at multiple phases of production preceding consumption. Therefore, overcoming the limitations of current antimicrobial techniques is a vital step in improving future health and safety for consumers of products that are at risk of bacterial contamination.

## **4.3 Materials and Methods**

### **4.3.1 Materials**

Low molecular weight chitosan extracted from crab shells and sodium tripolyphosphate (TPP) were both purchased from Sigma-Aldrich (St. Louis, MO, USA). The chitosan had a deacetylation fraction of 90.85% and molecular weight range of 50190 kDa (viscosity 185 cP for a concentration of 1% w/w in 1% w/w acetic acid solution;

all data provided by supplier). NEB turbo competent *E. coli* (high efficiency) was obtained from New England Biolabs Inc. (NEB # C2984I) and transformed with the supplied pUC19 plasmid. Carbenicillin, LuriaBertani broth, and phosphate-buffered saline (PBS) were also obtained from Sigma-Aldrich. Electric field cuvettes with a 1-mm electrode gap were purchased from Sigma- Aldrich. Leads were adhered to the cuvette using nickel paint and applied alternating current (AC) potentials using a function generator (BK Precision 4078, CA) for the electric field experiments.

### **4.3.2 Preparation of chitosan microparticles(CSMP)**

Chitosan microparticles(CSMP) were prepared using ionic gelation interactions between chitosan(low molecular weight 50 to 190kDa and sodium tripolyphosphate (TPP) under mild, room-temperature conditions[110]. The simple ionic gelation procedure bypasses the need for detailed chemical synthesis. The mass ratio of chitosan/TPP was always kept at 5:1. Chitosan was dissolved in an acetic acid aqueous solution at 4.0 mg/ml. The acetic acid concentration was 1.75 times higher than the chitosan concentrations. TPP was dissolved in deionized water at the same concentration as for the chitosan solutions. Then, 1.0 ml of the TPP solution was added drop wise to 5.0 ml of the chitosan solution during continuous stirring on a magnetic stir plate. The mixture was stirred for an additional 30 minutes, and the suspension was equilibrated overnight. The particles were centrifuged at 49,410 g for 30 minutes. The resultant wet pellet was weighed and then subsequently washed several times and redispersed in deionized water by probe sonication for approximately 30 seconds.

The mass of the wet pellet was measured in order to approximate the concentration of the suspension, which was determined to be approximately 1.6 mg/ml (dry), based on measurements of the dry weight of one batch of particles made from the 4.0 mg/ml chitosan and TPP solutions.

### **4.3.3 Characterization of CSMP**

The particle size distribution and zeta potential of the chitosan and chitosan-coated alginate particles were characterized using the Zetasizer Nano-ZS. The particle suspension was freshly synthesized and each of the samples was analyzed in triplicate. The size readings were measured for 1000 seconds, and each zeta potential reading was 100 runs long. Both measurements were performed in aqueous environments at approximately pH 6.85. CSMP were synthesized from the solutions containing 4.0 mg/ml of chitosan and TPP yielded a highly positive zeta potential of  $51.1 \pm 2.2$  mV with the average diameter of  $380 \pm 57$  nm.

### **4.3.4 Bacteria culture and inhibition assay**

*E. coli* derived from BL21(DE3) expressing the mCherry fluorescent protein were cultured overnight in 2 ml of Luria-Bertani broth containing  $100\mu\text{g}/\text{ml}$  ampicillin or carbenicillin in polystyrene culture tubes. Cells were agitated using an Innova 4080 Incubator Shaker at 37C at 250 rpm. Furthermore, the cells were grown to an initial optical density at 600 nm (OD600) of approximately 0.1 ( $\sim 15.7 \times 10^7$  cells/ml) as measured on a NanoDrop ND-1000 spectrophotometer. The cells were centrifuged

at 20,000 g for 2 minutes, and then resuspended in phosphate buffered saline (PBS) (pH 7.4) according to the desired optical density values. Freshly cultured cells were centrifuged at 14,000 g and resuspended in PBS. For experiments investigating the combined effect of CSMP and electroporation, cells were tuned to an optical density (OD<sub>600</sub>) of approximately 0.1. *Escherichia coli* cells were first introduced to CSMP gently pipetted to ensure a uniform distribution. The final suspension was composed of 100  $\mu$ l bacteria suspension and 20  $\mu$ l CSMP suspension. The mixture contained 0.267 mg/ml CSMP(dry concentration). 100  $\mu$ l of the resulting suspension was placed in an electroporation cuvette. The exposed electrodes were placed under the desired AC voltage at a frequency of 60 Hz for 2 minutes in an electro-cuvette with 1 mm electrode gap. After washing with PBS, the cells were cultured onto agar plates and incubated overnight at 37 C. The colonies were counted to estimate viable cells. For experiments investigating solely the effect of CSMP, cells were suspended to an OD<sub>600</sub> of approximately 0.3. Note that OD<sub>600</sub> was adjusted according to optimal conditions of different lysis experiments. 60  $\mu$ l of bacteria were then pipetted with 60  $\mu$ l of particles at different concentrations. The final suspension contained between 0.8 and 3.2 mg/ml CSMP(dry concentration) and approximately  $55.7 \times 10^7$  cells/ml bacteria. Control experiments utilized distilled water in the place of microspheres.

## 4.4 E. coli inhibition: Effect of CSMP concentration

The effect of CSMP without electroporation for inhibiting bacteria at neutral pH was investigated. Colony forming (units/ml) (Figure 4.1) were used to examine the ability of CSMP to inhibit the growth of *E. coli*. These values indicate particularly strong inhibition when large numbers of cells are inactivated. The serial plate dilution method allows rapid accurate comparison of different treatments, even if they are able to inhibit the vast majority of the *E. coli* present.

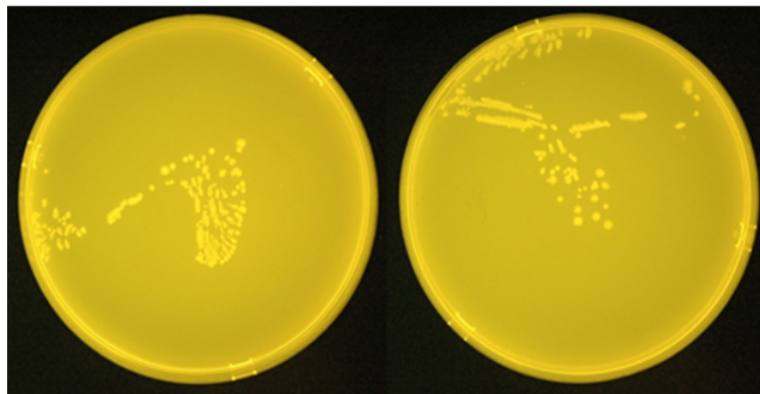


Figure 4.1: Colony forming units formed following overnight incubation after subsequent treatment with deionized water or CSMP. The left pane illustrates a representative result obtained after treating cells with deionized water only; the right pane shows cells that grew following introduction of CSMP at a concentration of 1.6 mg/ml suspended in deionized water. Both panes were obtained using dilutions of 1:100,000.

The multiple colonies were counted to estimate viable cells. As shown in Figure 4.2, there was about 28% reduction of viable cells due to incubation with 0.8 mg/ml microspheres. Similarly, 41% difference between the distilled water control and 3.2

mg/ml CSMP was observed. Although inhibition occurred, it was not complete, due to the suboptimal, neutral pH of the environment. The bacteria, following aggregation, were able to retain significant if not total viability. It is likely that the minimally charged chitosan was not completely effective in compromising both inner and outer membranes of the gram-negative bacteria.

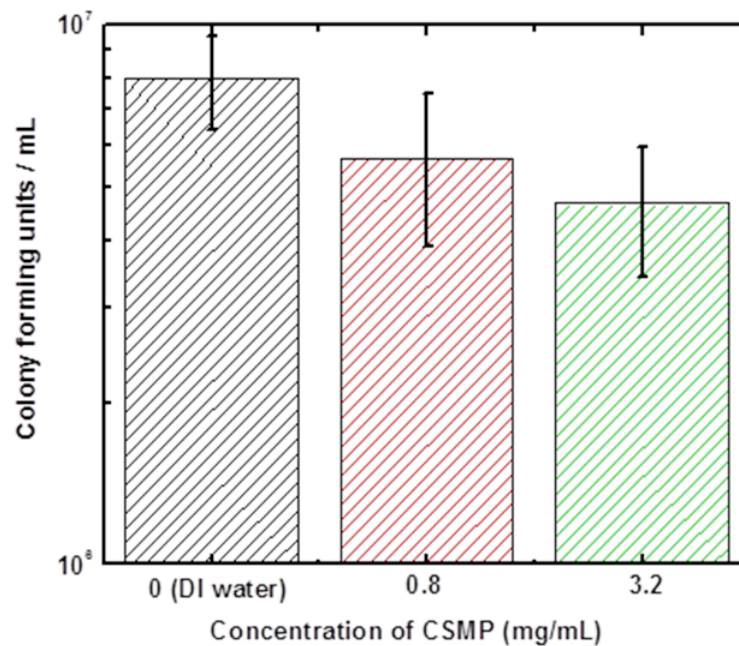


Figure 4.2: Growth of cells following treatment with different concentrations of CSMP. DI represents deionized water and values of 0.8 and 3.2 represent the concentration of CSMP in mg/ml prior to serial dilution.

In a study by Helander et al.[57], a minimum concentration (250 ppm) of molecular chitosan in solution was required to observe reproducible increases in outer membrane permeability of *E. coli*, while higher concentrations are needed for lethality (2000-5000 ppm or higher). In the work of Fernandes et al.[38], solutions of molecular chitosan with a minimum concentration of 5.0 mg/ml were needed for lethal action on an *E. coli* population inoculated at  $10^5$  CFU/ml. Similarly, in this study, we observe chitosan

to sensitize the bacterial membrane to an additional treatment (electroporation) at concentrations below bactericidal levels (0.8 to 3.2 mg/ml)

## 4.5 *E. coli* inhibition: combination of CSMP and electric field

Following the serial dilution experiments of CSMP, the synergistic effects of small sustained electric fields and chitosan were investigated using a similar method. Deionized water was used in place of chitosan to explore the effects of small electric fields that alternated at 60Hz for a period of two minutes. Fields of 50 V/cm and 100 V/cm were investigated. Two representative plates used in the cell counts are shown in Figure 4.3. When comparing the acquired plate images, it is important to note the dilution used to create each plate. All plates in these experiments were countable. Plates created using less diluted bacteria samples for deionized water controls, for example, consistently grow as a lawn with indistinct colonies. The multiple plates were counted to estimate viable cells. As shown in Figure 4.4, the electric field effect of 50 V/cm inhibited more bacteria (37% colony survival), compared to chitosan alone (58% colony survival). In the confined geometry of the cuvette, an electric field of 100 V/cm significantly reduced the colony survival rate. Over 98% of the bacteria were removed, a reduction in viability that almost spanned two orders of magnitude. Given the result that 100 V/cm substantially promoted bacteria inhibition, it was desirable to increase the effectiveness of this treatment using CSMP. A combined

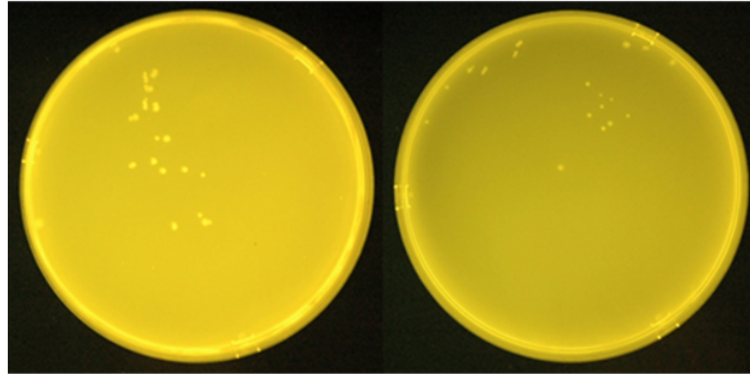


Figure 4.3: Colony forming units formed following overnight incubation after subsequent treatment with deionized water or CSMP at 100V/cm. The left pane illustrates a representative result obtained after treating cells with deionized water only with dilution factor of 1:100,000, the right pane shows survived colonies after chitosan treatment with dilution factor of 1:1000.

treatment was performed at low chitosan concentration (0.267 mg/ml during electric field treatment). This concentration was sufficient, however, to increase cell inhibition by another order of magnitude (over 99.9% of bacteria removed), a significant difference from the cell inhibition experienced using 100 V/cm electric field alone. This notable increase in cell death strongly supports the hypothesis that the two different treatments are able to act in synergy, significantly altering the inner and outer membrane of *E. coli*. The presence of chitosan causes flocculation of bacteria keeping them in close contact with chitosan particles. Once the electric field is applied, electroporation of the membrane enhances the inhibition effect of chitosan, and reduces bacteria viability by almost three orders of magnitude. The efficiency of chitosan inhibition was enhanced by increasing concentration. This effect, illustrated in Figure

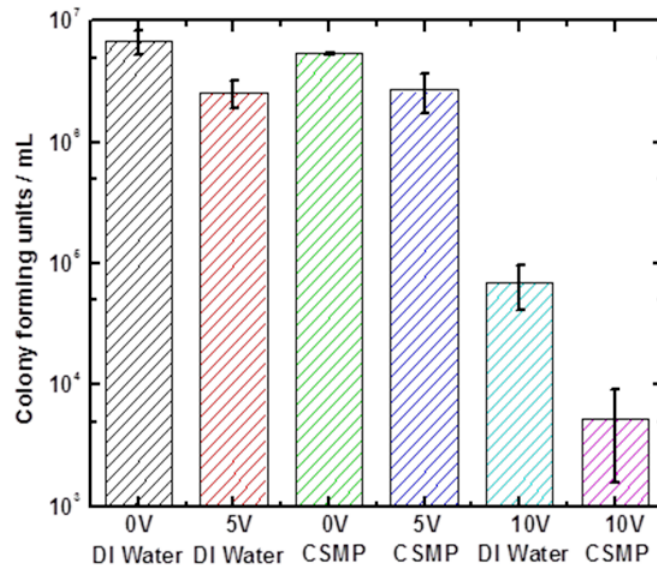


Figure 4.4: Cell colony counts after electroporation, chitosan introduction, or both. Electrical potentials of 5V and 10V applied across a 1 mm gap correspond to electric field strengths of 50 V/cm and 100 V/cm, respectively. The 0V CSMP data set was performed in triplicate, but the error bar is not visible on the chosen scale. The vertical axis contains a logarithmic scale.

4.5, shows that a 50 V/cm electric field is effective when combined with significant chitosan concentrations, where the viable population is reduced by approximately a factor of four at 3.2 mg/ml chitosan. Only a much smaller effect was observed previously at 50 V/cm with 0.267 mg/ml chitosan (Figure 4.4). Inhibition was also observed to be more consistent when chitosan was used in conjunction with electric fields. The results shown in Figure 4.5 suggest that further reduction in the applied electric field below 100 V/cm is possible as the chitosan concentration increases.

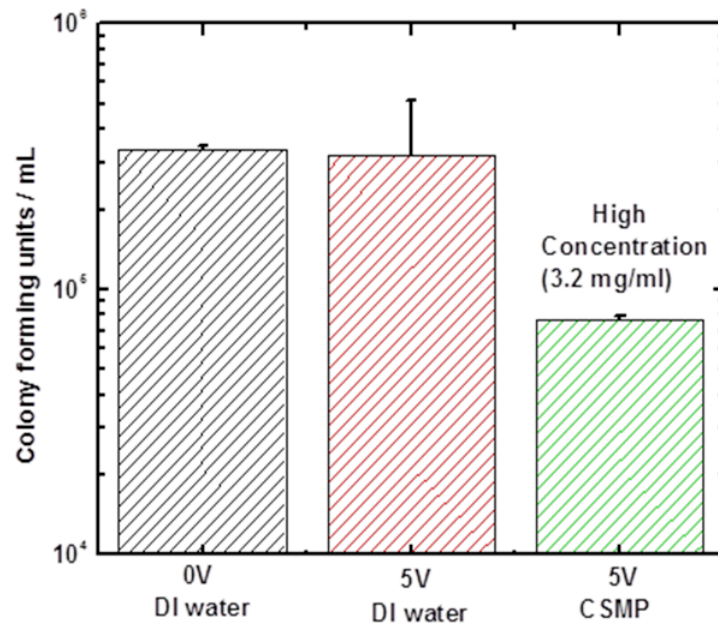


Figure 4.5: Comparison of electroporation treatment alone and combined treatment of electroporation and CSMP at high concentration. Final CSMP concentrations of 3.2 mg/ml were able to increase the inhibition effect of electroporation. Electroporation with electric field strengths of 50 V/cm were used.

## 4.6 E. coli inhibition: Colony growth results

Figure 4.6 illustrates the various potential colony growth types observed following overnight incubation of a small quantity of cells that were exposed to the treatments. An uncountable lawn is shown in Figure 4.6A, where a 1:1,000 dilution yielded a large number of viable bacteria following treatment with 50 V/cm electric field and chitosan (5V applied to the cuvette). Were this plate countable, it would signify a CFU/ml value on the order of that observed using 100 V/cm with particles (103-104). The number of colonies observed in Figure 4.6A agrees well since the dilution factor used to create this plate is a 1:100 dilution of Figure 4.6B. Although the population values for bacteria treated to only electric fields were less consistent, when particles

were introduced results were highly reproducible. Clearly, a smaller population of viable bacteria remains after the combined treatment of 50 V/cm electric field and 1.6 mg/ml chitosan (Figure 4.6B) compared to that remaining after the electric field alone at 50 V/cm (Figure 4.6E) or after the control treatment (Figure 4.6F), where the three plates are all displayed at the same dilution of 1:100,000.

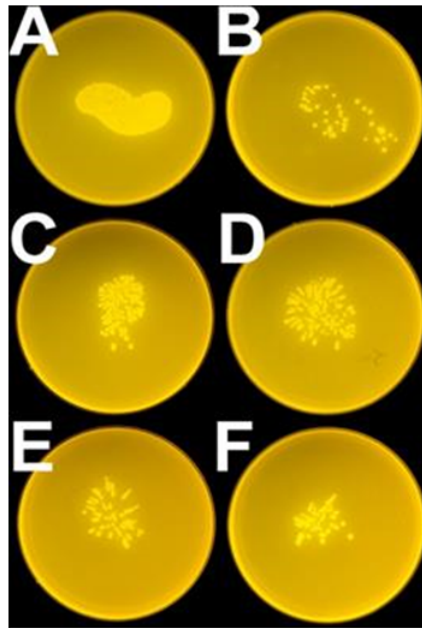


Figure 4.6: Viable colonies following various treatment combinations involving CSMP and 50 V/cm electroporation. Panes (A-C) depict cells that grew following combined treatment with 50 V/cm sustained electric field and 1.6 mg/ml CSMP. The respective dilution factors were: (A) 1:1,000, (B) 1:100,000, and (C) 1:10,000. (D) and (E) experienced electroporation only and had dilution factors of 1:1,000 and 1:100,000 respectively. The control treatment using deionized water and no electroporation appears in frame (F). This control plate was created from bacteria that were diluted by a factor of 1:100,000.

## 4.7 Conclusions

The results presented here shows that microbial inhibition methods can be significantly improved through the synergistic utilization of two charge-dependent methods that affect the cell membrane layers of gram-negative bacteria. Although chitosan did not significantly inhibit bacteria alone, presumably due to the neutral pH environment used, the combination of CSMP and a sustained electric field was successful in reducing bacteria viability by 2-2.5 orders of magnitude. The incorporation of CSMP was successful in reducing the voltage necessary to inhibit a significant number of bacteria. Previous work demonstrates the potential for highly cationic biopolymers to enhance microbial inhibition and separation. In this study, significant numbers of gram-negative *E. coli* bacteria were flocculated and inhibited using highly cationic chitosan particles, small sustained electric fields of 100 V/cm or less, or both. Electroporation techniques were able to inhibit approximately 98.0% of the bacteria. This result, obtained using a modified electroporation cuvette, was improved through the incorporation of small concentrations of CSMP. This mixture was so effective that approximately 99.9% of the original bacteria were prevented from growing in a nutrient-rich medium. This value is encouraging and strongly supports the assertion that small geometries with low electric fields or moderately sized geometries with slightly more applied energy can be utilized to inhibit unwanted microbes effectively when used in conjunction with biopolymeric particles. Finally, this work provides confirmation of the feasibility of biopolymeric particles for incorporation into new treatment methodologies for pathogenic microbe control. Numerous gram-negative

bacteria, including the often-mentioned Shiga-toxin producing *Escherichia coli* (e.g. *E.coli* O157:H7), could be prevented from spreading in contaminated food if biopolymeric inhibition methods are applied. Although the potential for such treatments is substantial, application of this treatment is likely limited to gram-negative bacteria with relatively high concentrations of negatively-charged ions and proteins near the cell wall. The present research would be enhanced by future studies with different strains of bacteria, investigations into biopolymeric flocculation as a method of sanitization, and encapsulation of biocompatible proteins that are delivered to the aggregates subsequent to flocculation. This valuable research provides insight into the mechanisms, optimal conditions and future potential of the synergistic antimicrobial action of electric fields and biopolymeric particles.

# Chapter 5

## Effect of surfactant adsorption on the electrokinetic properties of poly methylmetcarylate(PMMA)

### 5.1 Abstract

Control of EOF in microfluidic devices is essential in applications such as protein/DNA sizing and high-throughput drug screening. With the growing popularity of poly(methyl methacrylate) (PMMA) as the substrate for polymeric-based microfluidics, it is important to understand the effect of surfactants on EOF in these devices. In this article, we present an extensive investigation exploring changes in EOF rate induced by SDS, polyoxyethylene lauryl ether (Brij35) and CTAB in PMMA microfluidic capillaries. In a standard protein buffer (Tris-Glycine), PMMA capillaries exhibited a cathodic EOF with measured mobility of  $1.54 \pm 0.1(\times 10^{-4} Cm^2/V.s)$ . In the pres-

ence of surfactant below a critical concentration, EOF was independent of surfactant concentration. At high concentrations of surfactants, the electroosmotic mobility was found to linearly increase/decrease as the logarithm of concentration before reaching a constant value. With SDS, the EOF increased by 257% (compared to buffer), while it was decreased by 238% with CTAB. In the case of Brij35, the electroosmotic mobility was reduced by 70%. In a binary surfactant system of SDS/CTAB and SDS/Brij35, addition of oppositely charged CTAB reduced the SDS-induced EOF more effectively compared to nonionic Brij35. We propose possible mechanisms that explain the observed changes in EOF and zeta potential values. Use of neutral polymer coatings in combination with SDS resulted in 50% reduction in the electroosmotic mobility with 0.1% hydroxypropyl methyl cellulose (HPMC), while including 2% poly (N,N-dimethylacrylamide) (PDMA) had no effect. We also investigate the effect of surfactant chain length and concentration on the electro-osmotic (EO) mobility induced by three cationic surfactants cetyltrimethylammonium bromide (CTAB), tetradecyltrimethylammonium bromide (TTAB), and dodecyltrimethylammonium bromide (DTAB) in PMMA microcapillaries. The presented EO measurements provide a simple and rapid method for characterization of surface hydrophobicity through adsorption of surfactants. The EO mobility as a function of concentration shows three regimes. First, at very low concentrations below 0.002mM the mobility is constant and approximately equal to the value obtained with the surfactant-free electrolyte (1mM KCl). Next, the EOF reverses and mobility increases linearly with surfactant concentration. Finally, the mobility reaches a plateau at a concentration well below critical micelle concentration (CMC), 0.2mM CTAB, 0.5mM TTAB and 2mM DTAB

and decreases at the vicinity of CMC. Our results show that the rate of change in mobility with respect to concentration is a linear function of chain length and increases with longer chain surfactants. In addition, we deduce the magnitude of Van der Waals or cohesive energy between the adsorbed alkyl chains from the EO mobility values. For the alkyltrimethyl ammonium surfactants adsorbed on the hydrophobic surface of PMMA, this energy was found to be  $0.114KT$ , smaller than the reported value for ionic surfactants adsorbed on a hydrophilic surface. These results will potentially contribute to the development of PMMA-based microfluidic devices.

## 5.2 Introduction

Miniaturized microfluidic devices have significantly improved the field of detection and separation of analytes. The tremendous potential of microfluidics has been obvious since the first application in a variety of biochemical analyses[52]. Miniaturization provides a number of advantages including minimum sample consumption, fast analysis and automation allowing for development of high demand portable point of care devices (POC). Despite revolutionary achievements in the field of microfluidics, research into development of cheaper and more sensitive devices is underway. Recently, the focus has shifted to polymeric microfluidic platforms which are easier to manufacture[150], cost effective[35]and more flexible in design and fabrication[65]. The most common materials for plastic chip fabrication are poly(methyl methacrylate) (PMMA), polycarbonate (PC), poly(dimethyl siloxane) (PDMS) and poly(ethylene terephthalate glycol) (PETG). However, control of electroosmotic flow (EOF) has

proven challenging in these substrates [94]. Despite a large volume of publications on EOF and its origin, the surface properties and the electrical double layer (EDL) at the polymer surface remain poorly understood[93]. Therefore, a fine adjustment of EOF is necessary to achieve high resolution separation in electrophoresis systems. Numerous coating techniques for controlling EOF and preventing nonspecific interaction of analytes with the channel surface have been developed. Among these methods are external electric fields[53], pH adjustments[84], high concentration of ionic salts[45] and covalent and dynamic wall coating[59, 85]. Polymer and surfactant coating is the most attractive technique for suppression or reversal of EOF due to low cost, simplicity and versatility[60, 120, 55].

Transparency and excellent electrical and mechanical properties[11] make PMMA the most popular polymer for chip fabrication. At neutral and alkaline pH, PMMA exhibits a negative zeta potential (-10mV to -20mV)[71, 37]. Both hydrogen bonding and Van der Waals forces have been reported as the possible mechanism of surfactant adsorption to PMMA surface[37, 30]. Little work has been done on measuring EOF mobility and understanding the surface chemistry of PMMA coated with surfactants. Even though surface modification by polymers and surfactants have been investigated in PMMA microchips [29, 94, 95, 160], a detailed explanation on the effect of surfactant on EOF at different concentrations has not been presented. Moreover, to the best of our knowledge, the effect of mixed surfactants (ionic/non-ionic) or a surfactant and a neutral polymer on EOF has not been reported yet. In this paper, we present electroosmotic flow measurements in PMMA microfluidic capillaries, using dynamic coatings of surfactants. Three surfactant systems are considered:

anionic (SDS), cationic (CTAB) and non-ionic (Brij35). We also show the results obtained using binary surfactant systems SDS/CTAB and SDS/Brij35. Additionally, we focus on electroosmotic flow reduction for the purpose of protein microchip electrophoresis, where the concentration of SDS is above the critical micellar concentration ( $\sim 8\text{mM}$ ). Finally, the effect of Hydroxypropyl Methyl Cellulose (HPMC), Poly (N,N-dimethylacrylamide) (PDMA) and a non-ionic surfactant(Brij35) on EOF under protein electrophoresis conditions are studied. Adsorption of additives such as surfactants, added on purpose or present as impurities, significantly affects the EK properties by altering the surface charge density. The induction of charges on the surface has a profound effect on EOF. Hence, significant effort has been directed toward understanding the adsorption mechanism of surfactants at the solid-liquid interface. This includes surface modification in microfluidic devices for suppression of EOF or reduction of analyte adsorption[6, 94]. Even though surfactant adsorption can be directly characterized by techniques such as atomic force microscopy[83], ellipsometry[16], surface plasmon resonance[19], and neutron reflectivity[103], EK properties such as surface potential(zeta potential) and electro-osmotic(EO) mobility can be used as an indirect measurement of surfactant adsorption. Despite extensive research on surfactant adsorption at the solid-liquid interface[5, 87], there is a lack of fundamental understanding on the effect of surfactant concentration and structure on the EOF mobility in microfluidic channels or capillaries. In addition, a great volume of research has focused on the adsorption of ionic surfactants on hydrophilic surfaces. With the advent of polymeric (hydrophobic) microchips as substitutes for glass based devices, a fundamental understanding of surfactant induced EOF in these devices is

needed. Only a couple of studies examined the EO mobility as a function of surfactant concentration in PMMA devices. A significant volume of literature focused on the surface modification for the adjustment of EOF in microfluidics[94, 29]. To this end, more fundamental insights are needed to understand this mechanism in systems of surfactant with different structures. To the best of our knowledge, no study has been performed on understanding the effect of surfactant chain length and concentration of cationic surfactants on the EO mobility in PMMA microcapillaries. Adsorption of surfactants on silica shows an increase in surface excess and a shift of adsorption isotherms to lower concentrations with longer chain surfactants[43, 139]. However, despite few studies, a clear understanding of the effect of chain length on EK properties has not been presented. Comparing zwitterionic surfactants of different chain lengths (C16 and C12), constant EO mobility was observed below CMC with a small difference ( 20%) in the mobility of the two surfactants above CMC13. In another study comparing the EO mobility of non-ionic Tween surfactants(C12, C16, C18) above CMC, maximum mobility was reported with C16, with no correlation between the chain length and mobility[134]. Although these studies show a small difference in mobility values, others reported a more pronounced change. The effect of chain length of cationic surfactants(C10 to C18) below CMC on zeta potential of quartz showed a shift to lower concentrations with longer chain surfactant[122]. This observation is consistent with the reported shift in adsorption isotherm to lower concentration. Although concentrations at and above CMC were not studied, the authors concluded that significant changes in zeta potential occurs at concentrations well below CMC. In another report, comparing EO mobility of cationic surfactants(C16, C14, C12) below

and above CMC, a plateau in mobility was observed at 10% CMC with no difference above this point[131]. we compare the adsorption of three cationic surfactants of alkyl trimethylammonium bromides with different chain length on a hydrophobic surface of PMMA microcapillary. A wide concentration range below and above CMC has been selected in order to compare the differences in mobility values and also investigate the effect of CMC on the mobility. Based on the experimental data we present a correlation between the EOF mobility and the surfactant concentration. In addition we determine the magnitude of Van der Waals or cohesive energy between surfactant chains as the interaction between the adjacent chains facilitates the adsorption of more molecules on the PMMA surface. Considering the growing popularity of polymeric based microfluidic platforms, our results can be applied to investigate the effect of surfactants on EO mobility in these systems.

Molecular structures of the polymers and surfactants are given in Figure 5.1.

## 5.3 Materials and Methods

### 5.3.1 Materials and Reagents

Sodium dodecyl sulfate(SDS), cetyltrimethylammonium bromide (CTAB), tetradecyltrimethylammonium bromide (TTAB), dodecyltrimethylammonium bromide (DTAB), potassium chloride (KCl), hydroxypropyl methyl cellulose(HPMC) (viscosity of 2% aqueous solution at 20°C, 4060 cP) and Tris-Glycine buffer 10X (diluted to 1X, pH = 8.4) were purchased from Sigma-Aldrich (St.Louis, MO, USA). Polyoxyethylene

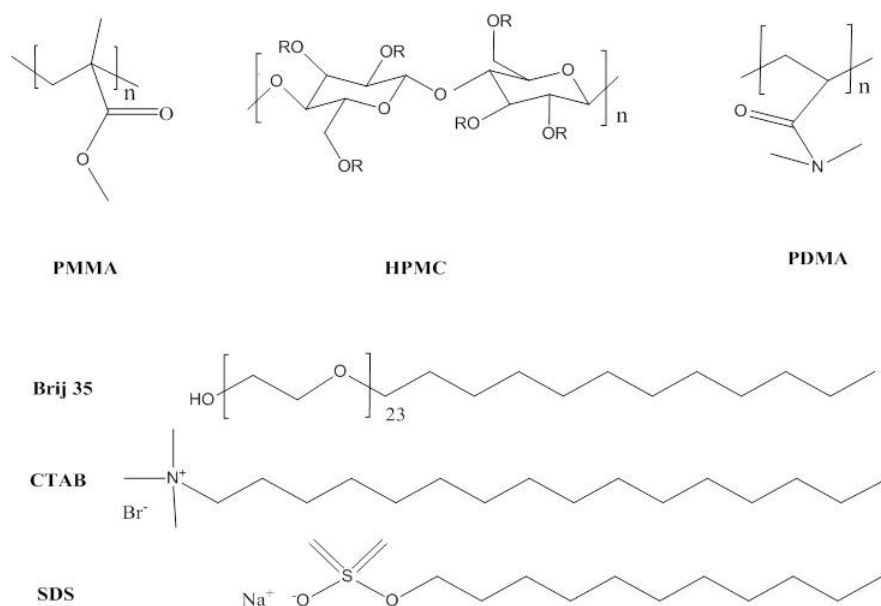


Figure 5.1: Chemical structures of surfactants, PMMA, PDMA and polymer used as a coating material.

lauryl ether (Brij35) (with 3% water) and Rhodamine B were obtained from Fisher Scientific (Pittsburgh, PA, USA). PDMA (MW:229000) was purchased from Polymer Source (Montreal, QC, Canada). PMMA capillaries (id/od 180/360  $\mu\text{m} \pm 5\%$ ) were purchased from Paradigm Optics (Vancouver, WA, USA). Aqueous solutions were prepared using ultra pure DI water (Elga Lab Water, Marlow, UK). All chemicals were used as received. Solutions of single and mixed surfactants/ polymer were prepared in Tris-Glycine buffer (25mM Tris and 192mM Glycine) and incubated on a shaker (Innova 4080 incubator shaker, New Brunswick Scientific) overnight at room temperature. After incubation, all the solutions were filtered using 0.2  $\mu\text{m}$  polypropylene syringe filters (VWR, Radnor, PA, USA) and degassed.

### 5.3.2 Instrumentation and Method

Microfluidic capillaries were first primed with the buffer by inserting one end of the capillary in the reservoir. As buffer filled the capillary due to surface tension, the other end was placed into the second reservoir (Figure 5.2). Care was taken to avoid the formation of air bubbles within the capillary. Both reservoirs (1ml volume) and the PMMA capillary ( $l_t = 12\text{cm}$ ) were filled with the same solution. Rhodamine B ( $0.2\mu\text{M}$ ) was added to one of the reservoirs, and the platform was placed on the stage of an inverted fluorescence microscope, Nikon Eclipse TE2000 with yellow fluorescence filter (540-580nm excitation range). The detection point was set at the middle of the capillary ( $l_d = 6\text{cm}$ ). Two platinum wires connected to the high voltage power supply equipped with current monitoring were placed in the reservoirs. Capillaries were pre-equilibrated for 5 minutes with the same solution by switching voltage configuration, directing the flow from the reservoir with no marker to the other. The pre-equilibration step was performed to establish near steady state conditions between the capillary wall and the bulk solution. This step also removes any transients due to inhomogeneities on the capillary wall. Equilibrium was achieved when no significant changes in the current ( $\pm 0.1\mu\text{A}$ ) were observed. The volume of the displaced fluid was not significant enough to create any measurable hydrostatic pressure difference. Finally, EOF measurements were performed under a constant voltage of  $V = 1500\text{V}$  at room temperature. The data was collected at 1 Hz as a plot of PMT signal versus time, by monitoring the migration time of the neutral marker, Rhodamine B. The arrival time of the marker was considered at the position where PMT signal reached a

constant value. Each measurement was repeated three times with a new capillary. In order to compare theoretical and experimental current, the conductivity of surfactant solutions (bulk) was measured with a Vernier probe.

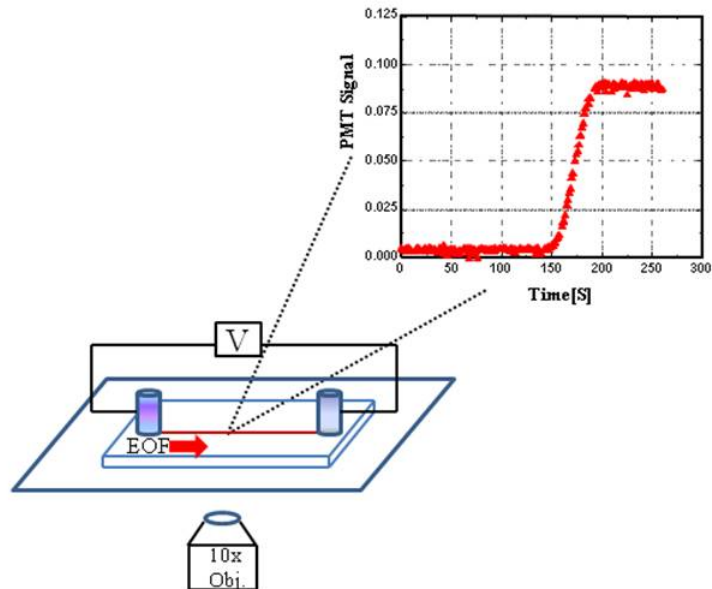


Figure 5.2: Schematic of the EOF detection platform. Microfluidic PMMA capillary (length 12 cm, i.d.  $180\mu\text{m}$ ) connected between two reservoirs. Microscope detection system consists of HV power supply (voltage 1500 V), microscope optics, excitation lamp and photodiode. Detection point was located at 6 cm. The migration time of the neutral dye is taken at the point where the photomultiplier (PMT) signal reaches a steady value.

## 5.4 Surface chemistry of PMMA

EOF measurements were first performed in Tris-Glycine buffer with 25mM Tris and 192mM Glycine. This combination provides pH value of 8.4 higher than isoelectric point (pI) of most proteins, making Tris-Glycine a common buffer in protein

electrophoresis[47, 102]. EOF mobility ( $\mu_{eo}$ ) is given by:

$$\mu_{eo} = \frac{u_{eo}}{E} \quad (5.1)$$

where  $u_{eo} = l_d/t$  is the measured electroosmotic velocity and  $E = V/l_t$  is the applied electric field. A constant electric field of was applied in all experiments. The migration time of the marker in the buffer was measured to be 3125 seconds, resulting in a EOF mobility of  $1.54 \pm 0.1(\times 10^{-4}) \text{ cm}^2/V.s$ . The positive value of mobility suggests that PMMA surface attains a net negative charge in the presence of Tris-Glycine buffer at 8.4 pH. The source of the acquired charge can be attributed to the adsorption of the buffer ions (Tris and Glycine) on the inner capillary wall. If the surface of PMMA is completely uncharged, the mechanism of the adsorption is governed by hydrophobic interactions only, which results in low electroosmotic mobility for the buffer as a mixture of ionic compounds. However, in case of slightly charged PMMA surface, depending on the ratio of charged to hydrophobic sites, there will be a contribution of ionic interactions between buffer ions and the PMMA surface. Mobility values within the same range as in Tris-Glycine buffer  $1.3 \pm 0.4(\times 10^{-4}) \text{ cm}^2/V.s$  [9] and  $1.68 \pm 0.08(\times 10^{-4}) \text{ cm}^2/V.s$ , pH 6.93 have been reported in PMMA in a phosphate buffer[31].

In the presence of the electric filed, the electromigration current is given by:

$$I = \sigma AE \quad (5.2)$$

where  $\sigma$  is the bulk conductivity and  $A$  is the cross sectional area of the capillary. Here, we have assumed that the net current is generated from bulk motion of ions. The bulk conductivity of buffer solution was measured to be  $462 \pm 5 \mu S/cm$  resulting in a theoretical current of  $14.7 \pm 1 \mu A$  for a capillary of cross sectional area  $2.54 \times 10^{-4} cm^2$ . This value agrees well with the measured value of  $13.4 \pm 0.3 \mu A$ . We believe a slightly higher theoretical value resulted from the 5% uncertainty in the capillary diameter ( $180 \pm 9 \mu m$ ).

The thickness of EDL for symmetric electrolytes is given by:

$$\kappa = \left( \frac{\varepsilon K_B T}{2n_\infty Z^2 e^2} \right)^{1/2} \quad (5.3)$$

where  $n_\infty$  is the ionic number concentration in the neutral electrolyte,  $Z$  is the electrolyte valency,  $e$  is the electric charge,  $\varepsilon$  is the electric permittivity of the solvent,  $K_B$  is the Boltzmann constant and  $T$  is the absolute temperature. Considering  $n_\infty = 1.31 \times 10^{26} m^{-3}$  and  $\varepsilon = 7.08 \times 10^{-12} C/V.m$  for Tris-Glycine buffer, Eq 5.3 results in EDL thickness  $\kappa = 0.066$  nm. Under this condition, where the EDL thickness is significantly less than the capillary radius, the contribution of the surface conductance is negligible[64] and the bulk conductance can be used directly in the electric current calculations. Considering a thin double layer, Eq 5.2 represents the electromigration current. The electroosmotic mobility for an infinitely thin double layer is expressed by Helmholtz-Smoluchowski equation as:

$$\mu = \frac{\varepsilon \zeta}{\eta} \quad (5.4)$$

where  $\zeta$  is the zeta potential of the PMMA surface and  $\eta$  is the viscosity of the buffer. Using this equation our experiments shows that the zeta potential of PMMA capillary walls in Tris-Glycine buffer is  $-21.8 \pm 0.1$  mV at 25°C. Here, the measured viscosity and the relative permittivity of the buffer are 1cP and 80 respectively. The change in viscosity is negligible for the concentrations of surfactants used in this study. After establishing the base mobility value in the buffer, we then performed experiments to understand the surfactant induced electroosmotic flow in PMMA capillaries.

## 5.5 Effect of ionic and non-ionic surfactants

The effect of surfactant coating on EOF in a PMMA capillary was studied in the presence of ionic (SDS,CTAB) and non-ionic (Brij35) surfactants. Adsorption or interactions of surfactants to the surface directly affects the rate of EOF by changing the net surface charge density. The concentration range for each surfactant was varied in order to cover a range below and above the bulk Critical Micelle Concentration (CMC) of the surfactant in Tris-Glycine buffer. For each concentration three independent measurements were performed. Surfactant CMC values in Tris-Glycine buffer were determined fluorometrically using a hydrophobic dye (Sypro Orange, Ex/Em 470/570). CMC was detected at a concentration where a sudden jump in fluorescent signal was observed, suggesting the formation of micelles where the dye molecules reside within the micelles and exhibit higher fluorescent signal. Figure 5.3 shows the measured fluorescence as a function of surfactant concentration. Based on data ob-

tained in Figure 5.3, the CMC values for SDS, CTAB and Brij35 are estimated to be 4mM, 0.3mM and 0.1mM, respectively.

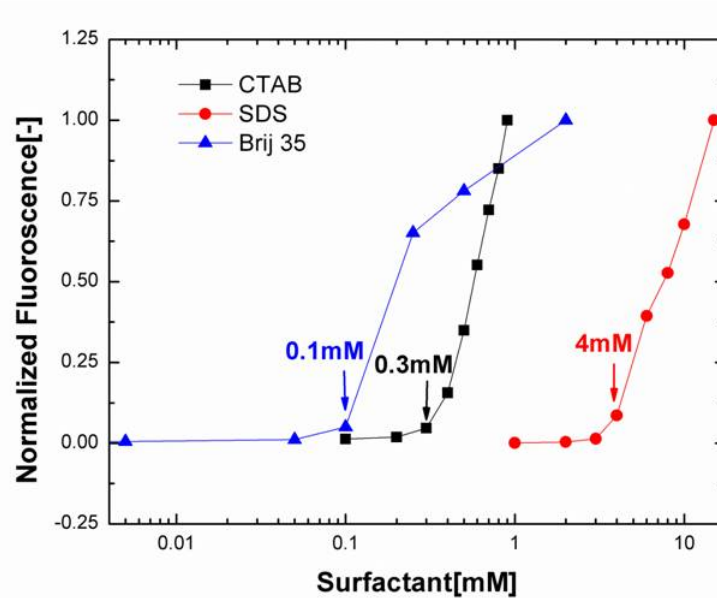


Figure 5.3: Critical micelle concentration (CMC) determination of the surfactants. The fluorescence signal is normalized with respect to maximum and minimum values. Sypro orange concentration was constant at 5x.

### 5.5.1 Effect of negatively charged ionic surfactant: SDS

Figure 5.4 shows the effect of SDS concentration on  $\mu_{eo}$  in a PMMA capillary. The electroosmotic flow exhibits three distinctive regions[79]. In region A, where SDS concentrations are less than 0.005mM, the EOF mobility remains constant at  $\mu_{eo} = 1.7 \pm 0.2(10^{-4} \text{ cm}^2/V.s$  which is in the same range as the mobility of the buffer. The negative zeta potential of the PMMA surface obtained with buffer only suggests that there is a tendency for the adsorption of the negative ions to the PMMA surface. This means that SDS molecules can compete with the negative buffer ions in adsorption to

the surface. However, in region *A* where SDS concentration is significantly less than buffer ions, there is minimum interaction between SDS molecule and the surface. As the SDS concentration increases beyond 0.005mM, a transition from region *A* to region *B* occurs, where SDS monomers can be arranged in opposite direction, minimizing the repulsion between the head groups and increasing the number of molecules adsorbed to the surface. The linearity of  $\mu_{eo}$  with the logarithm of SDS concentration in region *B* suggests that, upon adsorption of SDS hydrophobic tails onto the surface, all the shielding of the negatively charged head group is performed by the diffused portion of the double layer[70]. Since the length of the hydrophobic tail (1.7nm) is larger than the EDL thickness ( 0.066 nm, in presence of SDS in buffer), the diffused layer is expected to become slightly thicker even with a monolayer of SDS molecules. In the limit of  $\zeta \gg K_B T/e = 51$  mV, the dependence of zeta potential on the mobile ion concentration can be approximated as:

$$\zeta = a + b \log(c) \quad (5.5)$$

where  $a$  and  $b$  are constants and  $c$  is the concentration of the adsorbed ion. Given that EOF mobility is related to zeta potential(Eq 5.4), zeta potential varies in region B between -26mV and -78mV. Even though this range is not much greater than 51mV, Eq 5.5 agrees well with our experimental data with  $a = 2.7$  mV and  $b = 5.8$  mV/log(mM). This observation is consistent with the reported values in the literature[71]. This linearity is not valid in region *A* with low surfactant concentration and region *C* where the surface is saturated with the surfactant molecules. It is

believed that surfactant molecules in region *C* can form hemimicelle[42, 79] or a bilayer[13] on the surface. The mobility plateaus at  $\mu_{eo} = 5.5 \pm 0.2(10^{-4} \text{ cm}^2/\text{V}\cdot\text{s})$  which is 257% higher than that observed in pure buffer. It is important to note that this plateau is reached at a concentration below the measured bulk CMC of 4mM (as shown in Figure 5.4).

The experimental and theoretical currents for different concentrations of SDS are also shown in Figure 5.4(inset). The measured bulk conductivity increased linearly with increasing concentration which is supported by increasing current in Figure 5.4. The agreement between experimental and theoretical current values suggests that the role of surface conductance is negligible compared to the bulk conductance.

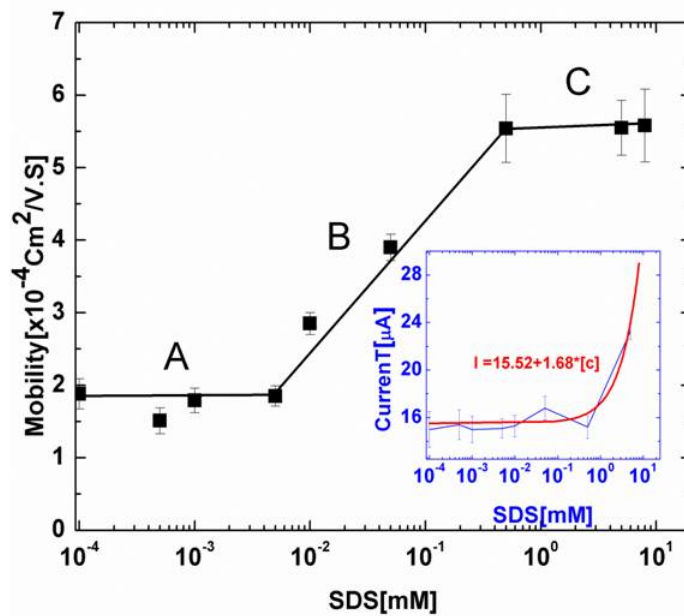


Figure 5.4: Effect of SDS on EOF in PMMA microcapillaries. The inset shows the plot of theoretical and experimentally measured current values. Error bars are obtained from three independent experiments.

### 5.5.2 Effect of positively charged ionic surfactant: CTAB

Figure 5.5 shows the effect of CTAB concentration on  $\mu_{eo}$  in a PMMA capillary. As for SDS, the adsorption of CTAB on the surface exhibits three distinctive regions with similar behavior in each region. In region A, where CTAB concentration is less than 0.005mM, the EOF mobility remains constant at  $\mu_{eo} = 1.63 \pm 0.2 (10^{-4} \text{ cm}^2/\text{V}\cdot\text{s})$ . Comparing this mobility with buffer mobility, there is minimum interaction between CTAB molecules and the PMMA surface in region A. As the concentration of CTAB increases beyond 0.005mM, the transition from region A to region B occurs. In region B, the electroosmotic flow decreases and finally reverses to an anodic EOF, due first to neutralization and then, to the formation of a positive charge layer near the surface. The EOF mobility decreases linearly with the logarithm of CTAB concentration. The zeta potential varies in this region between -35mV and +70mV. Once again Eq 5.5 agrees well with our experimental data with  $a = 1.7\text{mV}$  and  $b = -140.5\text{mV}/\log(\text{mM})$ . The rate of decrease of EOF with increase in CTAB concentration is much higher than the rate of increase observed with increase in SDS concentration, suggesting a faster adsorption rate of CTAB hydrophobic tails. Compared with the EDL thickness (0.066 nm) observed in pure buffer solutions, the length of CTAB hydrophobic tail (2.06nm) is much larger; hence the diffused layer thickness is expected to change even with a monolayer of CTAB molecules. Adsorption of CTAB changes the net charge of the diffused layer on PMMA from negative to positive (negative slope), and reverses the direction of EOF at approximately 0.01mM. The critical concentration (0.01mM) for transition from cathodic to anodic EOF is expected to depend on pH and the ionic

properties of the buffer. This transition has been achieved at a higher concentration of CTAB in silica(0.5mM)[67]. An order of magnitude lower value obtained in PMMA can be explained by the difference in the mechanism of adsorption of CTAB on these surfaces. CTAB concentrations greater than 0.05 mM (region *C*) result in a constant EOF with mobility, 238% higher than that of the buffer. In comparison to CMC value of CTAB(0.3mM), the constant mobility achieved at 0.05mM supports the formation of bilayers or hemimicelle structures on the PMMA surface, below CMC. The good agreement between theoretical and experimental current values (Figure 5.3, inset) further shows the negligible effect of surface conductance.

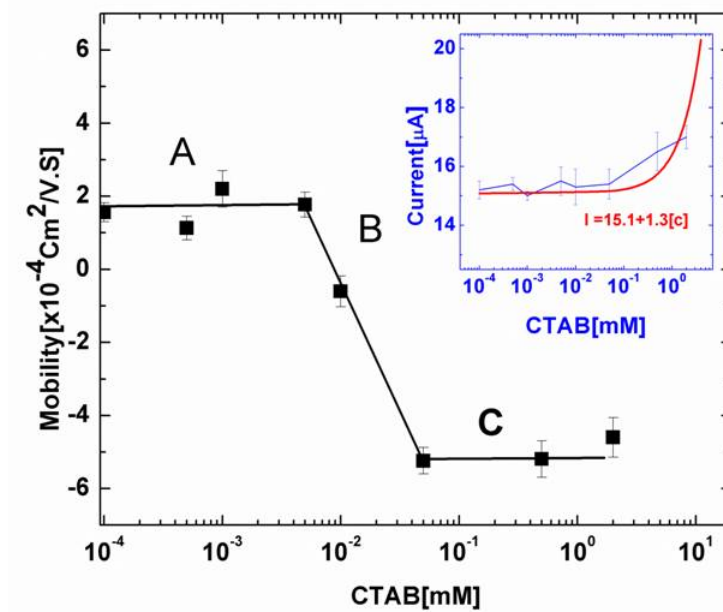


Figure 5.5: Effect of CTAB on EOF in PMMA microcapillaries. The inset shows the plot of theoretical and experimentally measured current values. Error bars are obtained from three independent experiments.

### 5.5.3 Effect of non-ionic surfactant: Brij35

As shown in Figure 5.6, the effect of Brij35 on  $\mu_{eo}$  in PMMA capillary shows a similar trend as SDS and CTAB at low concentrations. In region *A*, at concentrations below 0.0005,  $\mu_{eo}$  remains constant at  $\mu_{eo} = 1.75 \pm 0.1(\times 10^{-4}) \text{ cm}^2/V.s$ . However, unlike, CTAB, the decrease in EOF mobility is more gradual with Brij35. It is important to note that even though Brij35 is non-ionic, Eq 5.5 fits the data in region *B*, with  $a = 0.0001\text{mV}$  and  $b = -4 \times 10^{-4} \text{ mV}/\log(\text{mM})$ . The rate of change of EOF with increasing Brij35 concentration is quite small. In this region, the zeta potential varies between -19.5mV and -6.32 mV. Unlike SDS or CTAB no clear plateau region *C* was observed with Brij35. It is possible that even higher concentrations of Brij35 are required to achieve a constant  $\mu_{eo}$ . Since the length of the hydrophobic tail (7.5 nm) is two orders of magnitude larger than EDL thickness( 0.066 nm), the adsorption of a Brij35 molecule will not significantly alter the charge distribution of EDL. The exact mechanism for the reduction of EOF with Brij35 is unknown. We can only hypothesize that the shielding of the surface charges by Brij35 molecules can result in minimizing the surface charge density and possibly reducing the EOF mobility. The mechanism of reducing  $\mu_{eo}$  by Brij35 can possibly be explained by a replacement of buffer ions with Brij35 molecules, at higher concentrations, which can provide a moderate shielding of charges and hence reduce  $\mu_{eo}$ . The effect of Brij35 in suppressing EOF in silica or PDMS substrates has been already reported[134, 22]. As for SDS and CTAB, the mechanism of nonionic surfactant adsorption to a hydrophobic surface such as PMMA is expected to be dominated by hydrophobic interactions between

the hydrocarbon tail of the surfactant the PMMA surface; however, non-ionic surfactants with a polyoxyethylene(POE) chain are able to create hydrogen bonds with the PMMA surface[115], making the adsorption more effective. As expected with a non-ionic surfactant, the theoretical and experimental currents remain approximately constant (Figure 5.6, inset).

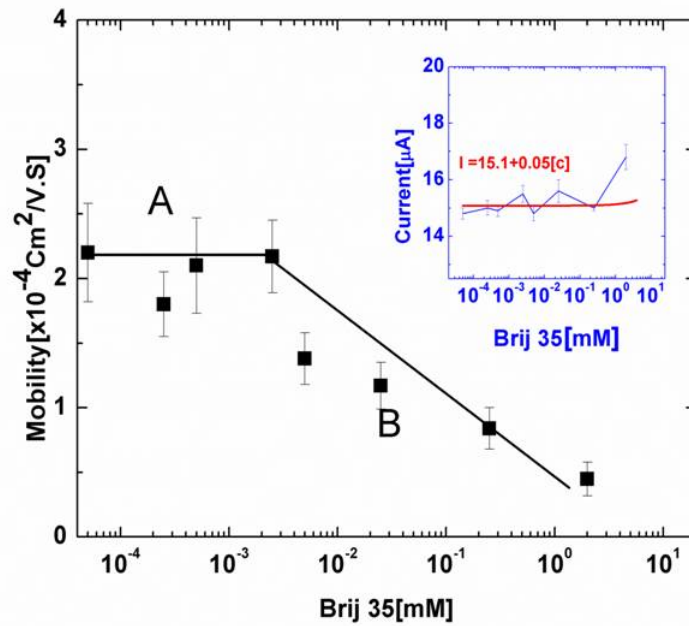


Figure 5.6: Effect of Brij35 on EOF in PMMA microcapillaries. The inset shows the plot of theoretical and experimentally measured current values. Error bars are obtained from three independent experiments.

## 5.6 Effect of mixed surfactants

Although the phase diagrams of SDS/CTAB and SDS/Brij35 systems are unavailable in Tris-Glycine buffer, it is expected that the addition of associating counter or neutral molecules will alter the aggregation morphology (micelles, vesicles or bilayer). Hence, mixtures of the cationic and anionic surfactants affects the adsorption be-

havior of individual surfactants which results in changes in electroosmotic flow[143]. After establishing the individual effect of each surfactant on electroosmotic mobility in a PMMA capillary, we investigated the combined contribution of surfactants in a binary system of anionic/cationic and anionic/non-ionic. Since the protein sizing is performed using denaturing concentrations of SDS ( $\sim 8\text{mM}$ ), we used a constant concentration of SDS at  $0.5\text{mM}$  above which  $\mu_{eo}$  was measured to be constant (Figure 5.4). The concentration of CTAB and Brij35 were varied as in the single surfactant case. Figure 5.7 shows no significant change in the magnitude of  $\mu_{eo}$  with CTAB at concentrations below  $0.05\text{mM}$ . This suggests that in the mixed CTAB/SDS solution with  $0.5\text{mM}$  SDS (10 times higher than CTAB), SDS is dominant in the adsorption into the surface charge layer. As the concentration of CTAB increases, the interaction between the two oppositely charged surfactant results in the neutralization of SDS molecules and the reduction of  $\mu_{eo}$ . Finally, at  $\sim 0.5\text{mM}$ , where equal numbers of SDS and CTAB molecules are present  $\mu_{eo}$  is reduced to  $9.6 \times 10^{-5} \text{ Cm}^2/\text{V.s}$ . Electroosmotic mobility is further reduced as the concentration of CTAB increases above the SDS concentration, and is finally reversed as CTAB becomes the dominant surfactant adsorbed to the surface. In case of SDS mixed with Brij35,  $\mu_{eo}$  remains constant at low Brij35 concentration and is slowly reduced with increasing concentration above  $2.5 \times 10^{-3} \text{ mM}$ . Unlike CTAB, addition of Brij35 reduces the electroosmotic mobility at much lower concentrations. However, even at a concentration higher than SDS, the addition of Brij35 does not reduce the mobility as effectively as CTAB at equimolar concentration with SDS. This can be explained by a comparison between the geometry of SDS and Brij35 molecules (Figure 5.1). Both molecules have the same

hydrophobic chain length consisting of 12 carbon atoms. However, with the addition of 23 polyoxyethylene (POE) groups, Brij35 is a much larger molecule. This is more evident when considering the surface area of each surfactant molecule. Using the aggregation numbers of each surfactant (in water) the surface areas of Brij35 and SDS were calculated as  $1.9\text{nm}^2$  and  $0.57\text{nm}^2$  respectively[63]. The surface area of a CTAB molecule is  $0.66\text{nm}^2$  which is within the same range as SDS. Thus, for SDS-CTAB mixture geometry does not significantly affect the adsorption mechanism.

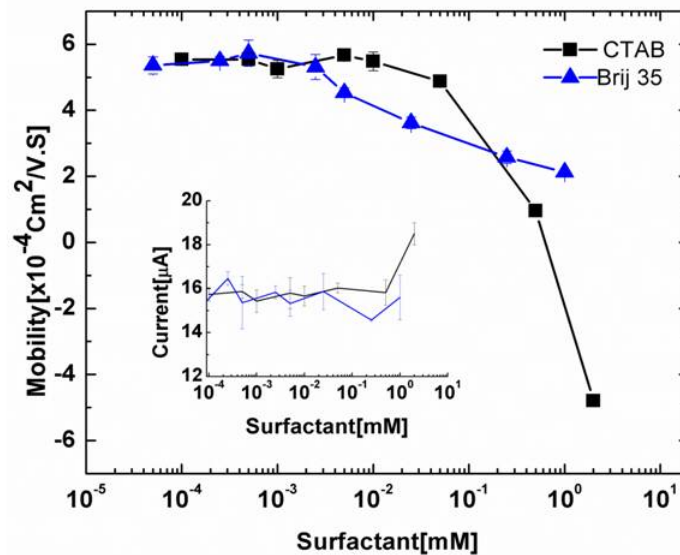


Figure 5.7: Effect of mixed surfactants on EOF in PMMA microcapillaries. For each data point the concentration of SDS was fixed at 0.5mM. The inset shows the experimental current.

The current profile for the mixed surfactant system is given in Figure 5.7(inset). As expected, the current remains approximately constant in the case of non-ionic Brij35. Addition of CTAB at concentrations below 0.5mM has negligible contribution to the current, however, a sudden jump in the current is observed above 0.5mM(at 2mM

CTAB+0.5mMSDS), where the concentration of CTAB is 4 times SDS.

The decrease in cathodic EOF is more pronounced (~60%) with Brij35. At a constant concentration of SDS, mixed SDS/Brij35 micelles should become increasingly less ionic as the concentration of nonionic surfactant increases. Reduction in EOF mobility can be the result of both increasing hydrophobicity and viscosity of the mixed micelles.

## 5.7 Effect of neutral polymers

Poly dimethylacrylamide (PDMA) has been widely used in gel electrophoresis as both a sieving matrix and a coating reagent for EOF suppression on silica and PDMS substrates[69, 34, 145]. Concentration of PMMA as the separating matrix is optimized according to the size of proteins between 2% to 4%(w/v). Even though the suppression in EOF has been achieved in the literature, the absolute value of EOF mobility and the degree of suppression have not been reported. Protein separation in PDMA gels has been performed in a PMMA microchip, using a variety of methyl cellulose (MC) compounds as EOF suppressor[123, 124, 125, 97, 144]. In these studies, the concentration of MC was varied from 0.01 to 1%(w/v). Due to an increase in viscosity, filling the capillaries is challenging with higher concentrations of MC[31]. We performed EOF measurements using 2% PDMA in the buffer solution. As shown in Figure 5.8, for 0.5mM SDS,  $\mu_{eo}$  is suppressed by ~60% and ~90%, with 2%PDMA and 0.1% HPMC respectively. At 8mM SDS, PDMA has no effect on  $\mu_{eo}$ , while HPMC reduces  $\mu_{eo}$  by 50%. We also performed experiments to quantify the effect

of mixed surfactant solution at 8mM SDS concentration, using Figure 5.7 as a reference. As shown in Figure 5.7, the greatest reduction in EOF is achieved when the mole fraction of SDS is  $\sim 0.66$  with Brij35 and 0.5 with CTAB. Solutions of SDS at 8mM with CTAB and Brij35 were prepared with the same mole fraction. However, only SDS/Brij35 could be filtered with a  $0.2 \mu\text{m}$  filter. This is possibly due to the formation of large mixed SDS/CTAB micelles at these particular concentrations. Addition of 4mM Brij35 had a similar effect as 0.1% HPMC in reducing by 50%.

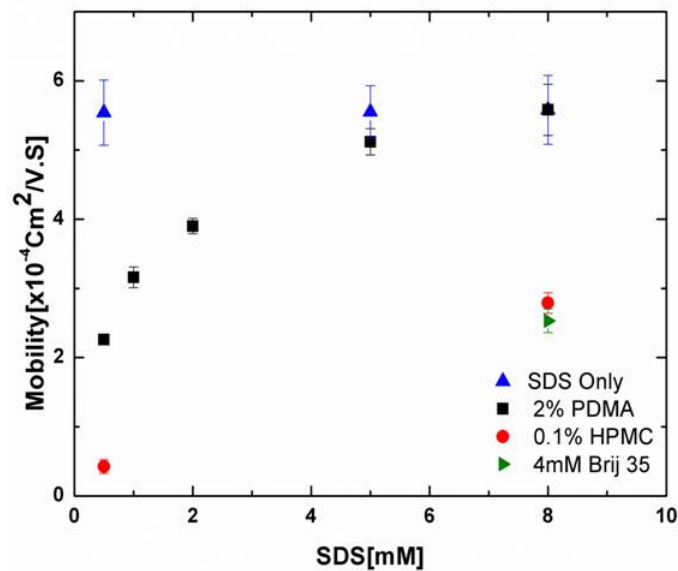


Figure 5.8: Effect of HPMC, PDMA and Brij35 mixed with SDS on EOF mobility in a PMMA microcapillary.

## 5.8 Effect of surfactant structure: chain length

In order to study the effect of surfactant chain length on the electrokinetic properties of PMMA, we compare the adsorption of three cationic surfactants of cetyltrimethy-

lammonium bromide (CTAB), trimethylammonium bromide (TTAB), and dodecyltrimethylammonium bromide with similar head group structure and various chain length. Solutions of surfactant were prepared in 1mM KCl (pH  $\sim$ 8.4) as the electrolyte. A wide concentration range below and above CMC has been selected in order to compare the differences in mobility values and also investigate the effect of CMC on the mobility. Baseline mobility was determined for surfactant-free electrolyte, with average flow velocity at  $u_{eo} = 0.18 \pm 0.1$  mm/s. A cathodic EO mobility (flow of positive ions) was observed at room temperature, indicating a slightly negatively charged PMMA surface with the surfactant free solution. Under this condition the surface potential was calculated  $\zeta = -21.3 \pm 0.4$  mV (using water viscosity 0.001 Pa.s), which was smaller than the conditional thermal scale of 51.4mV. The diffusion time of the fluorescent marker is neglected due to a much larger diffusion time compared to the experimental time scale. Surfactants were chosen based on alkyl chain length, as the only difference in structure. The chain length of CTAB with 16 carbons, TTAB with 14 carbons and DTAB with 12 carbons is 2.18, 1.67 and 1.42 nm respectively[113]. First, we measured the critical micelle concentration (CMC) of each surfactant in 1mM KCl as shown in Figure 5.9. The CMC of CTAB, TTAB and DTAB was measured at 1mM, 3.5mM and 15mM respectively. The CMC values are in good agreement with the reported values in water[91]. Compared to water at room temperature, no significant difference in the viscosity of surfactant solutions was observed.

The electromigration current was measured for each surfactant solution using Eq 5.2 and is presented in Figure 5.10. The current  $I$  is directly proportional to the bulk conductivity, which increases with concentration or number density of the sur-

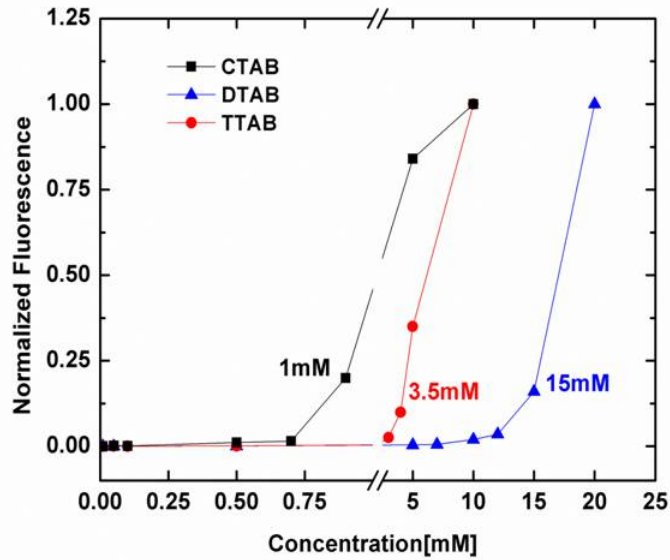


Figure 5.9: Critical micelle concentration (CMC) determination of the surfactants. The fluorescence signal is normalized with respect to maximum and minimum values. Sypro orange concentration was constant at 5x.

factant ions. The degree of counterion micellar binding has a direct effect on the electromigration current. The interaction between positively charged micelles of the surfactants and negatively charged chloride and bromide ions can be evaluated with respect to the counterion association constant  $f$ . This constant is defined as the ratio of postmicellar to premicellar slope from the plot of bulk conductance versus the surfactant concentration[91]. Figure 5.10 inset shows that  $f$  linearly decreases with the chain length. This observation agrees well with the reported trend in literature[91]. A higher number of counterions was observed with the shorter chain DTAB, resulting in an increase in current compared to CTAB and TTAB.

The measured EO mobility as a function of surfactant concentration is shown in Figure 5.11. The mobility curve comprises of three distinct regions. The first region

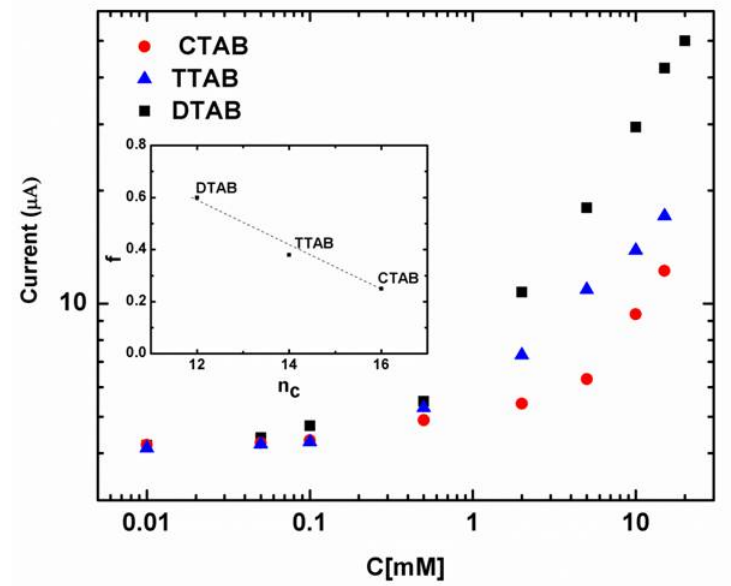


Figure 5.10: Experimental currents measurements. The inset shows the counterion association constant with respect to chain length  $n_c$ .

is characterized by a constant mobility value similar to the surfactant free solution. The second region is the linear region where increasing surfactant concentration first neutralizes the PMMA surface charges by reducing the mobility to zero and then reverses the surface charge, resulting in negative mobility values. Finally, the third region corresponds to a plateau in mobility. At this point the PMMA surface is saturated with surfactant molecules and addition of more surfactant has no effect on the mobility.

The saturation point is observed at 0.2mM CTAB, 0.5mM TTAB and 2mM DTAB, below the bulk CMC. At low concentrations from 0.0005mM to 0.002mM cathodic EOF was observed with CTAB and TTAB. For DTAB the cathodic range was extended to 0.005mM. At 0.01mM and above all surfactants showed an anodic EOF. The magnitude of EO mobility stays approximately constant with all three

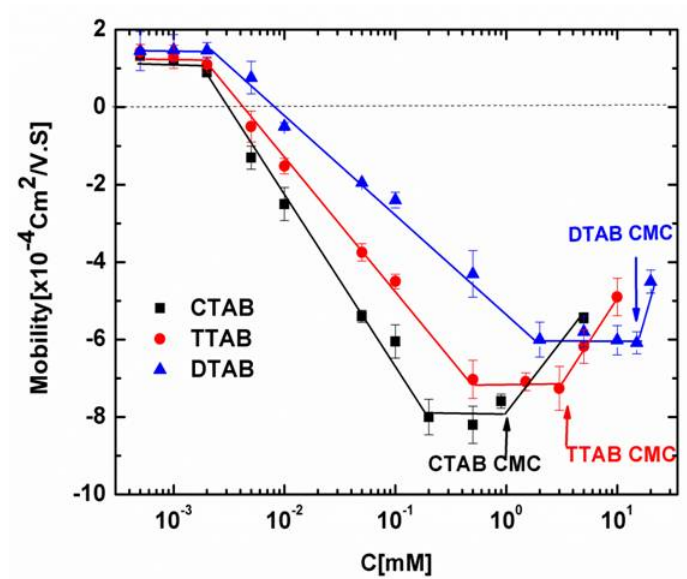


Figure 5.11: The effect of surfactant concentration on EO mobility in a PMMA microcapillary. Solid lines were added to guide the eye. Conditions: 1mM KCl, pH 8.5 at 25°C. Constant Voltage:1500 V.

surfactants from 0.0005mM to 0.002mM. Beyond 0.002mM, EO mobility is first reduced compare to 1mM KCl (surfactant free solution) and finally reaches zero at 0.0028mM, 0.0042mM and 0.008mM with CTAB, TTAB and DTAB respectively. The magnitude of zeta potentials at the studied concentration range varied from 18.64mV to 76.84mV with CTAB, 20.06mV to 69.21mV with TTAB and 20.48mV to 63.56mV with DTAB. The trend observed in Figure 5.11 is in a good agreement with the reported adsorption isotherms of these surfactants[4]. The mobility values are shifted to lower concentrations as the chain length (hydrophobicity) increases. The longest chain CTAB displays higher mobility values, suggesting an increase in adsorption with longer chain length. A valuable insight from Figure 5.11 is that at concentrations above CMC, all the mobility curves show a sudden decline. This could

be attributed to either the smaller diffusion coefficient of the micelles compared to monomers (CTAB:  $5.5 \times 10^{-10} m^2/s$ , TTAB:  $5.73 \times 10^{-10} m^2/s$ , DTAB:  $6 \times 10^{-10} m^2/s$  and  $8.36 \times 10^{-11} m^2/s$  for the micelles)[4] or the slow kinetics of micellar rearrangement to the adsorbed structures at the surface[49]. The mobility data indicates that the degree of binding of counterions to the micelles can be another reason for a drop in the mobility. This possibility can be supported by comparing the rate of mobility reduction ( $d\mu_{CTAB}/dc = 0.52$ ,  $d\mu_{TTAB}/dc = 0.34$ ,  $d\mu_{DTAB}/dc = 0.31$ ) with surfactant concentrations, which is most pronounced with CTAB showing the minimum counterion association (Figure 5.10 inset). Our data suggests that, in the linear region, the mobility slope increases with the chain length  $n_c$ , with  $n \geq 1$ . This correlation is presented in Figure 5.12 as:

$$\frac{d\mu}{d\log(c)} = -0.5n_c + 3.1 \quad (5.6)$$

## 5.9 Estimation of cohesive energy of adsorption

Adsorption of the hydrophobic chain of surfactants is assisted by the hydrophobic interactions between the adjacent alkyl chains. This effect becomes significant above a certain concentration at which the zeta potential (or mobility) increases significantly. The adsorption density  $\Gamma$  [moles/cm<sup>2</sup>] in the inner Stern-Grahame plane is given as[40]:

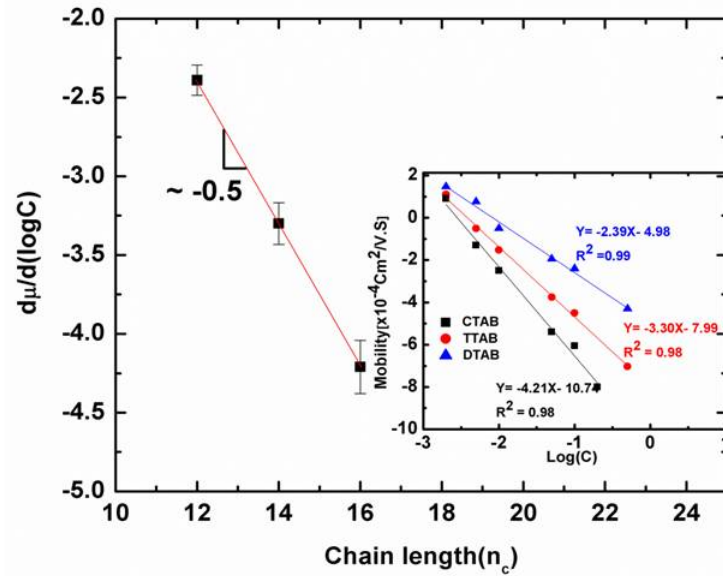


Figure 5.12: Variation of the slope of the mobility curve as a function of alkyl chain length. The inset shows the linear portion of the mobility curve plotted with logarithmic scale of concentration. Solid lines represent linear fits.

$$\Gamma = 2cr \exp\left(\frac{-zF\zeta + n_c\varphi}{K_B T}\right) \quad (5.7)$$

where  $c$ ,  $r$  and  $z$  are the concentration, the radius and the charge of adsorbed ion respectively, and  $n_c$  is the number of carbons in the alkyl chain.  $F$  is the Faraday constant and  $\zeta$  is the potential at the plane of adsorbed counter ions. The first term in the exponential accounts for the electrostatic contribution and the second term accounts for the cohesive or Van der Waals energy  $\varphi$  per mole  $\text{CH}_2$  adsorbed. This energy is associated with the removal of the alkyl chain from the aqueous solution and its adsorption at the solid-liquid interface. If the potential after the association of alkyl chains is extrapolated to zero, then Eq 5.7 deduces to [122, 90]:

$$\ln c = \frac{-n_c \varphi}{K_B T} - \ln \frac{2r}{\Gamma} \quad (5.8)$$

With the assumption of adsorption density at  $\zeta = 0$  being independent of chain length, the natural logarithm of the concentration of alkyl surfactant ions at  $\zeta = 0$  is a linear function of the alkyl chain length with a slope equal to  $\varphi/K_B T$ . Our results show that for alkyltrimethyl ammonium bromides (C12 to C16) adsorbed on the hydrophobic surface of PMMA the Van der Waals energy is approximately  $0.114K_B T$  as shown in Figure 5.13.

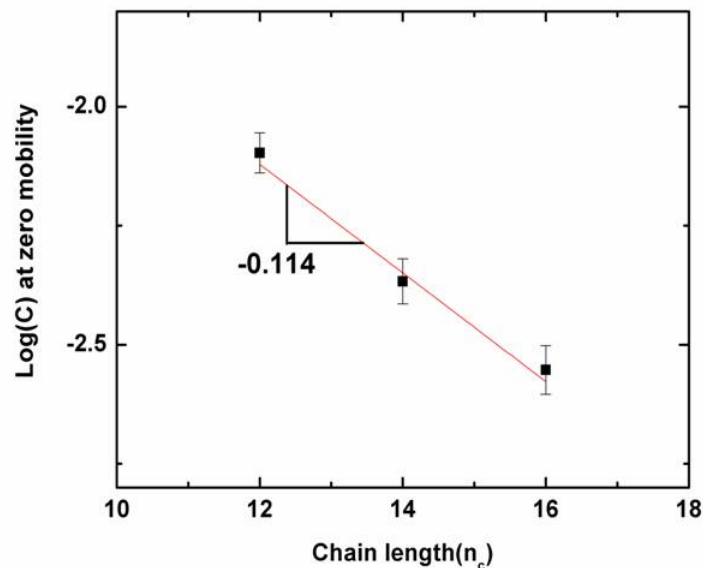


Figure 5.13: Variation of the concentration of alkyltrimethyl ammonium bromides at zero-mobility as a function of alkyl chain length.

A value of  $0.97K_B T$  and  $0.68K_B T$  was reported for the adsorption of alkylammonium acetates (C10 to C18) on quartz and alkyltrimethyl ammonium bromides (C8 to C16) on lysozyme[90] respectively. The reduction of the Van der Waals energy is likely due to the hydrophobic surface of PMMA facilitating the adsorption of alkyl

chains through hydrophobic interactions.

## 5.10 Mechanism of surfactant adsorption on PMMA

In order to explain the adsorption mechanism of the surfactants to PMMA surface, it is important to understand the surface chemistry of PMMA. At neutral and alkaline pH, PMMA exhibits a negative zeta potential with values ranging from -10mV to -20mV in 10mM KCl[140, 37]. The origin of the surface charges is argued to arise from the adsorption of hydroxide ions due to the enhanced autolysis of water at the hydrophobic surface and is independent of anions in the electrolyte solution[10]. Both hydrogen bonding and Van der Waals forces (hydrophobic interactions) have been reported as the possible mechanism of surfactant adsorption on PMMA surface[37, 30]. Even though PMMA is hydrophobic, the direction of EOF confirms that its surface is slightly negative and electrostatically attracts  $K^+$  ions as shown in figure 5.14(a). Due to the existence of surface charges and the hydrophobic nature of PMMA, both electrostatic and hydrophobic interactions contribute to the adsorption of surfactant molecules. At low concentrations (constant mobility), surfactant monomers are either electrostatically adsorbed with the positive head group or hydrophobically with the hydrophobic chain(Figure 5.14(b)). The orientation of the adsorbed molecules changes from parallel to vertical[2], as the concentration increases, allowing for formation of a packed monolayer at the surface (Figure 5.14(c)). This corresponds to the linear region of the mobility curve. The exact orientation of surfactant molecules at saturation point of the surface is debatable. This point corresponds to a plateau

in mobility curve. It is speculated that surfactants form hemimicelles, or bilayers at saturation concentrations[8, 5, 96](Figure 5.14(d)). It is important to note that this saturation occurs at concentration below the bulk CMC of the surfactants. Correlations between surfactant adsorption and surface charges have been studied on hydrophilic silica[44]. It was shown that at low electrolyte and low surfactant concentration the surface charge and adsorption isotherms are almost identical. This observation suggests that at monomeric concentrations (below CMC) the adsorption of each surfactant molecule imparts a single charge on the surface. At concentrations above the charge compensation point (ccp) where the substrate surface charges are neutralized by the adsorption of surfactants, no significant change in surface charge was observed whereas the adsorbed surfactant concentration continued to increase[5]. It is speculated that the increase in adsorption is facilitated by formation of a bilayer through the hydrophobic interactions between the chains. In this configuration, the additional surfactant molecules are adsorbed with the head groups in the opposite direction (towards the surface) of the formerly adsorbed chains. Given that the surface charge is influenced by the orientation of charged head groups towards the solution, even though more surfactant molecules are adsorbed by their head groups away from the solution, there is no contribution to the surface charge. Based on this result, it can be concluded that the adsorption of surfactants at low concentrations is governed by electrostatic adsorption, however at higher concentrations the driving force is hydrophobic interactions. In comparing the adsorption of CTAB, TTAB and DTAB, the degree of hydrophobicity is the driving force and increases with chain length. This is evident by lower CMC values obtained with longer chain surfactants due to

an increase in the aggregation force. The effect of increased hydrophobicity is also confirmed by the displacement of the adsorption isotherms to lower bulk concentrations with longer chained surfactants[5]. This trend was also shown with our results shifting the mobility values to lower concentrations with increasing chain length. The electrolyte counterions do not directly contribute to the adsorption mechanism. However, they change the curvature of the adsorbed hemimicelles by charge screening and reduction of electrostatic repulsion between head groups[129].

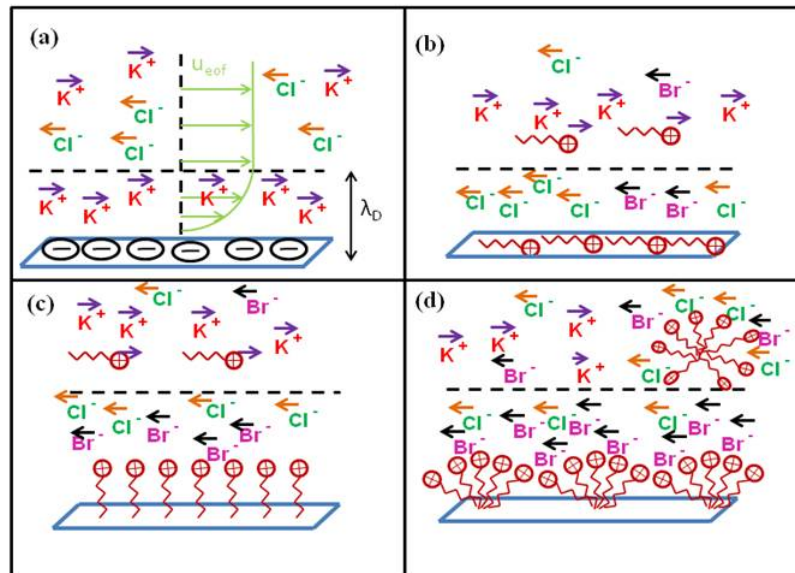


Figure 5.14: (a) Electro-osmotic flow in KCl electrolyte.(b) Monomeric surfactant adsorption through electrostatic and hydrophobic interactions.(c) Transition from dilute to packed surfactant monolayer at higher concentrations.(d) Formation of hemimicelles above critical micelle concentration (CMC).

## 5.11 Conclusions

EK properties at the solid-liquid interface are greatly influenced by the adsorption of surfactants and thus can be utilized in understanding the adsorption mechanism. In studying the effect of surfactant charge, our results show that ionic and non-ionic surfactant act oppositely by increasing and decreasing EOF respectively. Surface saturation occurs at a concentration much smaller than the bulk CMC. For SDS and CTAB, increase in the charge density at the surface results in higher EOF mobilities. In the case of Brij35, EO mobility is reduced due the shielding of PMMA charges by Brij35. In binary surfactant systems of SDS/CTAB and SDS/Brij35, the concentration of SDS was kept constant at the saturation point (0.5mM). We showed that addition of an oppositely charged surfactant such as CTAB significantly reduces EOF at equimolar concentration by neutralization of charges. In comparison to CTAB, addition of Brij35 to SDS does not suppress EOF as effectively, but it reduces EOF at concentrations less than CTAB. We also presented the result of PMMA capillary coating with neutral polymers PDMA and HPMC, focusing on 8mM SDS concentration used in microchip analysis and showed that HPMC at 0.1% reduced EOF by 50% where 2% PDMA had no effect. Furthermore, addition of 4mM Brij35 to 8mM SDS solution had a similar effect as 0.1% HPMC in suppressing EOF by 50%. Considering the effect of chain length, we have demonstrated that the adsorption of cationic alkyl bromide surfactants on the hydrophobic PMMA surface follows three main steps as a function of concentration. In the first step, adsorption of low concentration surfactants neutralizes some of the negative surface charges on the PMMA surface and

decreases the magnitude of the mobility. As more surfactant molecules are adsorbed, the surface charge changes from negative to positive, reversing the direction of EOF from cathodic to anodic. The magnitude of EOF mobility increases linearly with concentration in the second step of the adsorption model. Finally, at higher concentrations, the surface is saturated by formation of hemimicelles which is marked as the third step in the adsorption model. It is important to note that surface saturation occurs below the bulk CMC. In addition, a slight decrease in mobility is observed above CMC due to either lower diffusion coefficient of micelles compare to monomers or the rearrangement of micelles to form hemimicells at the surface. As zeta potential and EO mobility are closely related under the applied experimental conditions, EO mobility values can be used to measure the Van der Waals energy between the alkyl chains of the surfactants. Based on our experimental results, this energy is less than the reported values in the literature, possibly due to the hydrophobic nature of PMMA surface. Comparing EO mobility values of three alkyltrimethyl ammonium bromide surfactants with different chain length, we showed that the mobility curve is shifted to lower concentrations with longer chain length as the hydrophobic interactions between the surfactant chain length and PMMA surface are enhanced. More importantly, EO mobility increases linearly with the chain length. Finally, our work highlights the effect of surfactant structure on EO mobility in PMMA microcapillaries and can be used in understanding the electrophoretic separation of biomolecules in polymeric based microfluidic devices.

# Chapter 6

## Dispersion of a semi-infinite suspension plug under oscillatory flow

### 6.1 Abstract

We have investigated the dispersion of a semi-infinite suspension plug of particles inside a capillary, subjected to an oscillatory flow. The plug is created inside a vertical capillary filled with particle-free fluid. The transient growth of the suspension front is measured at the end of each oscillation cycle. The dispersion of the plug is studied at three volume fractions( $\phi$ ) 1%, 24% and 42% and at different strain amplitudes( $\gamma$ ) ranging from 0.7 to 5.4. Our experimental results show that the plug extension significantly increases after the first cycle. However, the growth is more gradual and follows a linear trend for the following consecutive cycles. In comparing the effect of

$\phi$ , particles at  $\phi = 1\%$  display a reversible behavior even at high strain amplitudes. The transition to an irreversible state occurs at smaller  $\gamma = 1.7$  for  $\phi = 42\%$ , versus  $\gamma = 2.4$  for  $\phi = 24\%$ . In addition the extension of the plug is more pronounced with  $\phi = 42\%$  at higher  $\gamma$  values (0.4 to 0.8) compared to  $\phi = 42\%$ (0.3-0.4).

## 6.2 Introduction

Dispersion of a plug of biological cells/particles in microfluidic devices is an important area of research. Many applications such as cell sorting and particle synthesis consist of multiple steps in which the plug is diluted by addition of necessary reagents or buffers. Further dilution minimizes the detection intensity, as the sample concentration/cell number is often limited. In addition, the dispersion is enhanced in microscale geometries, due to the effects of channel walls and the hydrodynamic interactions between the particles. To this end, the design of a dilution channel that limits the dispersion of the plug is crucial in microfluidic fabrication. Non-Brownian particles in a concentrated suspension experience a time-dependence rheological response as a result of hydrodynamic interaction between particles in low Reynolds number regimes. Among these responses is the irreversible particle migration in a suspension under non-homogenous shear flow, first observed in the pioneering work of Gadala-Maria and Acrivos and later by Leighton and Acrivos[41, 75]. The existence of this phenomenon has been acknowledged in various flow systems such as pressure driven flow between flat plates, cylindrical tubes and between rotating, concentric cylinders[72, 105, 80, 17] and in oscillatory flow of suspensions[106]. Understanding

the non-hydrodynamic particle interaction provides significant insights in modeling rheology of suspensions and the nature of particle migration. Due to the importance of this class of fluids in chemical, biological and industrial application, numerous theoretical and experimental studies have been directed towards understanding the dispersion of suspension fluids[46, 86, 117, 153]. These studies show that the onset of irreversibility strongly depends on the initial conditions, such as the volume fraction and the strain amplitude. Even though valuable insights have been obtained from numerous experimental and simulation studies, the significant volume of these studies have focused on fully populated suspensions[17, 46, 62, 104, 28, 39]. To the best of our knowledge, no study on the dispersion of a semi-infinite suspension plug has been reported. This class of suspension plug mimics the mixing of suspension solution with the clear fluid (particle free) on a microchip, at the cross section of the two channels. The dispersion of the suspension plug can be minimized in an oscillatory flow versus constant flow in one direction. In this paper, we study the transient dispersion of a semi-infinite suspension plug in an oscillatory flow inside a capillary filled with the clear fluid. We focus on the transient effects by minimizing the entry length of the plug in order to analyze the short scale behavior of the plug. This phenomenon is studied at three suspension volume fraction (1%, 24% and 42%) under different strain amplitudes.

### 6.3 Experimental Method

Spherical paramagnetic particles (Spherotech Inc.) with  $100\mu\text{m} \pm 10$  diameter and  $1.58\text{g/cc}$ (Figure 6.1A) density were suspended in a solution consist of DI water and poly(ethylene glycol-rar-propylene glycol) monobutyl ether(UCON lubricant 50-HB-5100, Sigma-Aldrich), with  $170\text{ cP}$  viscosity measured at room temperature ( $22^\circ\text{C}$ ) by a rheometer(AR 2000, TA instruments). A glass capillary ( $1.16\text{mm ID}$ ,  $10\text{cm}$  length) was vertically secured in place and connected to a programmable syringe pump(PhD 2000, Harvard Apparatus) at the top. The pump was programmed with continuous infuse/refill cycles, generating a sinusoidal flow wave. Figure 6.1B shows the position of a tracer particle subjected to a continuous flow cycle with  $Q = 20\mu\text{l}/\text{min}$  and  $40\text{ sec}$  time period( $T$ ). The experimental values are in a good agreement with the fitted sine curve.

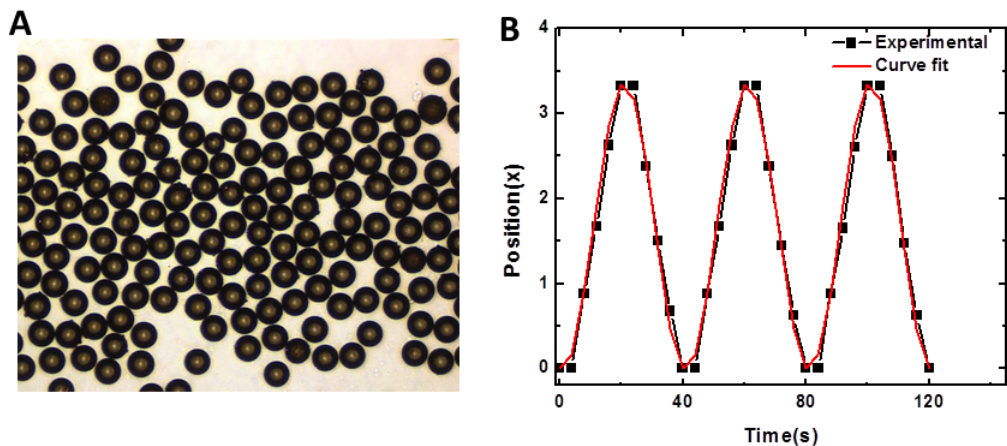


Figure 6.1: A: Paramagnetic spheres( $10\times$  Obj). B: Particle position as a function of time. Condition:  $Q = 20\mu\text{l}/\text{min}$ ,  $T=40\text{ sec}$ .

The capillary was filled with clear fluid(particle-free) with a small meniscus at

the bottom. This end was immersed in the suspension solution. The suspension was drawn into the capillary until a visible parabolic profile was observed. The semi-infinite suspension plug was then subjected to a continuous oscillatory flow at different strain amplitudes. Figure 6.2 shows the schematic of this set up.

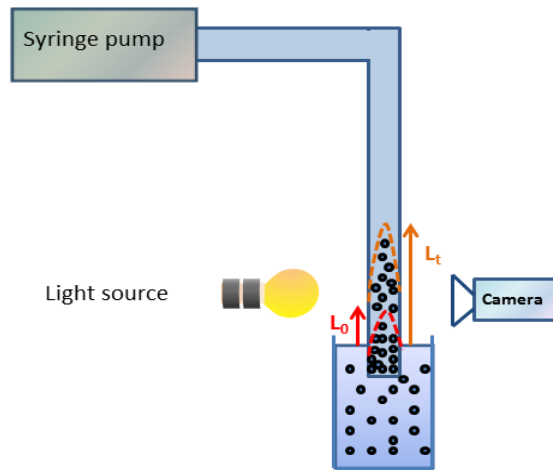


Figure 6.2: The glass capillary is connected to the syringe pump at one end, while the other end is placed vertically in the suspension solution. The semi-infinite plug is subjected to oscillatory flow for the duration of half period( $T/2$ ) in each direction at a set flow rate. Images are taken with a CCD camera at the end of each oscillation cycle.

### 6.3.1 Image Analysis

The capillary is positioned between a CCD camera(6.5X, 2.23mm field of view) and an illumination source. Images of the suspension front were taken at the end of each oscillation cycle. The plug length was determined after processing the images by Image J(Figure 6.3).

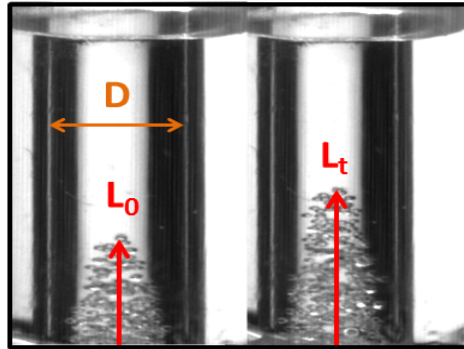


Figure 6.3: Image analysis by measuring the plug extension at the maxima of the parabolic profile.  $L_0$  and  $L_t$  are plug length at  $t = 0$  and  $t$  at the end of one cycle.  $D$  is the capillary diameter.

## 6.4 Theory

The flow rate is quantified with a dimensionless Peclet number as the ratio of shear induced to Brownian motion:

$$Pe = \frac{6\pi\eta\dot{\gamma}a^3}{K_B T} \quad (6.1)$$

where  $\eta$  is the fluid viscosity,  $\dot{\gamma}$  is the shear rate,  $a$  is the particle radius,  $K_B$  is Boltzmann constant, and  $T$  is the absolute temperature.

For flow inside a capillary, average shear rate is defined as:

$$\dot{\gamma} = \frac{2U_B}{R} \quad (6.2)$$

where  $U_B$  is the bulk flow velocity, and  $R$  is the capillary radius. Strain amplitude is given as  $\gamma = \frac{\dot{\gamma}T}{4}$ , where  $T$  is the oscillation period.

The required distance( $L$ )for a fully developed flow for shear-induced particle migration can be estimated as[17]:

$$\frac{L}{R} \sim 0.1 \frac{R^2}{a^2} \quad (6.3)$$

where  $R$  is the capillary radius, and  $a$  is the particle radius.

## 6.5 Results and Discussion

Suspension of particles were prepared at three volume fractions  $\phi = 1\%$ ,  $24\%$  and  $42\%$ . The high viscosity of the solution (170 cP) resulted in a settling velocity of  $\sim 10^{-8}$  mm/s. The large Peclet number calculated under the applied experimental conditions ( $\sim 10^7$ ) Eq. 6.1 ensures that the shear induced motion is dominant. Therefore, the Brownian diffusion of the particles can be neglected. After forming a visible suspension meniscus inside the capillary ( $\sim 4$  mm from the capillary entrance), the semi-infinite plug was subjected to forward and backward flow in a continuous cycle. The dynamics of plug extension was analysed at different strain amplitudes ranging from  $\gamma = 0.7 - 5.4$ . Furthermore, the results were compared at equal strain amplitudes  $\gamma = 2.7$  obtained by varying flow rate or time periods, using Eq. 6.2 ( $Q_1 = 10 \mu\text{l}/\text{min}$ ,  $T_1 = 20 \text{sec}$  and  $Q_2 = 20 \mu\text{l}/\text{min}$ ,  $T_2 = 10 \text{sec}$ ). Flow rates of  $10 \mu\text{l}/\text{min}$  and  $20 \mu\text{l}/\text{min}$  were chosen to ensure Stokes flow condition where Reynolds number  $Re \ll 1$ . The distance for fully developed flow was estimated by Eq. 6.3 as  $L = 7.8 \text{mm}$ , for capillary radius  $R = 0.58 \text{mm}$  and particle radius  $a = 0.05 \text{mm}$ . The suspension plug was formed at  $\sim 4$  mm of the capillary entrance, shorter than the length required for a fully developed flow.

At a dilute concentration,  $\phi = 1\%$ , a clear parabolic profile is not observed inside

the capillary. The average displacement of the particles is presented in Figure 6.4 in terms of dimensionless numbers,  $L/D$ , and  $N$ , where  $L$  is the plug length,  $D$  is the capillary diameter and  $N$  is the number of cycles.  $L$  is normalized by subtracting the initial length( $L_0$ ). At small  $\phi$ , there is no significant change in the position of the particles at different strain amplitudes due to minimum hydrodynamic interactions between the particles. Therefore, the position of the particles remained reversible even by increasing the strain amplitude.

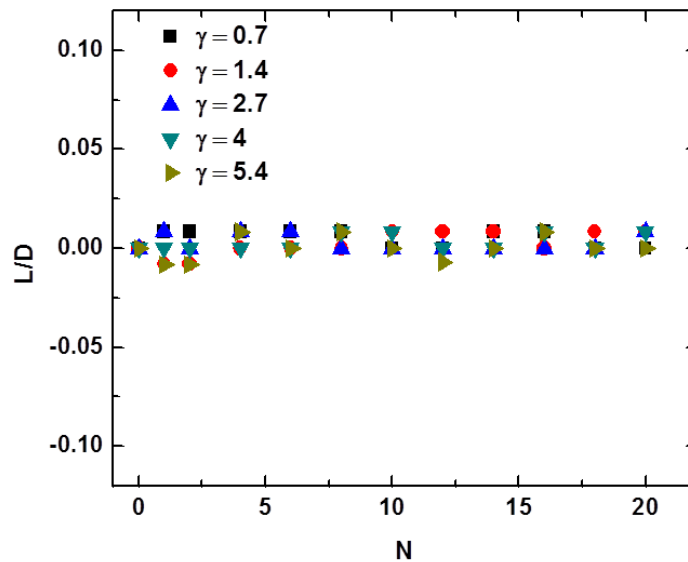


Figure 6.4: Average position of particles at  $\phi = 1\%$  at different strain amplitudes. The average shear rate varies from  $0.3s^{-1}$  to  $1.1s^{-1}$ , corresponding to  $5\mu l/min$ ,  $T = 10$  sec to  $20\mu l/min$ ,  $T = 20$  sec.  $N$  is the number of cycles,  $L$  is the plug length and  $D$  is the capillary length. Two sets of data for  $\gamma = 2.7$  was obtained by varying the flow rate and time period. The asterisk shows the resulting strain amplitude at  $20\mu l/min$  and  $T = 10$ .

A clear parabolic profile of particles was observed at higher  $\phi$ . Figure 6.5 shows the transient growth of the suspension front at 24% volume fraction. At the end of the first cycle there is a significant increase in plug extension for each  $\gamma$ . This could be the result of the entry effect induced by the particles or the viscous fluid. The transport

of the particles from the large geometry to a confined capillary creates a pressure gradient. As a result, more particles are drawn into the capillary. However, a gradual linear increase in the plug extension is observed after the first cycle at  $\gamma > 1.4$ . At  $\gamma = 0.7 - 1.4$ , the position of the plug remains approximately reversible. However, the plug transition to an irreversible state is archived at higher volume fractions by a gradual increase in plug length. In an study by Metzger and Butler[86], the extension of a cloud of particles in a clear solution was studied under periodic shear flow. They have reported that at  $\phi = 30\%$ , a cloud of particles with  $200\mu\text{m}$  diameter shows reversible behavior even at  $\gamma = 6$ . In comparison, our results show that the transition to an irreversible states occurs at  $\gamma = 2.7$  for a semi-infinite plug. The confinement of the plug by the capillary wall and the entry effects could contribute to this difference. In comparing the two equal strain amplitudes at  $\gamma = 2.7$ , a good agreement between the results shows that the plug behavior is only influenced by the strain value, independent of how the strain is defined by tuning either the flow rate or time period.

In order to further investigate the effect of volume fraction on the dispersion of the plug, we studied the dispersion of the plug at  $\phi = 42\%$ . Plug extension was enhanced due to increasing the interactions between the particles at higher concentration as shown in Figure 6.6. Compare to  $\phi = 24\%$ , the plug transition to an irreversible state occurs at smaller  $\gamma = 1.4$ . The extension of the plug increases by increasing  $\gamma$ , however the growth in length is more significant compared to  $\phi = 24\%$ . The plug extension after the first cycle for  $2.7 < \gamma < 5.4$  at  $\phi = 24\%$  varies from  $\sim 0.3 - 0.4$ , whereas this range increases to  $\sim 0.4 - 0.8$  at  $\phi = 42\%$ . This irreversible behavior

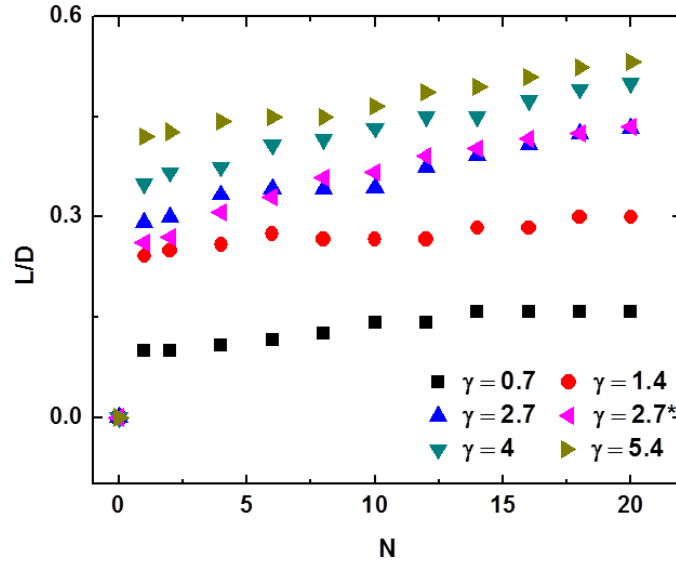


Figure 6.5: The transient growth of the semi-infinite suspension plug at 24% volume fraction at different strain amplitudes. The average shear rate varies from  $0.3s^{-1}$  to  $1.1s^{-1}$ , corresponding to  $5\mu l/min$ ,  $T = 10$  sec to  $20\mu l/min$ ,  $T = 20$  sec.  $N$  is the number of cycles,  $L$  is the plug length and  $D$  is the capillary length.

was also reported by [86], for a cloud of particles at  $\phi = 40\%$ .

At low strain amplitude the parabolic profile of the suspension front is persevered during the oscillations, as shown in Figure 6.7 A for the case of 42% volume fraction at 2.72 strain amplitude. However at higher strain amplitudes this profile is not maintained at  $\gamma > 5.4$ . Figure 6.7 B and C show the shape of the plug at  $\gamma = 6.8$  and  $\gamma = 8$  respectively.

Figure 6.7 shows that the transition between a full parabolic profile to when this profile is not maintained occurs at  $\gamma = 6.8$ . In a concentrated suspension, under Poiseuille flow a flux of particles towards the capillary wall is generated by particle stresses and pressure. At high strain amplitudes, by reversing the flow direction, particles which have migrated towards the capillary wall flow with at smaller velocity and change the plug profile.

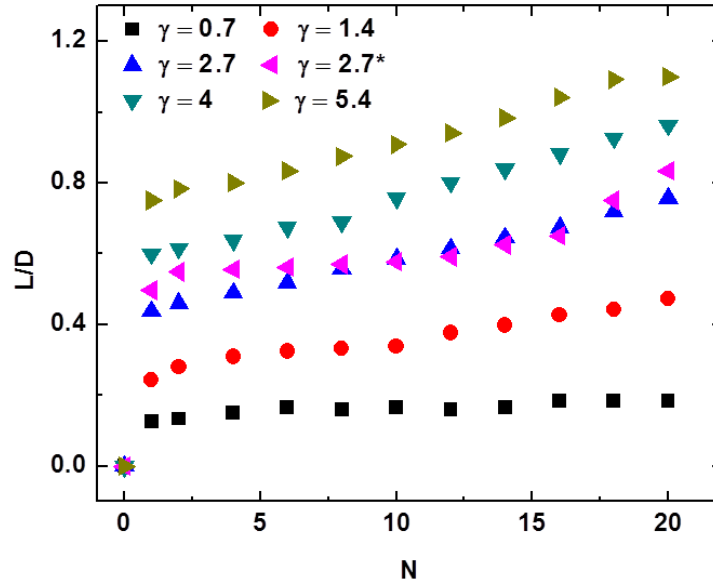


Figure 6.6: The transient growth of the semi-infinite suspension plug at 42% volume fraction at different strain amplitudes. The average shear rate varies from  $0.3s^{-1}$  to  $1.1s^{-1}$ , corresponding to  $5\mu l/min$ ,  $T = 10$  sec to  $20\mu l/min$ ,  $T = 20$  sec.  $N$  is the number of cycles,  $L$  is the plug length and  $D$  is the capillary length.

## 6.6 Conclusions

The transient (short time scale) dispersion of a semi-infinite plug in an oscillatory flow was studied in a clear fluid inside a capillary. Our results show that the dispersion is enhanced by at higher volume fractions. This is evident by an increase in plug extension from  $\phi = 24\%$  to  $\phi = 42\%$ . Furthermore, the plug displays an irreversible behavior by increasing  $\gamma$ . This was observed at by  $\gamma = 1.4$  at  $\phi = 42\%$ , whereas the transition occurred at higher strain amplitude,  $\gamma = 2.7$  for  $\phi = 24\%$ . Strain amplitude can be tuned by changes in the flow rate or the time period of oscillations. A good agreement between the result obtained at equal  $\gamma = 2.7$ , measured at different flow rates ( $10\mu l/min$  and  $20\mu l/min$ ) shows that the dispersion of the plug is a function of the magnitude of the strain amplitude, regardless of how this value is set. At 1% volume fraction, no significant change in the position of the particles indicates

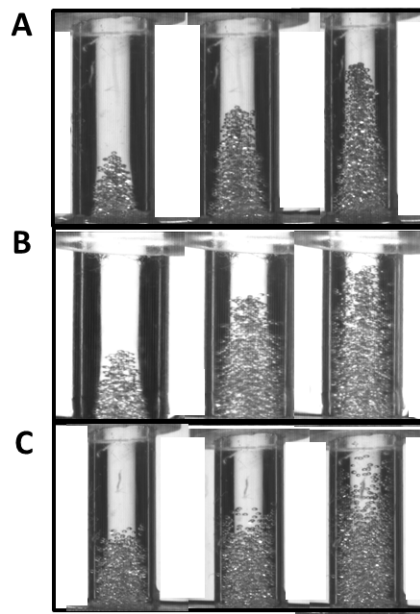


Figure 6.7: Profile of the suspension plug at cycles 2, 5 and 10. A :  $\gamma = 2.7$ , B:  $\gamma = 5.6$  and C:  $\gamma = 8$  for suspension with  $\phi = 42\%$ .

a reversible behavior even at higher strain amplitudes. This is due to minimum hydrodynamic interactions between the particles. As the volume fraction of particles increases (24% and 42%), a linear growth in the suspension front is observed with a significant increase in the plug length at the end of the first cycle. This observation can be attributed to the entry effects due to the particle-particle interactions or the high viscosity of the fluid. Our results show that the dispersion of a semi-infinite plug is a function of volume fraction( $\phi$ ) and the strain amplitude( $\gamma$ ). However, the dispersion is also affected by the capillary wall effects and the short entrance length.

## 6.7 Acknowledgement

Support for this work from the National Science Foundation under award number CBET 1133106 is gratefully acknowledged.

# Chapter 7

## Conclusions

The advantages of miniaturization and integration by microfluidics, as powerful analytical tools, are well established including speed, atomization, parallelization, portability and small sample volume. However, compared to conventional macroscale devices, fluid behavior is significantly different in small geometries. In microscale, fluid transport is governed by viscous forces, interfacial effects and diffusion. Therefore, understanding and controlling these effects is essential for improving the design and optimization of microfluidics.

The integration of protein electrophoresis on a microchip has allowed for rapid analysis of multiple samples. However, quantification of proteins based on the fluorescence intensity has not been achieved in the current designs. Furthermore, no optimum SDS concentration after dilution of protein–surfactant complex has been established. In electrophoresis, SDS is added at saturation (above CMC) in order to first unfold the protein coil and then create a constant charge to mass ratio where the structural differences in protein structure can be neglected. A hydrophobic fluorescent

dye is added to the protein-SDS complex in order to detect the fluorescent contribution of the protein, without the ability for parallel quantification. We hypothesize that quantification of proteins can be achieved by tuning the properties of the fluorescent dye. Towards this goal, in chapter 2 we analyzed the interactions of protein-SDS complex at different concentrations, using sypro orange as the hydrophobic fluorescent dye. The presented results showed that the protein peak height (fluorescence intensity) correlates with protein concentration if the dye quantum yield is constant. Optimum SDS concentration was found at 3mM (below CMC), where there are no free SDS micelles in the solution. At this concentration only bound micelles contribute to the overall fluorescence. Furthermore, a fluorescence model was proposed based on the interaction of dye with free and bound SDS micelles and was in a good agreement with the experimental results. Finally, the effect of addition of CTAB, as a cationic, more hydrophobic surfactant was studied. This is important as CTAB can be used in surface modification of microfluidics in order to reduce the undesirable effects of electroosmotic flow (EOF). Our results showed that protein peak was shifted to 4mM SDS by addition of CTAB at mole fractions above 0.1. At lower concentrations (0.5mM and 0.9mM), CTAB did not affect the dynamics of protein-SDS interactions and can be safely added in protein electrophoresis for dynamic surface modification. In chapter 2, we established that even though SDS binds to proteins with a constant stoichiometry, dye molecules behave differently with protein bound surfactant micelles. This means that the quantum yield of the dye and its fluorescence intensity varies with protein structure. Therefore, in the current designs the dye is added merely as a marker in detecting the protein peak without any correlation with

the sample quantity. A variety of fluorescent dyes should be studied in order to find an optimum dye for separation and quantification of proteins.

Even though microfluidic protein electrophoresis has been long established for separation of proteins, it can be used for detection of certain protein targets when combined with another analytical tool such as immunodepletion. The combination of these two techniques in comparison to the conventional tools such as Western blot, allows for parallel detection and quantification of multiples samples in orders of minutes versus hours or even days. In chapter 3, we presented a rapid and simple method for parallel detection and quantification of proteins by a combination of microchip electrophoresis and immunodepletion. First, the target is isolated using magnetic beads coated with an antibody against the target. After collecting the beads, the supernatant and the untreated sample(control) are simultaneously analyzed on a protein microchip electrophoresis. The target was detected by the depleted band visible on the electrophoresis gel. Quantification was achieved parallel to detection using the electropherograms(area under peak). Even though, analysis time is significantly improved in detecting the target compared to conventional detection techniques, this method is limited by factors such as concentration of the target, non-specific binding of other proteins present in the sample, and the concentration limit of the Bioanalyzer device. The target protein can not be detected if its concentration is much smaller than other proteins in the solution or has similar molecular weight as other proteins present due to the overlap of protein peaks. Sample treatments such as pre-concentration or isolation of target by antibody-antigen techniques can significantly improve the limitations of low concentration when used prior to the analysis by this

method.

Mild and low cost bacterial treatment is essential in minimizing bacterial contaminations in food products. To this end, bio compatible polymers such as chitosan can be safely utilized in combination with other mild treatment techniques such as low voltage pulsed electric field. In chapter 4, we explored the synergistic effect of chitosan microparticles(CSMP) with a low voltage pulsed electric field in inhibiting *E.coli* as a gram-negative bacteria. Chitosan as a positively charged polymer exhibits antibacterial properties by flocculating and inhibiting gram-negative bacteria at acidic pH. Short, high-voltage pulses on the nanosecond time scale is another effective method in bacteria inhibition when fields greater than approximately 16 kV/cm is applied. We showed that these techniques can be applied synergistically in order to provide a mild, low energy and bio compatible method for inactivating bacteria at neutral pH and lower intensity of electric field(100V/cm). These results can be applied in developing antibacterial methods for fresh and fresh-cut produce where low energy and bio compatible techniques are required. As a continuous study we hypothesise that the electric field can be eliminated by enhancing the efficiency of chitosan particles through addition of antibacterial peptides(lysine)that can be linked to the surface or encapsulated in these particles.

In recent years, polymeric devices have gained increasing attention as substitutes for glass microchips, mainly due to low cost. However, the surface charges of polymeric materials is not well known compare to glass substrate. One of the main challenges is the control of electroosmotic flow(EOF) which is a function of surface charges. Dynamic coating by surfactants provides a simple and low cost method for

surface modification and control of EOF. In chapter 5, we studied the influence of adsorption of surfactants on the electrokinetic properties of poly methylmethacrylate (PMMA) as a polymeric substrate for microchip fabrication. Our results showed that adsorption of neutral surfactant and polymers such as Brij35 and hydroxypropyl methyl cellulose (HPMC) significantly reduces the electroosmotic mobility in a PMMA microcapillary. Due to the neutral nature, Brij35 and HPMC can be safely added in dynamic coating of plastic microchips in protein electrophoresis with minimum influence on the dynamics of SDS-protein interaction. In exploring the effect of surfactant chain length, the kinetic of adsorption of surfactants on a hydrophobic substrate such as PMMA increased by chain length (hydrophobicity). Based on the presented results, we hypothesize that non-ionic (neutral) surfactants with a long chain length are the most effective additives for surface modification of polymeric microchips, allowing for performing the electrophoresis of proteins on polymeric devices. These results are not limited to PMMA, and can be applied to other optically clear polymers such as polycarbonate (PC) or poly dimethyl siloxane (PDMS).

Apart from the electrokinetic interactions, fluid transport in microfluidic is influenced by interfacial interactions. Dispersion of suspension particles is of special interest in biological applications such as cell sorting and sizing where a plug of cells is analyzed on a microfluidic chip. Multiple dilution steps integrated on a microchip for addition of specific reagents significantly affect the concentration of the cell plug by minimizing the detection sensitivity. To this end, a fundamental understanding of the dispersion behavior of a suspension plug is needed for an optimum design of a microchip where minimum reduction in concentration of a sample plug is desirable.

Even though numerous experimental and simulation studies have investigated the dispersion of a fully populated suspension of particles, no study on the dispersion of a plug or semi-infinite plug of particles has been reported. Moreover, the effect of channel wall and the entry length on the dispersion of a suspension plug in a microchannel needs to be addressed. In chapter 6 we investigated the transient dispersion of a semi-infinite suspension plug of particles in a continuous oscillatory flow as a function of strain amplitude( $\gamma$ ) and suspension volume fraction( $\phi$ ). Compared to a continuous unidirectional flow, oscillation of the plug in a forward and backward motion can significantly reduce the rate of dispersion inside the channel. Our results showed that the dispersion of a suspension plug can be minimized in an oscillatory flow by reducing the strain amplitude(small flow rates) or the concentration of the cell plug inside a microchannel. Therefore in design of dilution channels, minimum reduction in concentration of a plug of particles can be achieved in an oscillatory flow at low shear rates and volume fractions.

# Appendix A

## Dispersion of a suspension plug formed by magnetic sweeping

### A.1 Experimental Method

Spherical paramagnetic particles(Spherotech Inc.) with  $100\mu\text{m} \pm 10$  diameter were suspended in Newtonian fluid composed of DI water with 1mg/ml bovine serum albumin(BSA), Potassium iodide(KI, 8M) and polyethylene glycol(UCON lubricant 50-HB-5100, Sigma-Aldrich). The mixture has a viscosity of 2.95 cP as measured in room temperature ( $22^\circ\text{C}$ ) by a rheometer(AR 2000, TA instruments). KI was added to match the density of the solution with the particles. A glass capillary (1.16mm ID, 10cm length) connected to a 3-way valve was filled with the particle-free fluid using a syringe pump (PhD 2000, Harvard Apparatus). The direction of the flow was switched to the suspension fluid and magnets were placed around the capillary to form a plug inside the filled capillary by capturing the particles. The plug was

oscillated by programming the pump with continues forward and reverse direction for a preset number of times. The displacement of the particles can be approximated to an oscillatory square wave. The volume fraction of the plug was determined by comparing the volume of captured particles and comparing that with the volume of the formed plug. Figure A.1 shows the schematic of the experimental set up. The magnets where then removed, and the flow direction was switched to the clear fluid (particle-free).

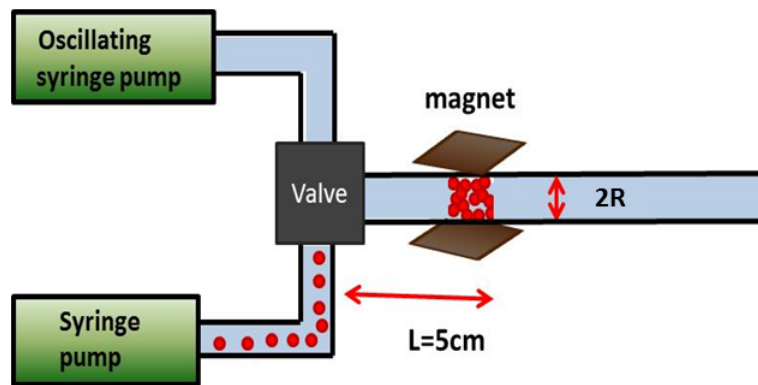


Figure A.1: The apparatus consists of a 3-way valve connected to particle-free syringe pump, suspension syringe pump, and the capillary.

### A.1.1 Image analysis

The plug length is calculated by the grayscale profile of the plug image in Image J as shown in Figure A.2. The capillary is placed horizontally between the camera(CCD, 6.5X optics and 2.23mm field of view) and the illumination source.

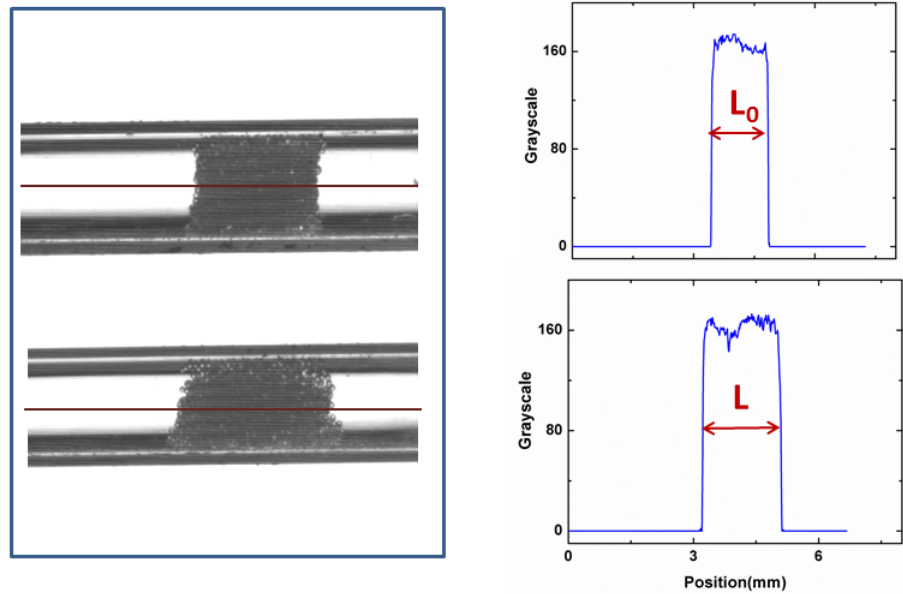


Figure A.2: Determination of the plug width by grayscale in Image J. The grayscale profile corresponds to the line chosen at the middle of the plug.

### A.1.2 Formation of force chains by magnetic sweeping

In a concentrated suspension, particles can form networks of force chains[20]. Under this condition, the particles are in direct contact and even the lubrication films around them can not prevent this contact. Particles in this state act as solid and resist dispersion even at a high shear rate. Our experimental results showed that magnetic sweeping facilitates the formation of these force chains. The response of the plug to the shear flow was significantly minimized. Based on these observations, it was established that the magnetic set up cannot be used in studying the dispersion of a plug of particles. In Figure A.3 the plug extension by time is shown for two volume fractions 33% and 53%. The extension is defined as  $L/L_0$ , where  $L_0$  is the plug length at  $t = 0$ . The volume fraction is calculated by the volume of the beads captured

divided by the total volume of the plug formed.

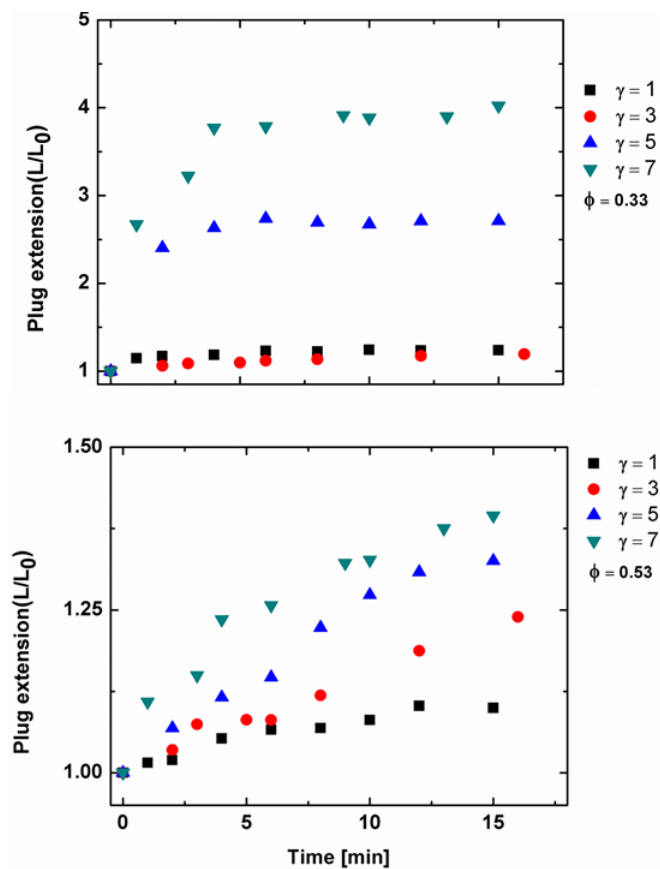


Figure A.3: Plug extension by time for two volume fractions 33% and 53% at various strain amplitudes.

# Bibliography

- [1] M. T. Alegre, M. C. Rodriguez, and J. M. Mesas. Transformation of lactobacillus plantarum by electroporation with in vitro modified plasmid dna. *Fems Microbiology Letters*, 241(1):73–77, 2004.
- [2] S. Alila, S. Boufi, M. N. Belgacem, and D. Beneventi. Adsorption of a cationic surfactant onto cellulosic fibers - i. surface charge effects. *Langmuir*, 21(18):8106–8113, 2005.
- [3] G. Allmaier, E. Herwig, M. Marchetti-Deschmann, C. Wenz, and A. Rufer. Immunoprecipitation combined with microchip capillary gel electrophoresis: Detection and quantification of beta-galactosidase from crude e. coli cell lysate. *Biotechnology Journal*, 6(4):420–427, 2011.
- [4] R. Atkin, V. S. J. Craig, E. J. Wanless, and S. Biggs. The influence of chain length and electrolyte on the adsorption kinetics of cationic surfactants at the silica-aqueous solution interface. *Journal of Colloid and Interface Science*, 266(2):236–244, 2003.

- [5] R. Atkin, V. S. J. Craig, E. J. Wanless, and S. Biggs. Mechanism of cationic surfactant adsorption at the solid-aqueous interface. *Advances in Colloid and Interface Science*, 103(3):219–304, 2003.
- [6] M. Y. Badal, M. Wong, N. Chiem, H. Salimi-Moosavi, and D. J. Harrison. Protein separation and surfactant control of electroosmotic flow in poly(dimethylsiloxane)-coated capillaries and microchips. *Journal of Chromatography A*, 947(2):277–286, 2002.
- [7] J. D. Badjic and N. M. Kostic. Effects of encapsulation in sol-gel silica glass on esterase activity, conformational stability, and unfolding of bovine carbonic anhydrase ii. *Chemistry of Materials*, 11(12):3671–3679, 1999.
- [8] S. Bandyopadhyay, J. C. Shelley, M. Tarek, P. B. Moore, and M. L. Klein. Surfactant aggregation at a hydrophobic surface. *Journal of Physical Chemistry B*, 102(33):6318–6322, 1998.
- [9] S. L. R. Barker, M. J. Tarlov, H. Canavan, J. J. Hickman, and L. E. Locascio. Plastic microfluidic devices modified with polyelectrolyte multilayers. *Analytical Chemistry*, 72(20):4899–4903, 2000.
- [10] J. K. Beattie. The intrinsic charge on hydrophobic microfluidic substrates. *Lab on a Chip*, 6(11):1409–1411, 2006.
- [11] H. Becker and L. E. Locascio. Polymer microfluidic devices. *Talanta*, 56(2):267–287, 2002.

- [12] A. K. Bhuyan. On the mechanism of sds-induced protein denaturation. *Biopolymers*, 93(2):186–199, 2010.
- [13] M. R. Bohmer and L. K. Koopal. Adsorption of ionic surfactants on constant charge surfaces - analysis based on a self-consistent field lattice model. *Langmuir*, 8(6):1594–1602, 1992.
- [14] C. Agay-D. Mari E. Roger T. Chancerelle Y. Boucard, N. Viton. The use of physical hydrogels of chitosan for skin regeneration following third-degree burns. *Biomaterials*, 28:3478–3488, 2007.
- [15] L. Bousse, S. Mouradian, A. Minalla, H. Yee, K. Williams, and R. Dubrow. Protein sizing on a microchip. *Analytical Chemistry*, 73(6):1207–1212, 2001.
- [16] J. Brinck, B. Jonsson, and F. Tiberg. Influence of long-chain alcohols on the adsorption of nonionic surfactants to silica. *Langmuir*, 15(22):7719–7724, 1999.
- [17] J. E. Butler, P. D. Majors, and R. T. Bonnecaze. Observations of shear-induced particle migration for oscillatory flow of a suspension within a tube. *Physics of Fluids*, 11(10):2865–2877, 1999. 233BH Times Cited:20 Cited References Count:25.
- [18] B. Cabane, R. Duplessix, and T. Zemb. High-resolution neutron-scattering on ionic surfactant micelles - sds in water. *Journal De Physique*, 46(12):2161–2178, 1985.

- [19] F. Caruso, T. Serizawa, D. N. Furlong, and Y. Okahata. Quartz-crystal microbalance and surface-plasmon resonance study of surfactant adsorption onto gold and chromium-oxide surfaces. *Langmuir*, 11(5):1546–1552, 1995.
- [20] M. E. Cates, J. P. Wittmer, J. P. Bouchaud, and P. Claudin. Jamming, force chains, and fragile matter. *Physical Review Letters*, 81(9):1841–1844, 1998. 114TY Times Cited:357 Cited References Count:36.
- [21] K. Chattopadhyay and S. Mazumdar. Stabilization of partially folded states of cytochrome c in aqueous surfactant: effects of ionic and hydrophobic interactions. *Biochemistry*, 42(49):14606–14613, 2003.
- [22] H. Y. Chen, Y. H. Dou, N. Bao, J. J. Xu, and F. Meng. Separation of proteins on surface-modified poly(dimethylsiloxane) microfluidic devices. *Electrophoresis*, 25(17):3024–3031, 2004.
- [23] S. Chodankar, V. K. Aswal, J. Kohlbrecher, R. Vavrin, and A. G. Wagh. Surfactant-induced protein unfolding as studied by small-angle neutron scattering and dynamic light scattering. *Journal of Physics-Condensed Matter*, 19(32):–, 2007.
- [24] K. Y. Chun and P. Stroeve. Protein transport in nanoporous membranes modified with self-assembled monolayers of functionalized thiols. *Langmuir*, 18(12):4653–4658, 2002.
- [25] Y. C. Chung and C. Y. Chen. Antibacterial characteristics and activity of acid-soluble chitosan. *Bioresource Technology*, 99(8):2806–2814, 2008.

- [26] Y. C. Chung, Y. P. Su, C. C. Chen, G. Jia, H. I. Wang, J. C. G. Wu, and J. G. Lin. Relationship between antibacterial activity of chitosan and surface characteristics of cell wall. *Acta Pharmacologica Sinica*, 25(7):932–936, 2004.
- [27] K.S Cole. *Membranes, Ions and Impulses*. California Press, Berkeley, 1972.
- [28] L. Corte, S. J. Gerbode, W. Man, and D. J. Pine. Self-organized criticality in sheared suspensions. *Physical Review Letters*, 103(24), 2009. 530YB Times Cited:5 Cited References Count:16.
- [29] F. Dang, L. Zhang, H. Hagiwara, Y. Mishina, and Y. Baba. Ultrafast analysis of oligosaccharides on microchip with light-emitting diode confocal fluorescence detection. *Electrophoresis*, 24(4):714–721, 2003.
- [30] F. Q. Dang, T. Hasegawa, V. Biju, M. Ishikawa, N. Kaji, T. Yasui, and Y. Baba. Spontaneous adsorption on a hydrophobic surface governed by hydrogen bonding. *Langmuir*, 25(16):9296–9301, 2009.
- [31] F. Q. Dang, K. Kakehi, J. J. Cheng, O. Tabata, M. Kurokawa, K. Nakajima, M. Ishikawa, and Y. Baba. Hybrid dynamic coating with n-dodecyl beta-d-maltoside and methyl cellulose for high-performance carbohydrate analysis on poly(methyl methacrylate) chips. *Analytical Chemistry*, 78(5):1452–1458, 2006.
- [32] R. Das, D. Guha, S. Mitra, S. Kar, S. Lahiri, and S. Mukherjee. Intramolecular charge transfer as probing reaction: Fluorescence monitoring of protein-surfactant interaction. *Journal of Physical Chemistry A*, 101(22):4042–4047, 1997.

- [33] S. De, A. Girigoswami, and S. Das. Fluorescence probing of albumin-surfactant interaction. *Journal of Colloid and Interface Science*, 285(2):562–573, 2005.
- [34] S. Descroix, Y. Shakalisava, M. Poitevin, and J. L. Viovy. Versatile method for electroosmotic flow measurements in microchip electrophoresis. *Journal of Chromatography A*, 1216(6):1030–1033, 2009.
- [35] D. C. Duffy, J. C. McDonald, O. J. A. Schueller, and G. M. Whitesides. Rapid prototyping of microfluidic systems in poly(dimethylsiloxane). *Analytical Chemistry*, 70(23):4974–4984, 1998.
- [36] P.D Adams E.A. Golemis. *Protein-Protein Interactions: A Molecular Cloning Manual*. Identification of associated proteins by coimmunoprecipitation. Cold Spring Harbor Laboratory Press, NY, 2002.
- [37] K. Q. Fa, V. K. Paruchuri, S. C. Brown, B. M. Moudgil, and J. D. Miller. The significance of electrokinetic characterization for interpreting interfacial phenomena at planar, macroscopic interfaces. *Physical Chemistry Chemical Physics*, 7(4):678–684, 2005. 902WE Times Cited:16 Cited References Count:65.
- [38] J. C. Fernandes, F. K. Tavora, J. C. Soares, O. S. Ramos, M. J. Monteiro, M. E. Pintado, and F. X. Malcata. Antimicrobial effects of chitosans and chitooligosaccharides, upon staphylococcus aureus and escherichia coli, in food model systems. *Food Microbiology*, 25(7):922–928, 2008.

- [39] M. Frank, D. Anderson, E. R. Weeks, and J. F. Morris. Particle migration in pressure-driven flow of a brownian suspension. *Journal of Fluid Mechanics*, 493:363–378, 2003. 739EG Times Cited:65 Cited References Count:24.
- [40] D. W. Fuerstenau and H. M. Jang. On the nature of alkylsulfonate adsorption at the rutile water interface. *Langmuir*, 7(12):3138–3143, 1991.
- [41] F. Gadalamaria and A. Acrivos. Shear-induced structure in a concentrated suspension of solid spheres. *Journal of Rheology*, 24(6):799–814, 1980. Kw237 Times Cited:244 Cited References Count:10.
- [42] Y. Y. Gao, J. H. Du, and T. R. Gu. Hemimicelle formation of cationic surfactants at the silica-gel water interface. *Journal of the Chemical Society-Faraday Transactions I*, 83:2671–2679, 1987. 8 K0310 Times Cited:123 Cited References Count:30.
- [43] T. P. Goloub and L. K. Koopal. Adsorption of cationic surfactants on silica. comparison of experiment and theory. *Langmuir*, 13(4):673–681, 1997.
- [44] T. P. Goloub, L. K. Koopal, B. H. Bijsterbosch, and M. P. Sidorova. Adsorption of cationic surfactants on silica. surface charge effects. *Langmuir*, 12(13):3188–3194, 1996.
- [45] J. S. Green and J. W. Jorgenson. Minimizing adsorption of proteins on fused-silica in capillary zone electrophoresis by the addition of alkali-metal salts to the buffers. *Journal of Chromatography*, 478(1):63–70, 1989. Au863 Times Cited:266 Cited References Count:20.

- [46] J. S. Guasto, A. S. Ross, and J. P. Gollub. Hydrodynamic irreversibility in particle suspensions with nonuniform strain. *Physical Review E*, 81(6), 2010. 1608ST Times Cited:3 Cited References Count:25.
- [47] K. L. Gudiksen, I. Gitlin, and G. M. Whitesides. Differentiation of proteins based on characteristic patterns of association and denaturation in solutions of sds. *Proceedings of the National Academy of Sciences of the United States of America*, 103(21):7968–7972, 2006.
- [48] EA Gustafson, M Yajima, C Juliano, and GM. Wessel. Post-translational regulation by gustavus contributes to selective vasa protein accumulation in multipotent cells during embryogenesis. *Developmental Biology*, in press, 2010.
- [49] C. Gutig, B. P. Grady, and A. Striolo. Experimental studies on the adsorption of two surfactants on solid-aqueous interfaces: Adsorption isotherms and kinetics. *Langmuir*, 24(9):4806–4816, 2008.
- [50] RC.Tabrizian M. Haidar, ZS. Hamdy. Protein release kinetics for core-shell hybrid nanoparticles based on the layer-by-layer assembly of alginate and chitosan on liposomes. *Biomaterials*, 29(9):1207–1215., 2008.
- [51] Lane D Harlow, E. *Antibodies: A Laboratory Manual*. Cold Spring Harbor, New York, 1999.
- [52] D. J. Harrison, K. Fluri, K. Seiler, Z. H. Fan, C. S. Effenhauser, and A. Manz. Micromachining a miniaturized capillary electrophoresis-based chemical-analysis system on a chip. *Science*, 261(5123):895–897, 1993.

- [53] N. K. Hartley and M. A. Hayes. Examination of theoretical models in external voltage control of capillary electrophoresis. *Analytical Chemistry*, 74(6):1249–1255, 2002.
- [54] M. D. Harvey, D. Bandilla, and P. R. Banks. Subnanomolar detection limit for sodium dodecyl sulfate capillary gel electrophoresis using a fluorogenic, noncovalent dye. *Electrophoresis*, 19(12):2169–2174, 1998.
- [55] R. Haselberg, L. van der Sneppen, F. Ariese, W. Ubachs, C. Gooijer, G. J. de Jong, and G. W. Somsen. Effectiveness of charged noncovalent polymer coatings against protein adsorption to silica surfaces studied by evanescent-wave cavity ring-down spectroscopy and capillary electrophoresis. *Analytical Chemistry*, 81(24):10172–10178, 2009.
- [56] M. He and A. E. Herr. Microfluidic polyacrylamide gel electrophoresis with in situ immunoblotting for native protein analysis. *Analytical Chemistry*, 81(19):8177–8184, 2009.
- [57] I. M. Helander, E. L. Nurmiäho-Lassila, R. Ahvenainen, J. Rhoades, and S. Roller. Chitosan disrupts the barrier properties of the outer membrane of gram-negative bacteria. *International Journal of Food Microbiology*, 71(2-3):235–244, 2001.
- [58] A. E. Herr, D. J. Throckmorton, A. A. Davenport, and A. K. Singh. On-chip native gel electrophoresis-based immunoassays for tetanus antibody and toxin. *Analytical Chemistry*, 77(2):585–590, 2005.

- [59] J. Horvath and V. Dolnik. Polymer wall coatings for capillary electrophoresis. *Electrophoresis*, 22(4):644–655, 2001.
- [60] B. Huang, S. Kim, H. Wu, and R. N. Zare. Use of a mixture of n-dodecyl-beta-d-maltoside and sodium dodecyl sulfate in poly(dimethylsiloxane) microchips to suppress adhesion and promote separation of proteins. *Analytical Chemistry*, 79(23):9145–9149, 2007. 236OH Times Cited:13 Cited References Count:31.
- [61] D.K Symes-K.C Hughes, J. Ramsden. The flocculation of bacteria using cationic synthetic flocculants and chitosan. *Biotechnology Techniques*, 4(1):55–60, 1990.
- [62] L. Isa, R. Besseling, and W. C. K. Poon. Shear zones and wall slip in the capillary flow of concentrated colloidal suspensions. *Physical Review Letters*, 98(19), 2007. 166XD Times Cited:53 Cited References Count:25.
- [63] Jacob N. Israelachvili. Intermolecular and surface forces, 1991.
- [64] S. B. Jacob, H. Masliyah. *Electrokinetic and Colloid Transport Phenomena*. John Wiley & Sons, Inc, Hoboken, New Jersey, 2006.
- [65] S. C. Jacobson, R. Hergenroder, L. B. Koutny, and J. M. Ramsey. Open-channel electrochromatography on a microchip. *Analytical Chemistry*, 66(14):2369–2373, 1994. Nx055 Times Cited:269 Cited References Count:27.
- [66] M. N. Jones. Surfactant interactions with biomembranes and proteins. *Chemical Society Reviews*, 21(2):127–136, 1992.

- [67] W. R. Jones and P. Jandik. Controlled changes of selectivity in the separation of ions by capillary electrophoresis. *Journal of Chromatography*, 546(1-2):445–458, 1991.
- [68] R. Sharma-A. Kanatt, SR. Chander. Chitosan glucose complex-a novel food preservative. *Food Chemistry*, 106:521–528, 2008.
- [69] J. W. Kang, Z. Y. Wang, J. F. Wang, and Z. D. Hu. Enantioseparation by ce with vancomycin as chiral selector: Improving the separation performance by dynamic coating of the capillary with poly(dimethylacrylamide). *Electrophoresis*, 28(6):938–943, 2007.
- [70] B. J. Kirby and E. F. Hasselbrink. Zeta potential of microfluidic substrates: 1. theory, experimental techniques, and effects on separations. *Electrophoresis*, 25(2):187–202, 2004.
- [71] B. J. Kirby and E. F. Hasselbrink. Zeta potential of microfluidic substrates: 2. data for polymers. *Electrophoresis*, 25(2):203–213, 2004.
- [72] C. J. Koh, P. Hookham, and L. G. Leal. An experimental investigation of concentrated suspension flows in a rectangular channel. *Journal of Fluid Mechanics*, 266:1–32, 1994. Nm368 Times Cited:133 Cited References Count:34.
- [73] B. T. Kurien and R. H. Scofield. Western blotting. *Methods*, 38(4):283–293, 2006.
- [74] M.U. Larsen, M. Seward, A. Tripathi, and N.C. Shapley. Biocompatible nanoparticles trigger rapid bacteria clustering. *Biotech. Prog.*, in press, 2009.

- [75] D. Leighton and A. Acrivos. The shear-induced migration of particles in concentrated suspensions. *Journal of Fluid Mechanics*, 181:415–439, 1987. J8319 Times Cited:570 Cited References Count:10.
- [76] B. Li, X. Wang, R. Chen, W. G. Huangfu, and G. L. Xie. Antibacterial activity of chitosan solution against xanthomonas pathogenic bacteria isolated from euphorbia pulcherrima. *Carbohydrate Polymers*, 72(2):287–292, 2008.
- [77] H. Liu, Y. M. Du, X. H. Wang, and L. P. Sun. Chitosan kills bacteria through cell membrane damage. *International Journal of Food Microbiology*, 95(2):147–155, 2004.
- [78] X. F. Liu, Y. L. Guan, D. Z. Yang, Z. Li, and K. De Yao. Antibacterial action of chitosan and carboxymethylated chitosan. *Journal of Applied Polymer Science*, 79(7):1324–1335, 2001.
- [79] C. A. Lucy and R. S. Underhill. Characterization of the cationic surfactant induced reversal of electroosmotic flow in capillary electrophoresis. *Analytical Chemistry*, 68(2):300–305, 1996.
- [80] M. K. Lyon and L. G. Leal. An experimental study of the motion of concentrated suspensions in two-dimensional channel flow. part 1. monodisperse systems. *Journal of Fluid Mechanics*, 363:25–56, 1998. Zw735 Times Cited:94 Cited References Count:39.

- [81] A. Mackie and P. Wilde. The role of interactions in defining the structure of mixed protein-surfactant interfaces. *Advances in Colloid and Interface Science*, 117(1-3):3–13, 2005.
- [82] E. Malinowska-Panczyk, I. Kolodziejska, D. Murawska, and G. Wolosewicz. The combined effect of moderate pressure and chitosan on escherichia coli and staphylococcus aureus cells suspended in a buffer and on natural microflora of apple juice and minced pork. *Food Technology and Biotechnology*, 47(2):202–209, 2009.
- [83] S. Manne, J. P. Cleveland, H. E. Gaub, G. D. Stucky, and P. K. Hansma. Direct visualization of surfactant hemimicelles by force microscopy of the electrical double-layer. *Langmuir*, 10(12):4409–4413, 1994.
- [84] R. M. McCormick. Capillary zone electrophoretic separation of peptides and proteins using low ph buffers in modified silica capillaries. *Analytical Chemistry*, 60(21):2322–8, 1988.
- [85] J. E. Melanson, N. E. Baryla, and C. A. Lucy. Dynamic capillary coatings for electroosmotic flow control in capillary electrophoresis. *Trac-Trends in Analytical Chemistry*, 20(6-7):365–374, 2001.
- [86] B. Metzger and J. E. Butler. Clouds of particles in a periodic shear flow. *Physics of Fluids*, 24(2), 2012. 901IH Times Cited:1 Cited References Count:17.
- [87] R. Miller, V. B. Fainerman, A. V. Makievski, J. Kragel, D. O. Grigoriev, V. N. Kazakov, and O. V. Sinyachenko. Dynamics of protein and mixed pro-

- tein/surfactant adsorption layers at the water/fluid interface. *Advances in Colloid and Interface Science*, 86(1-2):39–82, 2000.
- [88] A. K. Moren, M. Nyden, O. Soderman, and A. Khan. Microstructure of protein-surfactant complexes in gel and solution - an nmr relaxation study. *Langmuir*, 15(17):5480–5488, 1999.
- [89] J. Mosqueda-Melgar, R. M. Raybaudi-Massilia, and O. Martin-Belloso. Combination of high-intensity pulsed electric fields with natural antimicrobials to inactivate pathogenic microorganisms and extend the shelf-life of melon and watermelon juices. *Food Microbiology*, 25(3):479–491, 2008.
- [90] V. Mosquera, J. M. Ruso, G. Prieto, and F. Sarmiento. Characterization of the interactions between lysozyme and n-alkyltrimethylammonium bromides by zeta potential measurements. *Journal of Physical Chemistry*, 100(41):16749–16753, 1996.
- [91] S. P. Moulik, M. E. Haque, P. K. Jana, and A. R. Das. Micellar properties of cationic surfactants in pure and mixed states. *Journal of Physical Chemistry*, 100(2):701–708, 1996.
- [92] P.; Mukerjee and K. J. Mysels. *Critical Micelle Concentrations of Aqueous Surfactant Systems NSRDS-NBS 36*. U.S. Government Printing Office, Washington, DC, 1971.
- [93] R. W. Murray. Chips and more chips. *Analytical Chemistry*, 75(1):5A–5A, 2003.

- [94] H. Nagata, M. Tabuchi, K. Hirano, and Y. Baba. Microchip electrophoretic protein separation using electroosmotic flow induced by dynamic sodium dodecyl sulfate-coating of uncoated plastic chips. *Electrophoresis*, 26(11):2247–2253, 2005.
- [95] N. Naruishi, Y. Tanaka, T. Higashi, and S. Wakida. Highly efficient dynamic modification of plastic microfluidic devices using proteins in microchip capillary electrophoresis. *Journal of Chromatography A*, 1130(2):169–174, 2006.
- [96] S. O. Nielsen, G. Srinivas, C. F. Lopez, and M. L. Klein. Modeling surfactant adsorption on hydrophobic surfaces. *Physical Review Letters*, 94(22), 2005.
- [97] H. Okada, N. Kaji, M. Tokeshi, and Y. Baba. Poly(methylmethacrylate) microchip electrophoresis of proteins using linear-poly(acrylamide) solutions as separation matrix. *Analytical Sciences*, 24(3):321–325, 2008.
- [98] G. Oliver, C. Simpson, M. B. Kerby, A. Tripathi, and A. Chauhan. Electrophoretic migration of proteins in semidilute polymer solutions. *Electrophoresis*, 29(5):1152–1163, 2008.
- [99] D. E. Otzen. Protein unfolding in detergents: Effect of micelle structure, ionic strength, ph, and temperature. *Biophysical Journal*, 83(4):2219–2230, 2002.
- [100] D. E. Otzen, P. Sehgal, and P. Westh. alpha-lactalbumin is unfolded by all classes of surfactants but by different mechanisms. *Journal of Colloid and Interface Science*, 329(2):273–283, 2009.

- [101] J. C. Paton and A. W. Paton. Pathogenesis and diagnosis of shiga toxin-producing escherichia coli infections. *Clinical Microbiology Reviews*, 11(3):450–+, 1998.
- [102] J. Pei, J. F. Dishinger, D. L. Roman, C. Rungwanitcha, R. R. Neubig, and R. T. Kennedy. Microfabricated channel array electrophoresis for characterization and screening of enzymes using rgs-g protein interactions as a model system. *Analytical Chemistry*, 80(13):5225–5231, 2008. 320YH Times Cited:12 Cited References Count:48.
- [103] J. Penfold, E. Staples, L. Thompson, I. Tucker, J. Hines, R. K. Thomas, and J. R. Lu. Solution and adsorption behavior of the mixed surfactant system sodium dodecyl sulfate/n-hexaethylene glycol monododecyl ether. *Langmuir*, 11(7):2496–2503, 1995.
- [104] G. Petekidis, A. Moussaid, and P. N. Pusey. Rearrangements in hard-sphere glasses under oscillatory shear strain. *Physical Review E*, 66(5), 2002. 622DG Times Cited:68 Cited References Count:44.
- [105] R. J. Phillips, R. C. Armstrong, R. A. Brown, A. L. Graham, and J. R. Abbott. A constitutive equation for concentrated suspensions that accounts for shear-induced particle migration. *Physics of Fluids a-Fluid Dynamics*, 4(1):30–40, 1992. Gx510 Times Cited:371 Cited References Count:18.
- [106] D. J. Pine, J. P. Gollub, J. F. Brady, and A. M. Leshansky. Chaos and threshold for irreversibility in sheared suspensions. *Nature*, 438(7070):997–1000, 2005.

993EC Times Cited:78 Cited References Count:27.

- [107] M. E. Piyasena, T. Buranda, Y. Wu, J. M. Huang, L. A. Sklar, and G. P. Lopez. Near-simultaneous and real-time detection of multiple analytes in affinity microcolumns. *Analytical Chemistry*, 76(21):6266–6273, 2004.
- [108] O. Poetz, K. Luckert, T. Herget, and T. O. Joos. Microsphere-based co-immunoprecipitation in multiplex. *Analytical Biochemistry*, 395(2):244–248, 2009.
- [109] U. R. Pothakamury, A. Monsalvegonzalez, G. V. Barbosacanvas, and B. G. Swanson. Inactivation of escherichia-coli and staphylococcus-aureus in model foods by pulsed electric-field technology. *Food Research International*, 28(2):167–171, 1995.
- [110] Z. R. Jiang X. Qi, L. F. Xu, C. H. Hu, and X. F. Zou. Preparation and antibacterial activity of chitosan nanoparticles. *Carbohydrate Research*, 339(16):2693–2700, 2004.
- [111] H. Xiao Q. Liu Y. Zhu J. Du Y. Qin, C. Li. Water-solubility of chitosan and its antimicrobial activity. *Carbohydrate polymers*, 63(3):367–374, 2006.
- [112] F. Renault, B. Sancey, P. M. Badot, and G. Crini. Chitosan for coagulation/flocculation processes - an eco-friendly approach. *European Polymer Journal*, 45(5):1337–1348, 2009.
- [113] A. Rodriguez, M. D. Graciani, A. J. Moreno-Vargas, and M. L. Moya. Mixtures of monomeric and dimeric surfactants: Hydrophobic chain length and

- spacer group length effects on non ideality. *Journal of Physical Chemistry B*, 112(38):11942–11949, 2008.
- [114] M. A. Ren Z. F. Kempa K. Giersig M. Rojas-Chapana, J. A. Correa-Duarte. Enhanced introduction of gold nanoparticles into vital acidothiobacillus ferrooxidans by carbon nanotube-based microwave electroporation. *Nano Letters*, 4(5):985–988, 2004.
- [115] Milton J. Rosen. *Surfactants and Interfacial Phenomena*. Willey & Sons Inc., Hoboken, NJ, 3 edition, 2004.
- [116] A. I. V. Ross, M. W. Griffiths, G. S. Mittal, and H. C. Deeth. Combining nonthermal technologies to control foodborne microorganisms. *International Journal of Food Microbiology*, 89(2-3):125–138, 2003.
- [117] I. Santamaria-Holek, G. Barrios, and J. M. Rubi. Transition to irreversibility in sheared suspensions: An analysis based on a mesoscopic entropy production. *Physical Review E*, 79(3), 2009. 427GH Times Cited:6 Cited References Count:37.
- [118] G. Schmitt-Ulms, K. Markham, and Y. Bai. Co-immunoprecipitations revisited: an update on experimental concepts and their implementation for sensitive interactome investigations of endogenous proteins. *Analytical and Bioanalytical Chemistry*, 389(2):461–473, 2007.

- [119] D. Seth, P. Setua, A. Chakraborty, and N. Sarkar. Solvent relaxation of a room-temperature ionic liquid [bmim][pf6] confined in a ternary microemulsion. *Journal of Chemical Sciences*, 119(2):105–111, 2007.
- [120] X. W. Shao, Y. F. Shen, K. O’Neill, and M. L. Lee. Plexiglas column coatings for capillary electrophoresis of biomolecules. *Journal of Microcolumn Separations*, 11(5):325–329, 1999.
- [121] K. Shinzawa-Itoh, H. Aoyama, K. Muramoto, H. Terada, T. Kurauchi, Y. Tadehara, A. Yamasaki, T. Sugimura, S. Kurono, K. Tsujimoto, T. Mizushima, E. Yamashita, T. Tsukihara, and S. Yoshikawa. Structures and physiological roles of 13 integral lipids of bovine heart cytochrome c oxidase. *Embo Journal*, 26(6):1713–1725, 2007.
- [122] P. Somasundaran, D. W. Fuerstenau, and T. W. Healy. Surfactant adsorption at solid-liquid interface-dependence of mechanism on chain length. *Journal of Physical Chemistry*, 68(12), 1964.
- [123] S. A. Soper, A. Obubuafo, S. Balamurugan, H. Shadpour, D. Spivak, and R. L. McCarley. Poly(methyl methacrylate) microchip affinity capillary gel electrophoresis of aptamer-protein complexes for the analysis of thrombin in plasma. *Electrophoresis*, 29(16):3436–3445, 2008.
- [124] S. A. Soper, J. K. Osiri, H. Shadpour, S. Park, B. C. Snowden, and Z. Y. Chen. Generating high peak capacity 2-d maps of complex proteomes using pmma microchip electrophoresis. *Electrophoresis*, 29(24):4984–4992, 2008.

- [125] S. A. Soper and H. Shadpour. Two-dimensional electrophoretic separation of proteins using poly(methyl methacrylate) microchips. *Analytical Chemistry*, 78(11):3519–3527, 2006.
- [126] T. H. Steinberg, L. J. Jones, R. P. Haugland, and V. L. Singer. Sypro orange and sypro red protein gel stains: One-step fluorescent staining of denaturing gels for detection of nanogram levels of protein. *Analytical Biochemistry*, 239(2):223–237, 1996.
- [127] A. Stenstam, A. Khan, and H. Wennerstrom. The lysozyme-dodecyl sulfate system. an example of protein-surfactant aggregation. *Langmuir*, 17(24):7513–7520, 2001.
- [128] S. P. Strand, T. Nordengen, and K. Ostgaard. Efficiency of chitosans applied for flocculation of different bacteria. *Water Research*, 36(19):4745–4752, 2002.
- [129] V. Subramanian and W. A. Ducker. Counterion effects on adsorbed micellar shape: Experimental study of the role of polarizability and charge. *Langmuir*, 16(10):4447–4454, 2000.
- [130] C. X. Sun, J. H. Yang, X. Wu, X. R. Huang, F. Wang, and S. F. Liu. Unfolding and refolding of bovine serum albumin induced by cetylpyridinium bromide. *Biophysical Journal*, 88(5):3518–3524, 2005.
- [131] M. F. M. Tavares, R. Colombara, and S. Massaro. Modified electroosmotic flow by cationic surfactant additives in capillary electrophoresis - evaluation of

- electrolyte systems for anion analysis. *Journal of Chromatography A*, 772(1-2):171–178, 1997.
- [132] H. T Tien. *Bilayer Lipid Membranes (BLM): Theory and Practice*. Marcel Dekker, New York, 1974.
- [133] H. Towbin, T. Staehelin, and J. Gordon. Electrophoretic transfer of proteins from polyacrylamide gels to nitrocellulose sheets - procedure and some applications. *Proceedings of the National Academy of Sciences of the United States of America*, 76(9):4350–4354, 1979.
- [134] J. K. Towns and F. E. Regnier. Capillary electrophoretic separations of proteins using nonionic surfactant coatings. *Analytical Chemistry*, 63(11):1126–1132, 1991.
- [135] G. J. Tsai and W. H. Su. Antibacterial activity of shrimp chitosan against escherichia coli. *Journal of Food Protection*, 62(3):239–243, 1999.
- [136] T. Y. Tsong. Electroporation of cell-membranes. *Biophysical Journal*, 60(2):297–306, 1991.
- [137] T. Tsuda. Modification of electroosmotic flow with cetyltrimethylammonium bromide in capillary zone electrophoresis. *Journal of High Resolution Chromatography and Chromatography Communications*, 10(11):622–624, 1987.
- [138] A. Valstar, W. Brown, and M. Almgren. The lysozyme-sodium dodecyl sulfate system studied by dynamic and static light scattering. *Langmuir*, 15(7):2366–2374, 1999.

- [139] Wakamatsu.T and Fuerstenau.Dw. Effect of hydrocarbon chain length on adsorption of sulfonates at solid/water interface. *Advances in Chemistry Series*, (79), 1968.
- [140] S. L. Walker, S. Bhattacharjee, E. M. V. Hoek, and M. Elimelech. A novel asymmetric clamping cell for measuring streaming potential of flat surfaces. *Langmuir*, 18(6):2193–2198, 2002.
- [141] Weil. R Wallenfels. K. *The Enzymes*, volume 7. 3rd edition, 1972.
- [142] A. K. Lu C. Wang, H. Y. Bhunia. A microfluidic flow-through device for high throughput electrical lysis of bacterial cells based on continuous dc voltage. *Biosensors& Bioelectronics*, 22(5):582–588, 2006.
- [143] C. Z. Wang and C. A. Lucy. Mixed cationic/anionic surfactants for semipermanent wall coatings in capillary electrophoresis. *Electrophoresis*, 25(6):825–832, 2004.
- [144] J. Wang, Y. Zhang, M. R. Mohamadi, N. Kaji, M. Tokeshi, and Y. Baba. Exceeding 20 000-fold concentration of protein by the on-line isotachopheresis concentration in poly(methyl methacrylate) microchip. *Electrophoresis*, 30(18):3250–3256, 2009.
- [145] Y. M. Wang, J. Xu, L. Y. Yang, and Z. F. Luo. Synthesis of poly(n, n-dimethylacrylamide)-block-poly(ethylene oxide)-block-poly(n, n-dimethylacrylamide) and its application for separation of proteins by capillary zone electrophoresis. *Electrophoresis*, 31(10):1713–1720, 2010.

- [146] M Weber, K.; Osborn. The reliability of molecular weight determinations by dodecyl sulfate-polyacrylamide gel electrophoresis. *Journal of Biological Chemistry*, 1969:4406–4412, 1969.
- [147] C. Wenz and A. Rufer. Microchip cge linked to immunoprecipitation as an alternative to western blotting. *Electrophoresis*, 30(24):4264–4269, 2009.
- [148] A. T. Woolley and R. A. Mathies. Ultra-high-speed dna fragment separations using microfabricated capillary array electrophoresis chips. *Proceedings of the National Academy of Sciences of the United States of America*, 91(24):11348–11352, 1994.
- [149] S. Wu, J. J. Lu, S. Wang, K. L. Peck, G. Li, and S. Liu. Staining method for protein analysis by capillary gel electrophoresis. *Analytical Chemistry*, 79(20):7727–7733, 2007.
- [150] J. D. Xu, L. Locascio, M. Gaitan, and C. S. Lee. Room-temperature imprinting method for plastic microchannel fabrication. *Analytical Chemistry*, 72(8):1930–1933, 2000.
- [151] Q. Xu and T. A. Keiderling. Effect of sodium dodecyl sulfate on folding and thermal stability of acid-denatured cytochrome c: A spectroscopic approach. *Protein Science*, 13(11):2949–2959, 2004.
- [152] Q. Xu and T. A. Keiderling. Stop-flow kinetics studies of the interaction of surfactant, sodium dodecyl sulfate, with acid-denatured cytochrome c. *Proteins-Structure Function and Bioinformatics*, 63(3):571–580, 2006.

- [153] K. Yapici, R. L. Powell, and R. J. Phillips. Particle migration and suspension structure in steady and oscillatory plane poiseuille flow. *Physics of Fluids*, 21(5), 2009. 451WB Times Cited:14 Cited References Count:50.
- [154] R. Yousefi, N. Gheibi, A. Sharifzadeh, A. A. Moosavi-Movahedi, A. A. Saboury, J. M. Chobert, and T. Haertle. Chaperone-like activity of the dimeric beta-caseins: a first study towards development of gemini-like protein surfactant. *Febs Journal*, 276:353–353, 2009.
- [155] M. Yu, H. Y. Wang, and A. T. Woolley. Polymer microchip ce of proteins either off- or on-chip labeled with chameleon dye for simplified analysis. *Electrophoresis*, 30(24):4230–4236, 2009.
- [156] T. Yu, J. A. Traina, E. Pungor, and M. McCaman. Precise and comparative pegylation analysis by microfluidics and mass spectrometry. *Analytical Biochemistry*, 359(1):54–62, 2006.
- [157] G. Zardeneta and P. M. Horowitz. Prospective - detergent, liposome, and micelle-assisted protein refolding. *Analytical Biochemistry*, 223(1):1–6, 1994.
- [158] M. Allen C.Kumacheva E. Zhang, H. Oh. Monodisperse chitosan nanoparticles for mucosal drug delivery. *Biomacromolecules*, 5(6):24612468, 2004.
- [159] X. X. Zhang, H. Y. Li, V. Dauriac, V. Thibert, H. Senechal, G. Peltre, and S. Descroix. Micropillar array chips toward new immunodiagnosis. *Lab on a Chip*, 10(19):2597–2604, 2010.

- [160] Y. Zhang, G. C. Ping, B. M. Zhu, N. Kaji, M. Tokeshi, and Y. Baba. Enhanced electrophoretic resolution of monosulfate glycosaminoglycan disaccharide isomers on poly(methyl methacrylate) chips. *Electrophoresis*, 28(3):414–421, 2007.
- 139IN Times Cited:12 Cited References Count:30.